

Instituto Tecnológico y de Estudios Superiores de Monterrey

Campus Monterrey

School of Engineering and Sciences



Wavelets for Spindle Health Diagnosis

A thesis presented by

Silvia Cristina Villagómez Garzón

Submitted to the

School of Engineering and Sciences

in partial fulfillment of the requirements for the degree of

Master of Science

In

Manufacturing Systems

Monterrey, Nuevo León, December 4th 2017

Instituto Tecnológico y de Estudios Superiores de Monterrey

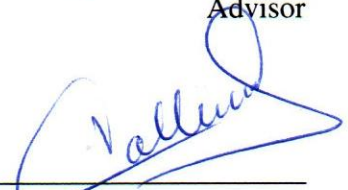
Campus Monterrey

School of Engineering and Sciences

The committee members, hereby, certify that have read the dissertation presented by Silvia Cristina Villagómez Garzón and that it is fully adequate in scope and quality as a partial requirement for the degree of Master of Science in Manufacturing Systems.



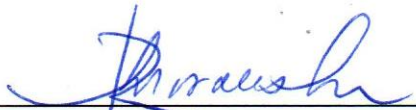
Dr. Rubén Morales Menéndez
Tecnológico de Monterrey
Advisor



Dr. Antonio Jr. Vallejo Guevara
Tecnológico de Monterrey
Committee Member



Dra. Diana Hernández Alcántara
Universidad de Monterrey
Committee Member



Dr. Rubén Morales Menéndez
Dean of Graduate Studies
School of Engineering and Sciences

Monterrey, Nuevo León, December 4th 2017

Declaration of Authorship

I, Silvia Cristina Villagómez Garzón, declare that this dissertation titled, *Wavelets for Spindle Health Diagnosis* and the work presented in it are my own. I confirm that:

- This work was done wholly or mainly while in candidature for a research degree at this University.
- Where any part of this dissertation has previously been submitted for a degree or any other qualification at this University or any other institution, this has been clearly stated.
- Where I have consulted the published work of others, this is always clearly attributed.
- Where I have quoted from the work of others, the source is always given. With the exception of such quotations, this dissertation is entirely my own work.
- I have acknowledged all main sources of help.



Silvia Cristina Villagómez Garzón

Monterrey, Nuevo León

December 4th 2017

@2017 by Silvia Cristina Villagómez Garzón
All rights reserved

Dedication

To my parents,
with their support and love they have raise bliss and happy children.
To my brothers,
because you taught me the "*iriomi*" of the purest and most sincere friendship.
To all my family,
for being and allowing me to be that great example of life.
To my extended family, my friends,
for giving me the privilege of sharing their lives.
And of course for you Agapimu,
for being more than I ever dreamed.

A mis padres,
con su apoyo y amor han formado hijos dichosos y felices.
A mis hermanos,
porque ustedes me enseñaron el "*iriomi*" de la más pura y sincera amistad.
A toda mi familia,
por ser y permitirme ser ese gran ejemplo de vida.
A mi familia ampliada, mis amigos,
por darme el privilejo de compartir sus vidas.
Y por supuesto para tí, Agapimu,
por ser más de lo que alguna vez soñé.

Acknowledgements

I would like to express my deepest gratitude to Mexico and its great people, who have received me with that charisma, affection and kindness that distinguish them so much. A country to which I will definitely always want to return.

I want to thank my adviser, Dr. Rubén Morales Menéndez, for his unconditional support, and his guidance during the development of this thesis. His willingness and commitment have allowed to satisfactorily fulfill the objectives of this investigation.

I also want to thank the committee members, Dr. Diana Hernández Alcántara and Dr. Antonio Jr. Vallejo Guevara, for their support and their valuable contributions and suggestions.

In addition, I would like to offer particular thanks to my colleague and co-author of this investigation; thank you, George Francisco Batallas Moncayo for your commitment, solidarity and dedication. But more than anything else, thank you for your friendship, for being my family during this stay in México.

Finally, I am very grateful to Tecnológico de Monterrey for the scholarship received and the support via Automotive Consortium, the project in collaboration with Bocar SA de CV and CONA-CyT for the maintenance support.

Thank you very much.

Me gustaría expresar mi más profunda gratitud a México y su grandiosa gente, que me ha recibido con ese carisma, ese cariño y esa amabilidad que tanto les caracteriza. Un país al que definitivamente siempre querré volver.

Quiero agradecer a mi asesor, Dr. Rubén Morales Menéndez, por su apoyo incondicional, y su orientación durante el desarrollo de esta tesis. Su disposición y compromiso han permitido cumplir satisfactoriamente los objetivos de esta investigación.

También quiero agradecer a los miembros del comite, Dra. Diana Hernández Alcántara y Dr. Antonio Jr. Vallejo Guevara, por su apoyo y sus valiosos aportes y sugerencias.

Además, quiero expresar un agradecimiento especial a mi colega y coautor de esta investigación; gracias George Francisco Batallas Moncayo por tu compromiso, solidaridad y dedicación. Pero más que nada, gracias por tu amistad, por ser mi familia durante esta estancia en México.

Finalmente, estoy muy agradecido con el Tecnológico de Monterrey por la beca recibida y el apoyo a través del Consorcio Automotriz, con el proyecto en colaboración con Bocar SA de CV y con CONACyT por el apoyo de manutención.

Dos mil gracias.

Wavelets for Spindle Health Diagnosis

By

Silvia Cristina Villagómez Garzón

Abstract

Industrial development and customer demands have increased the need to look for high-quality products at low cost and, at the same time, ensure safety during manufacturing. As a result, rotary machinery and its components have become increasingly complex, making their repairs more expensive. Therefore, many efforts must be focused in preventing breakdowns in machines, for which real-time fault diagnosis and prognosis are mandatory.

Considering that the element most prone to failure in a machining center is the spindle, and with it its bearing system, the diagnosis of failures of these elements is of paramount importance. To ensure the safe operation of the bearing, some methods of fault detection have been developed based on different techniques. One of the most commonly used is vibration analysis.

There are several difficulties when dealing with analyzing vibration signals, they are complex and non-stationary signals with a large amount of noise. Conventional analysis have not been able to solve this problem, thus, alternative methods such as Wavelet Transform have been gaining ground.

The following research is focused in detecting bearing faults, as well as the main shaft faults, which eventually also lead to bearing damage, by using wavelets. Different signals, presenting distinct bearing fault conditions, of different data sets are evaluated for validating the proposed methodology. An exhaustive analysis has been developed for selecting the best parameters of this methodology.

As results, an improvement around 20% in magnitude of bearing fault frequency peaks was found, compared to the traditional methodology. The proposal of giving more weight to high energy components allows increasing these fault frequencies, as well as reducing low frequency noise. This provides a great advantage in pursuit of an automatic fault detection.

An industrial approach was also validated, by proving that the proposed methodology is more immune to noise. Even though, the magnitudes of the bearing fault peaks are diminished by noise, a comparison between the proposal and the traditional methodology reveal an increase of approximately 70% of those magnitudes. Demonstrating that the fault information is barely attenuated by noise. Also, an early diagnosis was proved, which could benefit future studies of fault prognosis.

Finally, the filtering property of wavelet decomposition is exploited to limit the frequencies of the signal to few harmonics of the shaft speed. This with the aim of restricting the spectrum for detecting other faults, that mainly affect the spindle shaft, which are diagnosed by analyzing speed harmonics and subharmonics. Thus, a complete methodology is proposed to deal with the main spindle faults.

Contents

- 1 Introduction 1**
 - 1.1 Motivation 2
 - 1.2 Problem Description 3
 - 1.3 Research Question 4
 - 1.4 Solution Overview 4
 - 1.5 Main Contribution 5
 - 1.6 Dissertation 5

- 2 State of the Art 7**
 - 2.1 Literature Review 7
 - 2.2 Theoretical Background 15
 - 2.2.1 Wavelets 15
 - 2.2.2 Bearing Faults 16
 - 2.2.3 Unbalance, Misalignment and Mechanical Looseness 19

- 3 Experimental System 21**
 - 3.1 Introduction 21
 - 3.2 Experimental Data Sets 21
 - 3.2.1 Data 1 set: CWRU - Bearing Data Center 21
 - 3.2.2 Data 2 set: IMS - Bearing Data 22
 - 3.2.3 Data 3 set: Industrial Plant 23
 - 3.3 Design of Experiments 24
 - 3.3.1 Unbalance Holder 24

- 4 Proposal 27**
 - 4.1 Introduction 27
 - 4.2 Bearing Faults 27
 - 4.3 Unbalance, Misalignment and Mechanical Looseness 31

5	Results	33
5.1	Introduction	33
5.2	Results	33
5.2.1	Raw signal and preprocessing	33
5.2.2	Signal decomposition	36
5.2.3	Best nodes and weighting values	37
5.2.4	Signal reconstruction	37
5.2.5	Envelope and post processing	37
5.2.6	FFT and bearing fault detection	40
5.2.7	MA, ML, UB fault detection	43
5.3	Discussion	46
5.4	Comparison	54
6	Conclusions	57
6.1	Conclusions	57
6.2	Contributions	57
6.3	Publications	58
6.4	Future work	58
	Bibliography	59
A	Acronyms Definition	65
B	Wavelet Parameters Selection	67
B.1	Wavelet Transform Selection	67
B.2	Mother Wavelet Selection	69
C	Additional results of the proposed methodology	79
C.1	Bearing Faults	79
C.2	Unbalance, Misalignment and Mechanical Looseness	79
D	Published articles	87
E	Developed Programs	91
	Curriculum Vitae	97

List of Figures

2.1	Wavelet transforms evolution	15
2.2	Typical mother wavelets	16
2.3	Signals from local faults in bearings	17
2.4	Stages of bearing damage	18
3.1	<i>CWRU</i> Test Rig Schema	22
3.2	<i>IMS</i> Test Rig Schema	23
3.3	Signal acquisition schema of <i>GROB 550</i>	24
3.4	Vibration signal for <i>UB</i> analysis	25
4.1	Proposed methodology for spindle faults diagnosis	28
4.2	Entropy of each node for best tree selection	30
5.1	Signals considered to validate the proposed methodology (<i>CWRU</i> data)	34
5.2	Kurtosis calculation for detecting the initial stage of damage (<i>IMS</i> data)	34
5.3	Signals considered to validate the proposed methodology (<i>IMS</i> data)	35
5.4	Signal Preprocessing: Trend Removal	35
5.5	Best trees selected for each fault	38
5.6	<i>Kurtosis</i> , <i>RMS</i> and <i>KR</i> for the signal with <i>OR-Y</i> fault	39
5.7	Weighting values for the signal with <i>OR-Y</i> fault	39
5.8	Signal reconstruction scheme	40
5.9	Reconstructed signal from the <i>OR-Y</i> fault	40
5.10	FFT spectrum of the (a) original and the (b) reconstructed signal with the <i>OR-Y</i> fault	41
5.11	Envelope of the reconstructed signal with removed <i>DCC</i> from the <i>OR-Y</i> fault . . .	41
5.12	<i>FFT</i> of the enveloped reconstructed signal with removed <i>DCC</i> from the <i>OR-Y</i> fault	42
5.13	<i>FFT</i> of the enveloped reconstructed signal with removed <i>DCC</i> from the <i>IR-Y</i> fault	42
5.14	<i>FFT</i> of the enveloped reconstructed signal with removed <i>DCC</i> from the <i>RE-Y</i> fault	43
5.15	<i>FFT</i> spectrum of the (a) original signal and the (b) low nodes reconstructed signal - baseline of <i>CWRU</i>	44
5.16	<i>FFT</i> of the two low nodes reconstructed signal with <i>IR-P</i> fault (<i>CWRU</i> data)	44

5.17	<i>FFT</i> of the two nodes reconstructed signal 0 load baseline (<i>CWRU</i> data)	45
5.18	<i>FFT</i> of the two nodes reconstructed signals baseline (<i>CWRU</i> data)	46
5.19	<i>FFT</i> of the two nodes reconstructed signals baseline (<i>IMS</i> data)	47
5.20	<i>FFT</i> of the two nodes reconstructed signals baseline (<i>IMS</i> data)	48
5.21	Periodicity description of the additional peaks found in <i>IR-N</i> signal	49
5.22	Combined defects found in <i>OR-P</i> signal, explaining additional peaks	50
5.23	Combined defects found in <i>OR-N</i> signal, explaining additional peaks	50
5.24	Combined defects found in <i>RE-P</i> signal, explaining additional peaks	51
5.25	Combined defects found in <i>RE-N</i> signal, explaining additional peaks	51
5.26	Comparison of the traditional envelope <i>FFT</i> and the proposed methodology for the base line signal (without fault)	54
5.27	Comparison of the traditional envelope <i>FFT</i> and the proposed methodology for <i>IR-Y</i> signal (<i>CWRU</i> data)	55
5.28	Comparison of the initial signal and the obtained with the proposed methodology in time domain for <i>IR-Y</i> signal added white <i>Gaussian</i> noise <i>SNR</i> = 10 (<i>CWRU</i> data)	55
5.29	Comparison of the <i>FFT</i> spectrum of the initial signal and the proposed methodol- ogy for <i>IR-Y</i> signal added white <i>Gaussian</i> noise <i>SNR</i> = 10 (<i>CWRU</i> data)	56
5.30	Comparison of the traditional envelope <i>FFT</i> and the proposed methodology for <i>IR-Y</i> signal added white <i>Gaussian</i> noise <i>SNR</i> = 10 (<i>CWRU</i> data)	56
B.1	<i>WT</i> 3D scalogram comparison applied to a signal with <i>OR</i> fault	68
B.2	<i>WT</i> frequency-coefficients comparison applied to a signal with <i>OR</i> fault	69
B.3	Mother wavelet computing time for signals with <i>IR</i> , <i>OR</i> , and <i>RE</i> faults	70
B.4	Orthogonal vs Biorthogonal transfer modulus for decomposition and reconstruc- tion filters	71
B.5	<i>FFT</i> signals energy	73
B.6	Border Effects	75
B.7	<i>MW</i> quantitative parameters for 4 signals with <i>OR</i> fault	75
B.8	<i>MW</i> quantitative parameters for 4 signals with <i>IR</i> fault	75
B.9	<i>MW</i> quantitative parameters for 4 signals with <i>RE</i> fault	76
B.10	Averaged <i>MW</i> quantitative parameters for signals with <i>OR</i> fault	76
B.11	Averaged <i>MW</i> quantitative parameters for signals with <i>IR</i> fault	76
B.12	Averaged <i>MW</i> quantitative parameters for signals with <i>RE</i> fault	77
B.13	Quantitative parameters comparison for signals with <i>OR</i> faults	77
B.14	Quantitative parameters comparison for signals with <i>IR</i> faults	77
B.15	Quantitative parameters comparison for signals with <i>RE</i> faults	78
B.16	Averaged <i>MW</i> quantitative parameters for the three type of faults	78
B.17	Quantitative parameters comparison for the three type of faults	78

C.1	Spectrum of <i>IR</i> faulty signals considering harmonics and sidebands (<i>CWRU</i> data base)	80
C.2	Spectrum of <i>OR</i> faulty signals considering harmonics (<i>CWRU</i> data base)	80
C.3	Spectrum of <i>RE</i> faulty signals considering harmonics and sidebands (<i>CWRU</i> data base)	80
C.4	Cleared spectrum of <i>IR</i> faulty signals (<i>CWRU</i> data base)	81
C.5	Cleared spectrum of <i>OR</i> faulty signals (<i>CWRU</i> data base)	81
C.6	Cleared spectrum of <i>RE</i> faulty signals (<i>CWRU</i> data base)	81
C.7	Spectrum of <i>IR</i> faulty signals considering harmonics and sidebands (<i>IMS</i> data base)	82
C.8	Spectrum of <i>OR</i> faulty signals considering harmonics (<i>IMS</i> data base)	82
C.9	Spectrum of <i>RE</i> faulty signals considering harmonics and sidebands (<i>IMS</i> data base)	82
C.10	Cleared spectrum of <i>IR</i> faulty signals (<i>IMS</i> data base)	83
C.11	Cleared spectrum of <i>OR</i> faulty signals (<i>IMS</i> data base)	83
C.12	Cleared spectrum of <i>RE</i> faulty signals (<i>IMS</i> data base)	83
C.13	Spectrum of <i>IR</i> faulty signals considering speed harmonics and half speed harmonics (<i>CWRU</i> data base)	84
C.14	Spectrum of <i>OR</i> faulty signals considering speed harmonics and half speed harmonics (<i>CWRU</i> data base)	84
C.15	Spectrum of <i>RE</i> faulty signals considering speed harmonics and half speed harmonics (<i>CWRU</i> data base)	84
C.16	Spectrum of <i>IR</i> faulty signals considering speed harmonics and half speed harmonics (<i>IMS</i> data base)	85
C.17	Spectrum of <i>OR</i> faulty signals considering speed harmonics and half speed harmonics (<i>IMS</i> data base)	85
C.18	Spectrum of <i>RE</i> faulty signals considering speed harmonics and half speed harmonics (<i>IMS</i> data base)	85
E.1	<i>WPT</i> 2D scalogram function	92
E.2	<i>WPT</i> 3D scalogram function	92

List of Tables

2.1	Comparison between some fault diagnosis researches using <i>WT</i> for machining . . .	12
3.1	<i>CWRU</i> Bearing Defect Frequencies (multiple of running speed in Hz)	22
3.2	IMS Bearing Defect Frequencies (multiple of running speed in Hz)	23
3.3	Acquisition equipment characteristics of GROB 550	24
4.1	Sidebands considered for bearing fault diagnosis	31
5.1	Level of decomposition calculated for each signal	36
5.2	Results for bearing faults	52
5.3	Results for <i>MA</i> and <i>ML</i>	53
5.4	Comparison between traditional envelope <i>FFT</i> and proposed methodology for noiseless and noisy signals (<i>IR-Y CWRU</i> data)	56
A.1	Acronyms Definitions	65
B.1	Mother wavelets for <i>WPT</i>	70
B.2	Selected mother wavelets for <i>WPT</i>	71
B.3	<i>CWRU</i> signals considered for <i>MW</i> analysis	74

Chapter 1

Introduction

Industrial development and customers demands have increased the need to pursue high-quality products at low cost while ensuring safety during manufacturing. *High Speed Machining (HSM)*¹ offers high-quality and low machining times; however, its components are more complex and more expensive when they need repairs. For this reason, machine maintenance strategies have evolved from corrective over preventive to condition-based maintenance, for which real-time fault diagnosis and prognosis are needed, [Yan *et al.*, 2014]. Therefore, all efforts must be focused in preventing breakdowns in machines; thus, spindles must be monitored. A failure in the spindle can be catastrophic, leading to costly machine downtime, affecting the productivity in the company.

Bearings are one of the foremost cause of failures in a machine tool spindle, they are the most critical and vulnerable components in the mechanical transmission. According to statistics, approximately 30% of mechanical failures in rotating machinery are due to the failure of rolling bearings, [Cui *et al.*, 2016]. Hence, the bearing faults diagnosis has been gaining importance due to its detrimental effect on machines reliability. Additionally, spindle fault such as *MisAlignment (MA)*, *Mechanical Looseness (ML)* and *UnBalance (UB)* must also be monitored, as they might lead to bearing faults.

As bearings wear out, several defects may unleash. The principal defects affecting bearings are: distributed and local flaws. Distributed defects are divided in surface roughness, waviness, misaligned races and off-size *Rolling Elements (RE)*. On the other hand, local defects are splitted into, cracks, pits and spalls on the rolling surface, [Prabhakar *et al.*, 2002]. Most typical faults in bearings are produced by local defects, mainly cracks, pits and spalls in the *Inner Race (IR)*, the *Outer Race (OR)* or the *RE*.

During bearing operation, localized faults or wear produce successive periodic impacts when rollers pass over the defect and causes wideband impulses. The amplitude and period of these impulses depend on the shaft speed, the type of fault (location) and the bearing geometry. Mean-

¹All acronyms are defined in Appendix A

while, the other faults influence straightforward to the shaft speed characteristics. Vibration signal analysis is one of the most effective techniques for analyzing impulses to detect and diagnose flaws for a successful maintenance program.

Nevertheless, there are several difficulties in signal analysis for fault detection. The foremost problem to deal with are the characteristics of the signals, they are nonlinear and non-stationary. Another issue to solve is that the signature of a defective spindle can be undercovered by noise, and low frequency effects. In addition, as defect frequency is typically small it is not easily noticed. For bearing faults, it also needs to be considered that, in an initial stage of wear, the vibration signal shows up distinct peaks in the frequency domain, but after wear develops along the surface, the signal becomes more like random noise and it can not be easily detected, [Chancey *et al.*, 2002]. Among other difficulties, there is also a problem when trying to detect *OR* and *IR* defects at the same time, the *OR* defects are clear in the spectra, while the *IR* are not easily detected.

To cope with these problems many research have been developed, and a wide variety of techniques have been introduced such as *Short Time Fourier Transform (STFT)*, *Wavelet Transform (WT)*, *Hilbert-Huang Transform (HHT)*, *Wigner-Ville Distribution (WVD)*, *Statistical Signal Analysis (SSA)* among others.

Traditional approaches (conventional time domain and frequency domain analysis) are not useful as they tend to average out transient effects. Some defects such as *UB*, eccentricity and *Bent Shaft (BS)* or bowed rotor can display similar time traces with impulses of similar amplitude and frequency; therefore, defects can not be isolated. Also, the complexity and non-stationary characteristics of signals carrying out with a large amount of noise make spindle faults very difficult to detect with these traditional methods.

Signals have a vast information, but they are often tainted by noise. Signal processing techniques must have the ability to split close frequencies in real data.

Due to the high frequency nature of defect bearings impulses, it is required to handle bearing damage with a high frequency signal analysis. On the other hand, shaft faults must be analyzed at low frequencies. Signal processing techniques, such as *WT*, *Fast Fourier Transform (FFT)* and *HHT* are applied to extract features from the acquired signals.

1.1 Motivation

As industry develops, technological advances are needed to satisfy customers demands. When talking about manufacturing industry machining centers stand out, since they allow a high production of complex pieces with much shorter machining times. Five axis machining centers, for example, even allow speeds up to 80,000 RPM with superior precision and amazing surface finishing capabilities.

When working at these speeds it is necessary to keep an accurate control of everything that

happens during machining, to avoid damages in production as well as in the equipment. If the equipment has a fault, it will be reflected directly in the machined product, generating losses for the manufacturing enterprise.

To avoid damage in machining centers, maintenance procedures exist. These have been evolving along with existing technology. Initially machines were forced to work until they failed, giving maintenance to the equipment when they could no longer function. While this prolonged its useful life to the maximum, damages implied a sudden and prolonged breakdown with high costs of repair. To solve this type of inconveniences the preventive maintenance emerged, which sets dates to stop production and review the operation of the equipment. This maintenance allows to avoid unforeseen events; however, this is done with much shorter times to which the equipment can fail, wasting the capacity of the machines. Finally, as a balance between the two options described above appears the condition-based maintenance, which monitors the entire process to know when exactly it will require maintenance.

Currently, with the development of technology, industries are looking to migrate to more advanced monitoring and diagnostic systems, precisely to guarantee production. For this reason, the monitoring of machining centers is highly quoted.

Considering that the element most exposed to failure is the spindle, and with it its bearing system, the diagnosis of failures of these elements is of paramount importance for the manufacturing industry.

1.2 Problem Description

To ensure a healthy spindle some methods of fault detection, fault diagnosis and fault prognosis have been developed based on different techniques. One of the most commonly used is vibration analysis, this technique allows capturing periodic events, as faults produce peaks for every rotation this technique helps extracting features for monitoring spindles.

Vibration analysis is the single most important component of a successful maintenance program, [Chancey *et al.*, 2002], as it allows machine condition monitoring. This technique reacts immediately to changes, is more likely to point to the actual faulty component and most importantly, many powerful signal processing techniques can be applied to vibration signals to extract even very weak fault indications from noise and other masking signals, [Randall, 2011].

Faults, in the initial stage of wear, produce distinct peaks that can be seen in the frequency domain, as wear develops they become more like random noise. This makes vibration analysis a powerful tool for detecting incipient faults; but, it requires a good processing technique to show faults before they can not be detected.

There are several difficulties to deal with analyzing vibration signals, they are complex and non-stationary with a large amount of noise which makes very difficult to detect faults, especially

by conventional analysis, [Kankar *et al.*, 2011]. For bearings, the difficulties lie in the fact that the distinctive features of a defective bearing is spread across a wide frequency band and hence can be easily masked by noise and low frequency effects. Furthermore, the amplitudes of the defects are small so they are not easily noticed. Therefore, the main problems to be solved when proposing a methodology to detect spindle faults using vibration analysis are:

- Developing a powerful signal processing algorithm to filter noise and low frequency effects, separating close frequencies in real data.
- Deal with non-stationary signals, considering transient effects.
- Efficient extraction of features that vary in time.
- Isolate defects to deal with more than one fault at the time.

Based on the previous issues, non-traditional signal processing techniques such as *STFT*, *WT*, *HHT*, *WVD*, *SSA* can provide an efficient feature extraction method for fault detection.

1.3 Research Question

There are many problems when dealing with vibration analysis for spindle faults detection. Traditional signal processing can not deal with complex characteristics of signals, and are highly affected by noise.

Commonly, fault detection focuses on a specific spindle problem; however, a methodology that analyzes more than one defect can provide a complete overview of the state of the spindle. Nevertheless, leading with more than one defect requires good spectral resolution since, certain faults are analyzed at high frequencies, bearing faults, and others at low frequencies, *MA*, *UB* and *ML*.

The adaptive multi-resolution capability of the *WT* has made it a powerful mathematical tool for diagnostics of machine operation conditions in manufacturing. Though, many parameters must be evaluated for performing a good decomposition and reconstruction to extract the features that allow a good diagnosis. The type of *WT*, the mother wavelet, level of decomposition, indicators to extract the useful information, must be well studied.

1.4 Solution Overview

To generate a successful methodology, some aspects must be considered. First, it must be guaranteed that collected information is useful, signals should contain valid information with a good acquisition system and reliable sensors. To apply this methodology to industrial equipment, the

characteristics of the environment as well as of the inside of the machine should be well identified. A good characterization of the machine in good conditions must be established.

Wavelets have the ability of simultaneously gather information from time and frequency domains with a varying time-frequency window. This substantial insight of the method makes it ideal for processing transient and non-stationary signals as well as extracting features that vary in time. As *WT* can also be considered as a special filtering operation, it has a denoising nature. This helps to isolate defects to deal with more than one fault at the time.

After a good vibration signal is acquired, wavelets analysis is applied as a filter dividing high and low frequencies, obtaining more detailed information of the vibration signal. The spectrum of the signal is analyzed for identifying fault frequencies that previously are computed for every possible damage. For the faults that are analyzed in the harmonics of the rotational speed, the low frequencies are considered; while for bearing faults, high frequencies that contain more information about the fault are analyzed.

1.5 Main Contribution

The main contribution of this thesis is the development of a methodology based on *Wavelet Packet Transform (WPT)* for bearings faults diagnosis as well as for *MA*, *ML* and *UB* faults detection; which are the main cause of spindle machining centers breakdowns.

Additionally, for the development of the methodology, it was analyzed which were the best parameters for detecting spindle faults by using *WT*. Among the analyzed parameters were: the type of *WT*, the optimum decomposition level and the most suitable *MW*.

The proposed methodology, was validated with different data sets, showing effectiveness for the three of them. It was shown that *IR*, *OR*, *RE*, *MA*, *ML* and *UB* defects were efficiently determined.

In addition, a magnification of around 20% in magnitude of fault frequency peaks was found compared to traditional methodologies. This increase may benefit in future implementation of classifiers, as it gives more energy to the fault components and makes them more visible in the spectrum.

A possible application to industrial level was also identified, as the proposed methodology is more immune to noise. The magnitude comparison between the proposal and the traditional methodology reveal that the attenuation of the fault peaks, due to noise, was approximately 70% less for the proposed methodology.

1.6 Dissertation

This thesis is structured as follows:

Chapter 2 introduces the subject by means of a brief description of the state of the art, considering the evolution of the techniques for vibration signal analysis emphasizing the preference for wavelets.

Chapter 3 describes the experimental development, the management of data sets and the *DoE* for the data obtained from a *GROB 550* machining center or similar during its daily industrial operation.

Chapter 4 presents the theoretical-technical proposal with the development of the diagnosis methodology, and the used algorithms for applying the selected technique.

Chapter 5 shows the analysis of the results that validate the proposed methodology. A comparison with other methods is included.

Chapter 6 presents the conclusions from this research, highlights the contributions obtained and introduces some future works and research lines.

Chapter 2

State of the Art

2.1 Literature Review

The relationship between vibration signals and machine condition was first perceived by [Rathbone, 1939], where it was considered that the damage of the machine depend of the vibration amplitude. By 1960, it was recognized that periodic monitoring could be useful to avoid machine failures, so measurement and recording vibration signals experienced a great surge. In the next decade *FFT* analyzers were applied, expanding vibration analysis to more difficult and complex cases. From 1980s the technology of the accelerometers and digital computers improved, obtaining a better performance in the efficiency and effectiveness of the analyses, [Randall, 2011].

When analyzing vibration signals of *HSM* machines, efforts must be focused in detecting some paramount defects. The principal elements of the spindle that must be considered when monitoring a machine are the shaft and the bearings. These components are in charged of transmitting movement from the motor to the tool, so they are subjected to constant loads. When they present defects the cutting process is altered, originating defects in the rest of the components as well as in the quality of the machining.

Defects that emerge in spindles are basically *MA*, *UB*, *ML*, *BS* and bearings faults. A brief description as well as the causes and effects of these faults are described in [Mais, 2002]. A summary of these characteristics is:

- *Misalignment (MA)* is created when shafts, couplings and bearings are not properly aligned along their centerlines. One principle cause of this problem is a poor coupling, and as effect the bearing carries higher load than its design specification, leading to fatigue.
- *Unbalance (UB)* occurs when the shafts mass centerline does not coincide with its geometric centerline. This is often induced by the addition of shaft fittings without an appropriate counter balancing procedure. As *MA*, *UB* usually causes bearings fatigue.

- *Bent Shaft (BS)* problem is almost identical to *MA*. It is occasioned by excessive torque. Consequences are the same as the others: bearing's fatigue.
- *Mechanical Looseness (ML)* appear when a machine component is loose. This is not common, and as consequence it is possible that the component will become detached and cause secondary damage.
- Bearings are the principal reason of machine breakdowns, as they take up fatigue. Elements that show defects are *Inner Race (IR)*, *Outer Race (OR)*, *Cage (C)*, and *Rolling Element (RE)*.

Many research projects have been developed to identify faults from vibration signals. Nevertheless, many difficulties appear while trying to detect them. Within many methods of processing vibration signals focused in the field of fault diagnosis, a trend towards the study of wavelets has been noticed. In recent years, the theory and applications of wavelets have been deeply studied.

One of the first wavelet approach for detecting bearing faults was done by [Mori *et al.*, 1996] focused in analyzing just *OR* defects. By the same time [Paya *et al.*, 1997] developed another technique based on the application of *Continuous Wavelet Transform (CWT)* and the use of *Artificial Neural Network (ANN)* to detect automatically *IR* defects. In the next decade, many studies were developed to take advantage of the benefits of *WT* in the analysis of nonlinear and non-stationary signals.

Traditional approaches (conventional time domain and frequency domain analysis) are not useful as they tend to average out transient effects; hence a wide variety of techniques have been introduced such as *STFT*, *WT*, and *WVD*. Nevertheless, [Tse *et al.*, 2001] revealed that in *STFT*, the resolutions in the time and frequency domains are limited by the width of the analyzing window so this technique is deemed unsuitable for fault diagnosis. On the other hand, *WVD* may lead to the emergence of negative energy levels and spectrum aliasing, causing difficulty in interpreting results. This research proposed that *WT* is uniquely suitable to detect bearing faults and suggested a more convenient method to detect the existence of any bearing fault in a fast process and diagnose its cause of fault in the higher frequency bearing excitation range.

Considering that the first proposals used *CWT*, which has the disadvantage of requiring great computational effort due to overlapping and a large amount of redundant information, research has focused on the development of other techniques. [Prabhakar *et al.*, 2002] presented the diagnosis of single and multiple ball bearing race faults using *Discrete Wavelet Transform (DWT)*, where signals are decomposed in low frequency (approximations) and high frequency (details) signals. This helped to cope with the problem of detecting *IR* defects, which are not clear in the spectra as *OR*. Another alternative was proposed by [Tse *et al.*, 2004], a new method named *Exact Wavelet Analysis (EWA)* was developed to generate multiple mother wavelets that will generate various kinds of daughter wavelets that are adaptive to the characteristics of the inspected signal.

Other methods were proposed by [Chancey *et al.*, 2002] and [Nikolaou and Antoniadis, 2002], the first one uses the *Harmonic Wavelets (HW)* which has been shown to be a favorable choice for vibration analysis because of the use of the *FFT* and the *Inverse Fast Fourier Transform (IFFT)* in its *HW* algorithm. The second one proposed the use of *WPT* where the signal is decomposed in details and approximations, in turn, those are split into finer components. Some statistical indicators, such as, the mean and the standard deviation are used to compare results.

[Zhang and Gao, 2004] identified that the *WT* could detect faults in the *IR* and *OR* unlike the *FFT*, which deal only with *OR* faults. In [Zhang *et al.*, 2005] the investigation was expanded to shaft *UB* and finally in [Zhang *et al.*, 2006] some improvements of the methods were developed by using envelope and the *Analytic Wavelet Transform (AWT)*, as result, *RE* faults were distinguished.

In the last 10 years, more improvements and combined methods have been developed to achieve a better performance. [He *et al.*, 2009] aggregate *Sparse Code Shrinkage (SCS)* to wavelet filters, obtaining signals without any kind of noise. Also, an important contribution was made by [Rafiee *et al.*, 2010] analyzing the most suitable mother wavelet for detecting bearing faults. The research examined 324 mother wavelets concluding that *db44* has the most similar shape for comparing with bearing faults, but presents the disadvantage of requiring much computational resources. [Wang *et al.*, 2011] realized another study to select the best mother wavelet, in this analysis single-side models were considered, and it was found that they presented a better performance than the double-side ones for bearing localized fault detection. The transient model was selected by applying the technique of correlation filtering. Further researches handle several aspects: the different possible faults, the ideal mother wavelet and ideal classifier. [Kankar *et al.*, 2011] presented a procedure for fault diagnosis of bearings to detect not only *IR*, *OR* and *RE* faults, but also combined defects. The potential of various artificial intelligence techniques, to predict the type of defect in bearings, were also investigated. On the other hand, [Law *et al.*, 2012] combined wavelets (*WPT*) and Hilbert Transforms to perform an analysis without predefined basic functions; instead, using adaptive functions based on *Empirical Mode Decomposition (EMD)*. In [Khanam *et al.*, 2014] the developed methodology considers the estimation of the defect size, and analyzes that wavelet *sym5* is the best suited for detecting the size of the defects, due to its form.

Some statistical methods have been included to work together with wavelet analysis. In [Liu, 2012] a method using *Exponential Moving Average (EMA)* filtering for eliminating noise features and Shannon wavelet spectrum to detect faults frequencies was presented. Another study presented by [Pandya *et al.*, 2012] includes energy *Kurtosis* and *ANN*.

A compilation of many studies working with *WT* was done by [Yan *et al.*, 2014], their research presents a review of wavelets approach to machine fault diagnosis classifying the different transforms, and recognizing different new proposals.

In the very last years, more expanded analysis has been done. [Kedadouche *et al.*, 2016a] presented a method that combines *Empirical Wavelet Transform (EWT)* and *Operational Modal*

Analysis (OMA), *Kurtosis* values are used to select the performing of the envelope spectrum. In a complementary research, [Kedadouche *et al.*, 2016b] presented a comparison between the *Ensemble Empirical Mode Decomposition (EEMD)*, the *EMD* and the *EWT*. It was shown that *EWT* reduce computational time and shows a better effectiveness in decomposing a signal as compared with *EMD* and *EEMD* methods. Additionally, a selection method of the *Intrinsic Mode Function (IMF)* in the *WT* using the index selection variable was analyzed. Another method was proposed by [Cui *et al.*, 2016], where the detection of faults was done by comparing the high frequency band power. A first step considered a wavelet denoising and then extracting features in both time and frequency domain, for the fault detection the *Grey Correlation Method* was applied obtaining good results in *IR*, *OR* and *RE* faults detection.

Finally, a good contribution for detecting early stages of bearing faults was done by [Li *et al.*, 2017] using *Q Factor Wavelet Transform (QFWT)* and *Intrinsic Characteristic-scale Decomposition (ICD)*. The used *WT* presented better and faster results compared to *EMD*.

When analyzing shaft faults, *MA*, *UB*, *BS* and *ML* must be considered. Nevertheless, as *BS* and *ML* are occasioned by excessive torque and by machine components that are loose from fabrication, *HSM* centers already deal with quality and torque control. This make *ML* and *UB* the principal defects to be considered. These faults can be detected by looking at the frequency spectrum and evaluating the *1X* and *2X* speed harmonics, respectively; for other defects it is necessary other techniques.

Wavelets have also been applied to detect this kind of faults as they help to separate the signal in different frequency ranges. Some research have been done in this area. One of the first studies was made by [Yanping *et al.*, 2006]; a method to characterize the shaft status using parameters extracted from wavelet coefficients of the *CWT* was developed. For a good detection, some additional analysis was required, the use of *Wavelet Grey Moment (WGM)* and first-order *Wavelet Grey Moment Vector (WGMV)* when the second one shows overlapped results. The studied defects were *UB* and *MA*. On the other hand, [Peng *et al.*, 2007] combines the *Wavelet Transform Modulus Maxima (WTMM)*, a variance in the *CWT* which detects local maxima in the wavelet coefficients, and the *Lipschitz Exponent*, also known as *Holder Exponent*. The method is implemented for detecting *UB* and *MA*. [Chen *et al.*, 2013] reaffirm that *WT* have better results than other methods such as *FFT*. In their research an implementation of *DWT* and *Power Spectral Density (PSD)* was developed to analyze *UB*. *DWT* allows using lower sampling frequency making the storage space reduced and the processing speed improved.

WT applied on *UB* and *MA* have not been widely studied. Some research based their analysis in *Finite Element Model (FEM)* such as [Xul *et al.*, 2017] were it was determined a linear response between *UB* and sensed vibration amplitude. Other approaches like [Fan *et al.*, 2013] used filters, *FFT* and *EMA* to establish some limit values of peak amplitudes in different *UB* produced on a test rig.

A summary of *WT* approach research is shown in Table 2.1 where the techniques as well as the studied defects are presented considering a chronological order to compare new trends. At the beginning of the table bearing defects are considered, and at the end *UB*, *MA* and *ML* studies are shown.

Table 2.1: Comparison between some fault diagnosis researches using *WT* for machining

<i>References</i>	<i>Defects</i>	<i>Case Study</i>	<i>Technique</i>	<i>Additional Analysis</i>	<i>Classifier and efficiency</i>
[Mori <i>et al.</i> , 1996]	<i>OR</i>	Test rig 660 RPM	<i>DWT</i> <i>MW</i> : Daubechies	Does not apply	Maximum Value of coefficients
[Paya <i>et al.</i> , 1997]	<i>IR</i>	Test rig 470-4230 RPM	<i>CWT</i> <i>MW</i> : Db4	Does not apply	<i>ANN</i> & Back-Propagation 96%
[Tse <i>et al.</i> , 2001]	<i>IR, OR, RE</i>	Test rig 1200 RPM	<i>CWT</i> <i>MW</i> : Gaussian	Does not apply	Visual
[Nikolaou and Antoniadis, 2002]	<i>IR, OR</i>	Simulation / Test Rig 1500 RPM	<i>WPT</i> <i>MW</i> : Db12	Energy of coefficients	Visual
[Prabhakar <i>et al.</i> , 2002]	<i>IR, OR</i>	Vibration Tester 1800 RPM	<i>DWT</i> <i>MW</i> : Db4	<i>RMS</i> and Kurtosis, <i>FFT</i>	Visual
[Tse <i>et al.</i> , 2004]	<i>IR, OR</i>	Simulation / Test Rig 1398 RPM	<i>EWA</i> <i>MW</i> : Multiple	Does not apply	Visual
[Shi <i>et al.</i> , 2004]	<i>IR, OR, RE</i>	Test Rig 1020 RPM	<i>CWT</i> <i>MW</i> : Gaussian	Shannon Entropy	Visual
[Purushotham <i>et al.</i> , 2005]	<i>IR, OR, RE</i>	Test rig 1300 RPM	<i>DWT</i> <i>MW</i> : Db2	<i>MFCC</i>	<i>HMM</i> 99%
[Yan and Gao, 2005]	<i>OR</i>	Test rig 1200 RPM	<i>WPT</i> <i>MW</i> : Harmonic	<i>FDC</i>	<i>MLP, RBF</i> 99%, 100%
[Zhang <i>et al.</i> , 2006]	<i>IR, OR, UB</i>	Test Rig 1200-8400 RPM	<i>AWT</i> <i>MW</i> : C. Morlet	<i>Envelope Spectrum</i>	Visual
[Zhu <i>et al.</i> , 2009]	<i>IR, OR, RE</i>	Simulation / Test Rig 1430 RPM	<i>CWT</i> <i>MW</i> : Morlet	<i>K-S</i>	Does not apply
[He <i>et al.</i> , 2009]	<i>IR, OR</i>	Simulation / Test Rig 1500 RPM	<i>CWT</i> <i>MW</i> : Morlet	<i>SCS</i>	Does not apply

Table 2.1: Comparison between some fault diagnosis researches using *WT* for machining (Continued)

<i>References</i>	<i>Defects</i>	<i>Case Study</i>	<i>Technique</i>	<i>Additional Analysis</i>	<i>Classifier and efficiency</i>
[Rafiee <i>et al.</i> , 2010]	<i>IR, RE, C</i>	Test Rig 1420 RPM	<i>CWT</i> <i>MW</i> : Analyzed: 324, Best: Db44	Variance, Standard Deviation, Kurtosis and 4th Central Moment	Does not apply
[Tse and Leung, 2010]	<i>IR, OR, RE</i>	Test Rig 1400 RPM	<i>CWT</i> <i>MW</i> : Morlet	Kurtosis and RMS	Does not apply
[Kankar <i>et al.</i> , 2011]	<i>IR, OR, RE</i>	Test Rig 250-2000 RPM	<i>CWT</i> <i>MW</i> : Analyzed: 7, Best: Complex Morlet	MSEC, Kurtosis, Skewness, Standard Deviation.	<i>SVM</i> 100%
[Wang <i>et al.</i> , 2011]	<i>IR, OR, RE</i>	Simulation / <i>CWRU</i> Web Data 1796 RPM/ Test Rig 1496 RPM	Transient Modeling <i>MW</i> : Laplace, <i>HW</i> , Single-Side	Correlation Filtering	Automatic Estimation
[Yan and Gao, 2011]	<i>OR</i>	Test Rig 900-1500 RPM / 2000 RPM	<i>WPT</i> <i>MW</i> : Biorthogonal 5.5.	Kurtosis, Energy and PFA	<i>ANN</i> 93%
[Liu, 2012]	<i>IR, OR, RE</i>	<i>CWRU</i> Web Data 1796 RPM/ Test Rig 1500-1920 RPM	Shannon Wavelet Spectrum.	<i>EMA</i>	Visual
[Pandya <i>et al.</i> , 2012]	<i>IR, OR, RE</i>	Test Rig 1000-6000 RPM	<i>WPT</i> <i>MW</i> : Rbio5.5	Kurtosis, Energy, MSEC	<i>ANN</i> 93%
[Chandel and Patel, 2013]	<i>IR, OR, RE</i>	<i>CWRU</i> Web Data 1796 RPM	<i>DWT</i> <i>MW</i> : db10	Variance, Variance of autocorrelation	<i>ANN</i> 100%
[Cui <i>et al.</i> , 2016]	<i>IR, OR, RE</i>	<i>CWRU</i> Web Data 1796 RPM	Adaptive Wavelet Decomposition	Time-frequency features, ITD	Grey relational analysis 100%
[Kedadouche <i>et al.</i> , 2016b]	<i>OR</i>	Test Rig 600 RPM	<i>EWT</i>	Does not apply	Visual
[Li <i>et al.</i> , 2017]	<i>OR, IR</i>	Test Rig 1800 RPM	Q-factor <i>WT</i>	Does not apply	Visual

Table 2.1: Comparison between some fault diagnosis researches using *WT* for machining (Continued)

<i>References</i>	<i>Defects</i>	<i>Case Study</i>	<i>Technique</i>	<i>Additional Analysis</i>	<i>Classifier and efficiency</i>
[Yanping <i>et al.</i> , 2006]	<i>UB, MA, ML</i>	Test rig 0-10000 RPM	<i>CWT</i> <i>MW</i> : Morlet	<i>WGM</i> and <i>WGMV</i>	Numerical
[Chen <i>et al.</i> , 2013]	<i>UB</i>	Simulation 110 RPM	<i>DWT</i> <i>MW</i> : Db10	<i>PSD</i>	Visual
[Peng <i>et al.</i> , 2007]	<i>UB,MA</i>	Test rig 3000 RPM	<i>CWT</i>	<i>WTMM</i> and the Lipschitz exponent	Numerical

2.2 Theoretical Background

2.2.1 Wavelets

WT is capable of concentrating in transitory and high frequency phenomena. It decomposes a signal into a group of wavelets being added together, which are generated from a basic wave function, usually called *Mother Wavelet (MW)*, and maps it in a time-scale representation. Wavelets are limited in time and frequency thus their energy is finite. They are local in both frequency and time domain via dilations and translations respectively; hence, they have better resolution than other transformations. Principal side benefits are noise reduction, compressing data, filtering among others. The *WT* of a function $s(t)$ is defined in eqn. 2.1

$$S(a, b) = \int_{-\infty}^{\infty} s(t) \frac{1}{\sqrt{a}} \psi_{(a,b)}^* \left(\frac{t-b}{a} \right) dt \quad (2.1)$$

where $\psi_{(a,b)}^*$ is the complex conjugated of the *MW*, a the scale or dilatation (frequency range) of the *MW* and b the translation in time.

Different types of *WT* have been developed for analyzing signals, starting with *CWT* evolving to *Second Generation Wavelet Transform (SGWT)*. The evolution of *WT* as well as their principal characteristics are shown in Fig. 2.1, including some new research trends such as multi-wavelets.

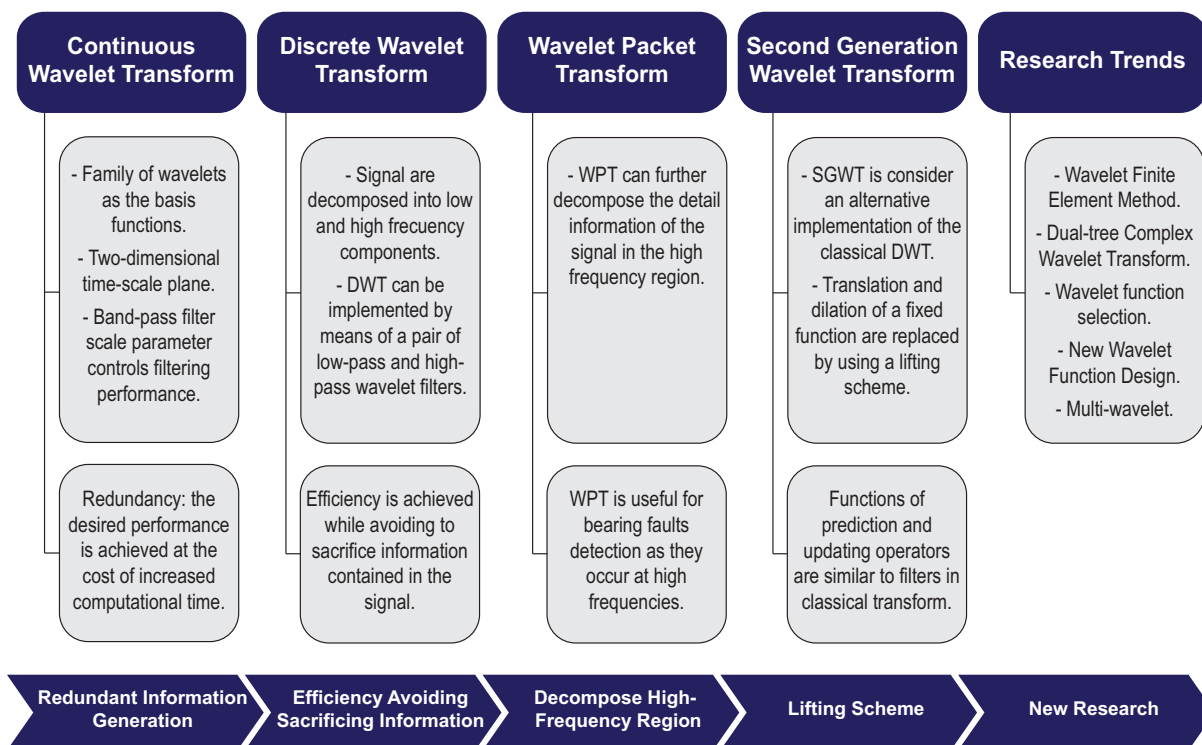


Figure 2.1: Wavelet transforms evolution

When analyzing a signal, in addition to considering the type of transformation, it is necessary to determine the *MW* to be used. Many studies have been carried out to compare and evaluate which *MW* is the best. Some of the most used wavelets for vibration signals analysis are shown in Fig. 2.2

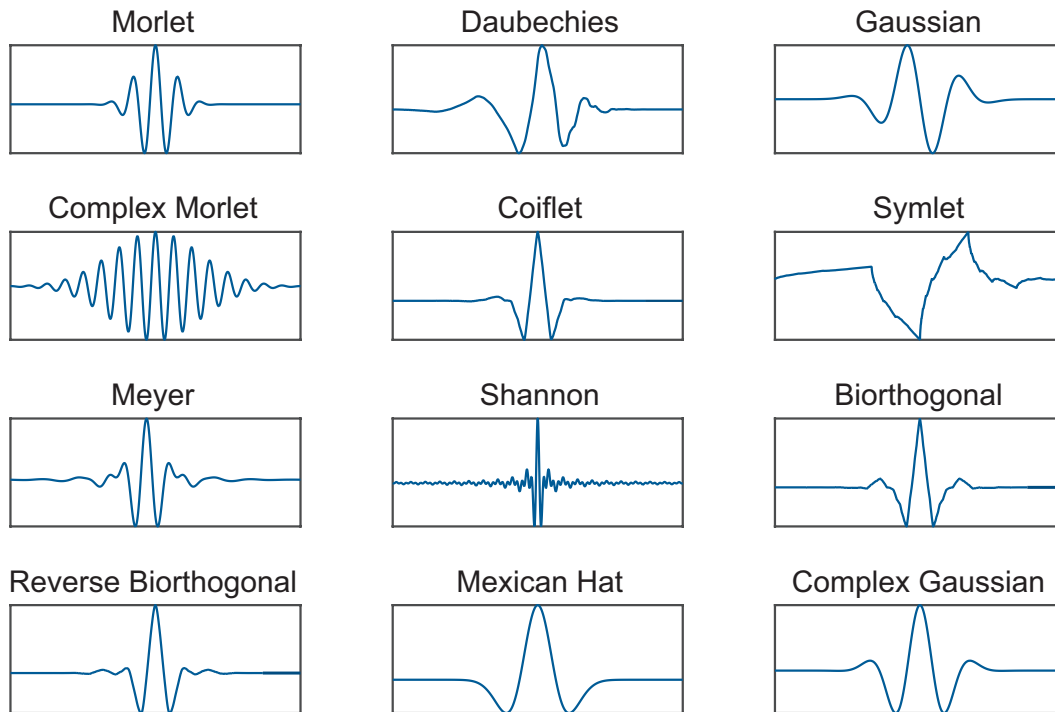


Figure 2.2: Typical mother wavelets

Nevertheless, for bearing faults the best behavior is obtained by the wavelet which is the most similar to the defect. It must be considered that the computational effort becomes higher when the complexity of the mother wavelet function grows up.

2.2.2 Bearing Faults

Bearings are one of the foremost cause of failures in a machine tool spindle, they are the most critical and vulnerable components in the mechanical transmission. Most typical faults in bearings are produced by local defects mainly cracks, pits and spalls in the *IR*, the *OR* or the *RE*, [Zhang and Gao, 2004].

Defects produce successive periodic impacts, which are characterized by the following frequencies:

- *Ball Pass Frequency Outer-race (BPFO)*
- *Ball Pass Frequency Inner-race (BPFI)*

- *Ball Spin Frequency (BSF)*
- *Fundamental Train Frequency (FTF)*

Fault frequencies can be obtained by:

$$BPFO = \frac{nf_r}{2} \left(1 - \frac{d}{D} \cos \alpha \right) \quad (2.2)$$

$$BPFI = \frac{nf_r}{2} \left(1 + \frac{d}{D} \cos \alpha \right) \quad (2.3)$$

$$BSF = \frac{Df_r}{2d} \left(1 - \left[\frac{d}{D} \cos \alpha \right]^2 \right) \quad (2.4)$$

$$FTF = \frac{f_r}{2} \left(1 - \frac{d}{D} \cos \alpha \right) \quad (2.5)$$

where, n is the number of *RE*, f_r the shaft rotating speed and α the angle of the load from the radial plane. Vibration signals as well as fault frequencies (*BPFO*, *BPFI*, *BSF*), D and d are shown in Fig. 2.3.

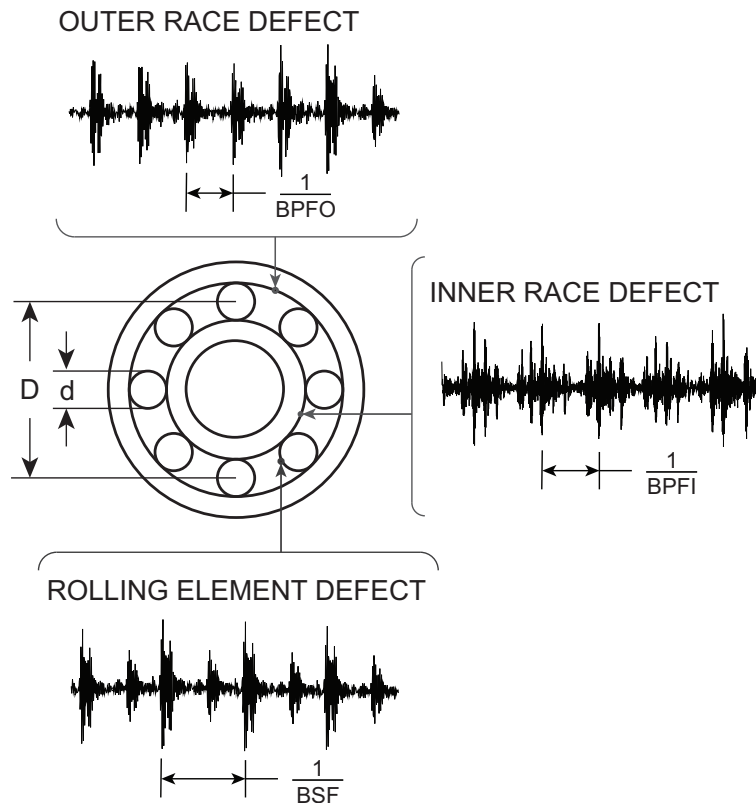


Figure 2.3: Signals from local faults in bearings

As it can be seen in Fig. 2.3, for the *RE* defect signal there is one extra peak between *BSF*. This is because the *BSF* frequency is calculated for each contact of the ball with the *OR*; however,

there is an additional periodic impact when the fault contacts the *IR*. Therefore, when analyzing the frequency spectrum, the harmonics of the *BSF/2* must be considered.

According to [Scheffer and Girdhar, 2004], there are four stages of bearing damage (*Stage 1*, *Stage 2*, *Stage 3* and *Stage 4*). Each stage is characterized by a different frequency spectrum as shown in Fig. 2.4. To analyze the severity of the fault the spectrum is divided in four zones:

- *Zone A*: machine RPM and their harmonics (0-85 Hz)
- *Zone B*: bearing fault frequencies (85-500 Hz)
- *Zone C*: bearing natural frequencies (500-2,000 Hz)
- *Zone D*: *High-Frequency-Detection (HFD)* (above 2,000 Hz)

First stage of bearing wear presents peaks at the ultrasonic frequency ranges, *Zone D*, besides the machine *RPM*, but, the spectrum is clear in *Zones A* and *B*, Fig. 2.4 (a). The next stage, Fig. 2.4 (b), generates the bearing component natural frequencies, *Zone C*, depending on the severity, sidebands frequencies might appear and the peak of *HFD* increases its amplitude; *Zone B* remains clear at this point. In the following stage fault frequencies are visible in the spectrum, Fig. 2.4 (c), a number of sidebands may also appear; amplitude of peaks at *Zones C* and *D* might increases. By the end of this stage the remaining bearing life is considered to be about 1 hour or 1% of its average life.

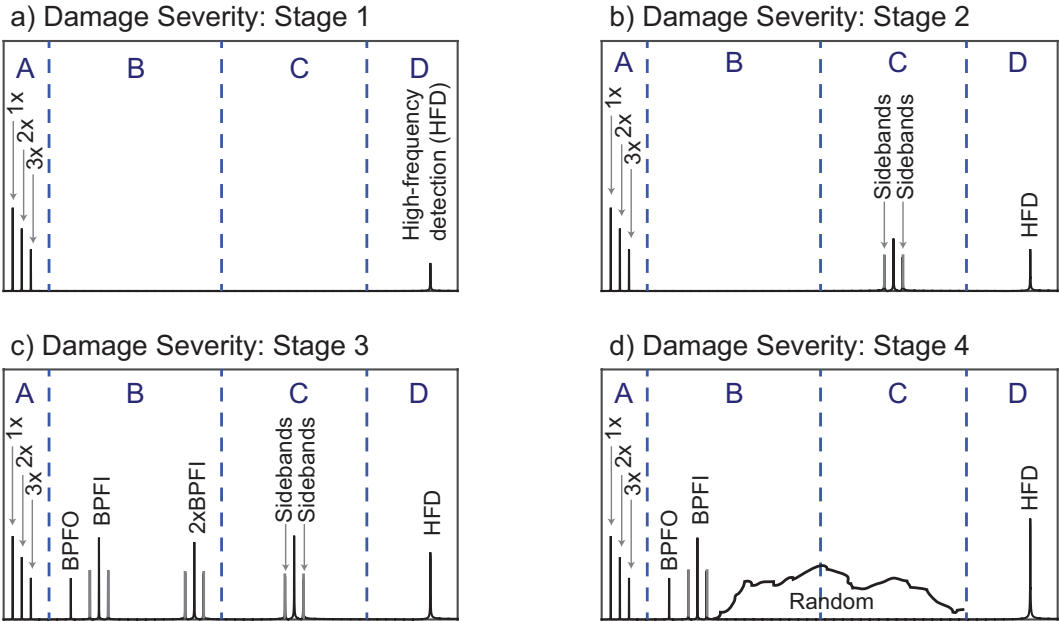


Figure 2.4: Stages of bearing damage

2.2.3 Unbalance, Misalignment and Mechanical Looseness

- **Unbalance**

UB occurs when the shafts mass centerline does not coincide with its geometric centerline. This malfunction is caused by improper manufacturing, blade erosion, non appropriate counter balancing procedure of shaft fittings among others. As a result of this, excessive forces that affect the equipment are caused, and due to it, bearings carry a higher dynamic load, which causes failure from early fatigue.

Vibration signal of an *UB* spindle is characterized by a single frequency occurring at once per revolution (1X) and it does not contain harmonics unless the failure is severe. It must be consider that amplitude of *UB* vibration signal increases with speed.

- **Misalignment**

MA is also an important fault that must be detected for preventing bigger damages. It is created when shafts, couplings and bearings are not properly aligned along their centerlines. This is mainly caused by thermal complications, expansion growth, bad alignment of components during coupling, imparted forces from piping and support members or uneven foundation, shifting in foundation or settling. *MA* leads to bearing failures due to early fatigue, as they carry a higher load than its design specification.

Detecting *MA* with vibration signals is very important, it helps avoiding damage in bearings and other elements of the machine. Commonly some overall vibration values are considered to distinguish this failure; but, a more practical way of analysis is to consider the second harmonic of the spindle speed (2X) and compare it with the first one (1X). If a higher than normal 2X amplitude is detected, *MA* is occurring, this amplitude can vary from 30% of the 1X amplitude to 100 to 200% of it.

- **Mechanical Looseness**

ML is produced when a machine component came loose from its mounting, when the mounting is cracked or broken or when the bearing wore down causing excessive clearance in the bearing. Looseness may provoke that a part become detached and cause secondary damage.

ML is identified in the frequency spectrum by abnormally high rotation speed amplitude peaks, followed by multiples or 1/2 multiples. These harmonics may be random and unorganized. If there are a series of three or more synchronous or 1/2 synchronous multiples of running speed in the range of 2X to 10X, and their magnitudes are greater than 20% of the 1X, there may be *ML*.

Chapter 3

Experimental System

3.1 Introduction

This chapter presents the description of the test rigs, the data obtained from them and the Design of Experiments (*DoE*) performed in an industrial machining center. Two different data sets were considered for bearing fault diagnosis. The *Data 1* set was obtained from *Case Western Reserve University (CWRU)* where single faults were introduced to bearings and the acquisition was made by accelerometers attached directly in the bearings. The *Data 2* set was obtained from a test rig developed by NSF I/UCR Center for *Intelligent Maintenance Systems (IMS)*. In this case bearings were in new condition and were tested until they fail. *MA* and *ML* were analyzed in both data sets.

For *UB*, the developed *DoE* in a *GROB 550 HSM* center is described, where different signals were recorded for 3 different unbalanced holder tools at different speeds. This corresponds to *Data 3* set.

3.2 Experimental Data Sets

3.2.1 Data 1 set: CWRU - Bearing Data Center

CWRU provides a group of signals for bearing faults analysis. They had developed a test rig, Fig. 3.1. The equipment consists of a 2 Hp motor, a torque transducer/encoder, a dynamometer, and control electronics, [CWRU, 1999].

Data was recorded for motor loads of 0 to 3 Hp with motor speeds of 1,720 to 1,797 RPM. For fault analysis, single points were introduced to the bearings using an electro-discharge machining. Defect diameters were of 7, 14, 21, 28, and 40 mils (1 mil = 0.001 inches). The test rig has two bearings: drive end and fan end. Data was collected at 12,000 samples/second and at 48,000 samples/second for drive end and at 12,000 samples/second for fan end. Fault characteristic frequencies for the bearings are shown in Table 3.1.

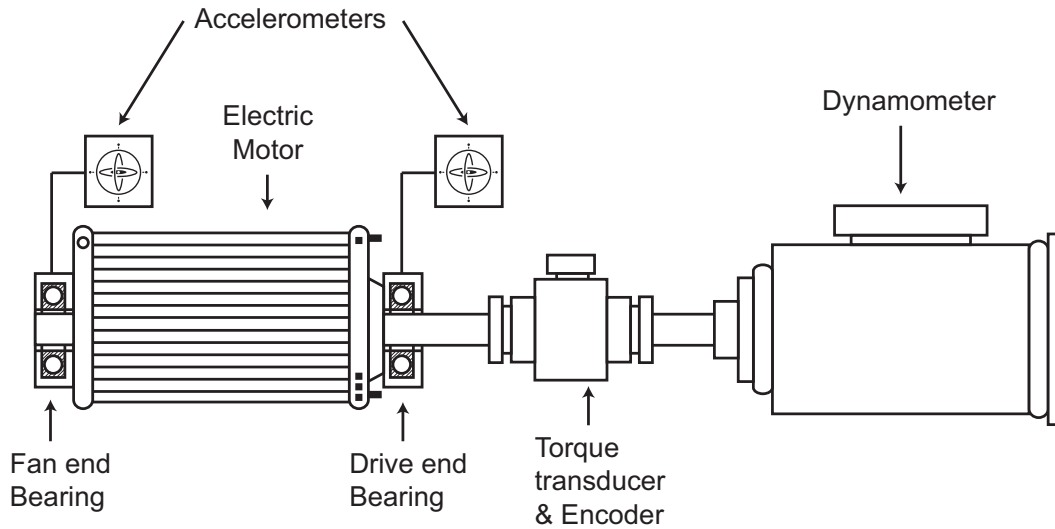


Figure 3.1: CWRU Test Rig Schema

Table 3.1: CWRU Bearing Defect Frequencies (multiple of running speed in Hz)

<i>Bearing</i>	<i>Inner Ring</i>	<i>Outer Ring</i>	<i>Cage Train</i>	<i>Rolling Element</i>
Drive end	5.4152	3.5848	0.39828	4.7135
Fan end	4.9469	3.0530	0.3817	3.9874

3.2.2 Data 2 set: IMS - Bearing Data

The NSF I/UCR Center for *IMS* with support from Rexnord Corporation in Milwaukee, USA, developed a test rig for bearing fault diagnosis considering the full life of these elements. All failures occurred after exceeding designed life time of the bearing, which is more than 100 million revolutions, [IMS, 2004].

As shown in Fig. 3.2, four bearings were installed on a shaft. The rotation speed was controlled at 2,000 RPM, and a radial load of 6,000 lbs was applied into the shaft and bearings.

Three data sets were generated, each data set describes a test-to-failure experiment. It consists of 1-second vibration signal snapshots recorded at specific intervals. The sampling rate was 20 kHz.

All bearings were the same; they were tested in new conditions. The fault characteristic frequencies were calculated based on the bearing geometry, Table 3.2. The following faults were recorded:

- Set 1: *IR* defect in bearing 3 and *RE* defect in bearing 4.
- Set 2: *OR* defect in bearing 1.
- Set 3: *OR* defect in bearing 3.

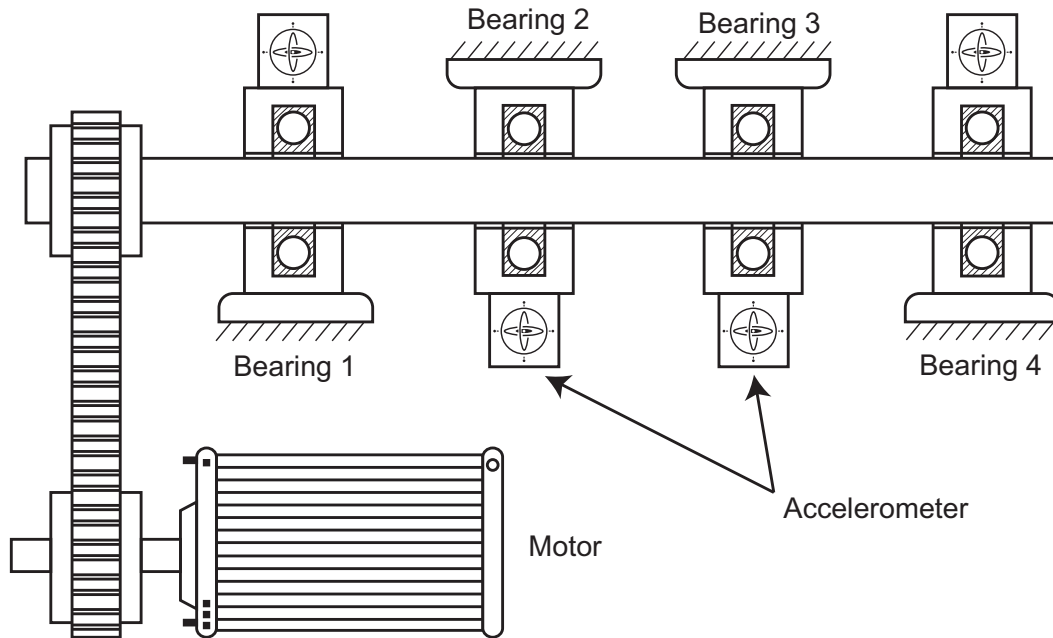


Figure 3.2: IMS Test Rig Schema

Table 3.2: IMS Bearing Defect Frequencies (multiple of running speed in Hz)

<i>Inner Ring</i>	<i>Outer Ring</i>	<i>Cage Train</i>	<i>Rolling Element</i>
8.907	7.092	0.444	4.197

3.2.3 Data 3 set: Industrial Plant

In addition, vibration signals obtained from *HSM* spindles (*GROB 550* machining center) from an industrial plant were considered.

The *GROB 550* is a compact, rigid, and highly flexible horizontal machining center, which enables single setup machining of 5 sides as well as the most complex 5-axis simultaneous 3-D surfaces. The maximum spindle speeds are available from 12,000 up to 28,000 RPM. Workpieces up to 836 lbs can be machined with ultra-fast rapid rates up to 3,540 IPM in the Z-axis.

Vibration signals of this equipment were obtained from two different sensors *VSA005* placed inside the housing of the spindle and an *ICP 621B41* sensor placed near the spindle. *VSA* signals is detached to the *VSE100* controller and to a Kristler 5134B amplifier. Signals were recorded in Labview and Octavis software. Figure 3.3 represents the data acquisition system for *GROB 550* machining center.

The spindle of the analyzed machining center can work up to 18,000 RPM. Velocity is recorded by a sensor connected to the *VSE* controller, which it was also connected to the *DAQ 9234*. Table 3.3 presents the characteristics of the equipment and the recording parameters of the spindle in the

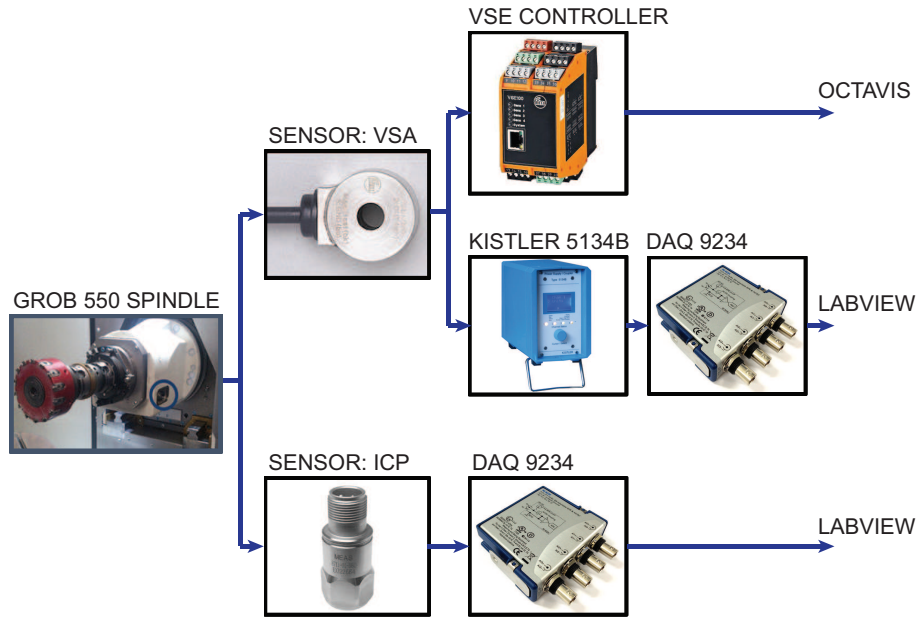


Figure 3.3: Signal acquisition schema of GROB 550

GROB 550 HSM center.

Table 3.3: Acquisition equipment characteristics of GROB 550

<i>Equipment</i>	<i>Model</i>	<i>Sensing Parameters</i>
Acquisition module DAQ	9234 / 4 Channels	Sample rate: 51.2 kS/s/ch / Output: ± 5 V
Acquisition module VSE	100 / 4 Channels	Sample rate: ≤ 100 kS/s / Output: 0-20 mA
Accelerometer VSA	005	fs: 0.10 kHz / Sensitivity: $0.2 [\text{mg}/\sqrt{\text{Hz}}]$ / Range: ± 25 [g]
Accelerometer ICP	621B41	fs: 144-600 kHz / Sensitivity: $10.2 [\text{mV/g}]$ / Range: ± 50 [g]
Amplifier Kristler	5134B / 4 Channels	Gain programmable 0.5-150 / Output: ± 5 V
Speed Sensor	Unknown	Output: 0-5 V (0-18000 RPM)

3.3 Design of Experiments

3.3.1 Unbalance Holder

The tests were performed using different levels of *UB* holder tools. The vibration signals were recorded at different spindle speeds. Two test were performed for each case of study to validate

results and various *GROB 550* machines were analyzed for comparing behaviors.

Different levels of *UB* were introduced in tool holders; for this research three test were analyzed: one with *UB* near 0 was considered as baseline and the other two with high levels of *UB* as a first approach to detect this type of fault.:

- Holder tool with *UB* of 1.1 baseline
- Holder tool with *UB* of 10.5 bad condition level 1
- Holder tool with *UB* of 26.1 bad condition level 2

For machining purpose, the allowed *UB* limit is 2.5. This value is considered adequate not to adversely affect the quality of machining in *HSM*.

The signals were recorded during 10 seconds with a sampling rate of 51,200 samples/s. Every two seconds the spindle speed was incremented considering the following velocities: 8,000, 10,000, 12,000, 14,000 and 18,000 RPM, which are commonly used in industry. Figure 3.4 shows the three signals that are acquired simultaneously, VSA sensor vibration, ICP sensor vibration and speed in RPM. It must be considered the speed input signal to avoid analyzing the initial slope, where transients can distort the analysis.

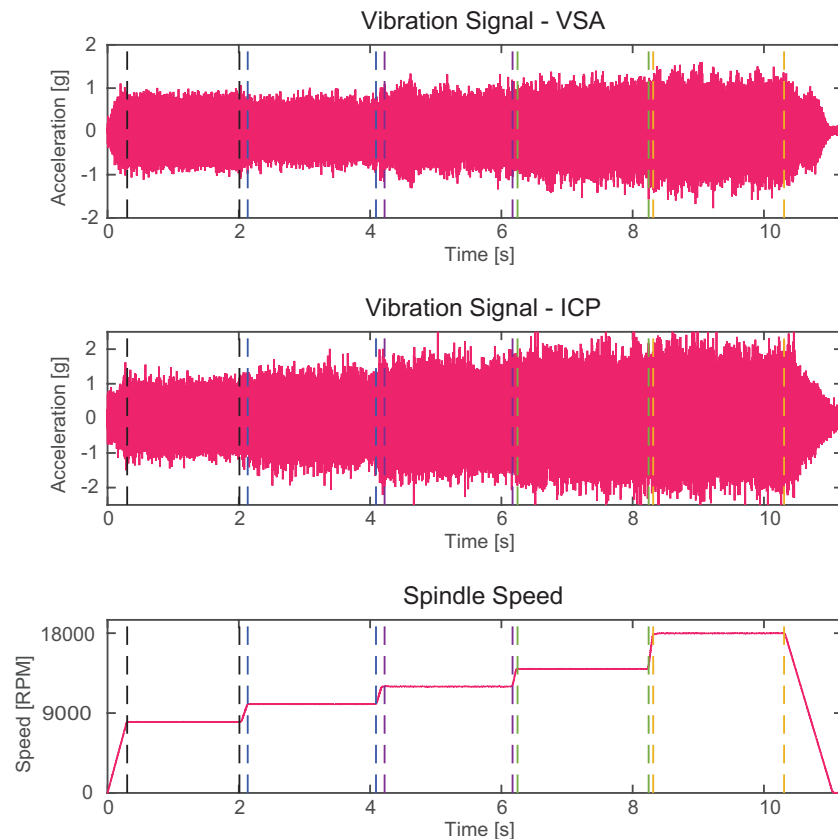


Figure 3.4: Vibration signal for *UB* analysis

Chapter 4

Proposal

4.1 Introduction

A methodology for detecting spindle faults using vibration signals via *WT* was developed. The analysis is presented in two sections, one for bearing faults and other for *UB*, *MA* and *ML*.

For bearing faults detection, a comparison between *CWT*, *DWT* and *WPT* was developed to select the best mathematical tool for diagnosis. Then, an analysis of different *MW* was performed for choosing the most suitable waveform for each fault. Once the transform and the *MW* have been selected, the proposed methodology was applied for different faults. Finally, different results are shown to validate the proposed methodology.

For *UB*, *MA* and *ML* the filtering property of *WT* was exploited, with the same decomposition as bearing faults signal was reconstructed removing high frequencies as a low pass filter. Harmonics and sub-harmonics of the shaft speed were evaluated.

4.2 Bearing Faults

Many techniques have been applied for bearing fault detection. Different *WT* as well as different *MW* have been used. For selecting the most convenient *WT*, a comparison between *CWT*, *DWT* and *WPT* was developed, results are shown in *Appendix B*. *WPT* has been selected as the best transform for these purposes.

Once the *WT* is selected, the remaining parameter that must be evaluated is the best *MW* for each bearing fault. *Matlab Wavelet Toolbox* has 125 different *MW* for *WPT*. To choose the most suitable *MW* computational effort as well as others quantitative indicators, summarized by [Ngui *et al.*, 2013], were taken into account. Results are shown in *Appendix B*. The analysis showed that *dmey* performs better for *OR* faults, while for *IR* and *RE* the best were *db41* and *db45*, respectively.

Once the principal parameters of *WT* have been selected, the presented methodology, Fig. 4.1,

is proposed for detecting spindle faults. The proposal consists of two branches, one for bearing faults and the other for *UB*, *MA*, and *ML*.

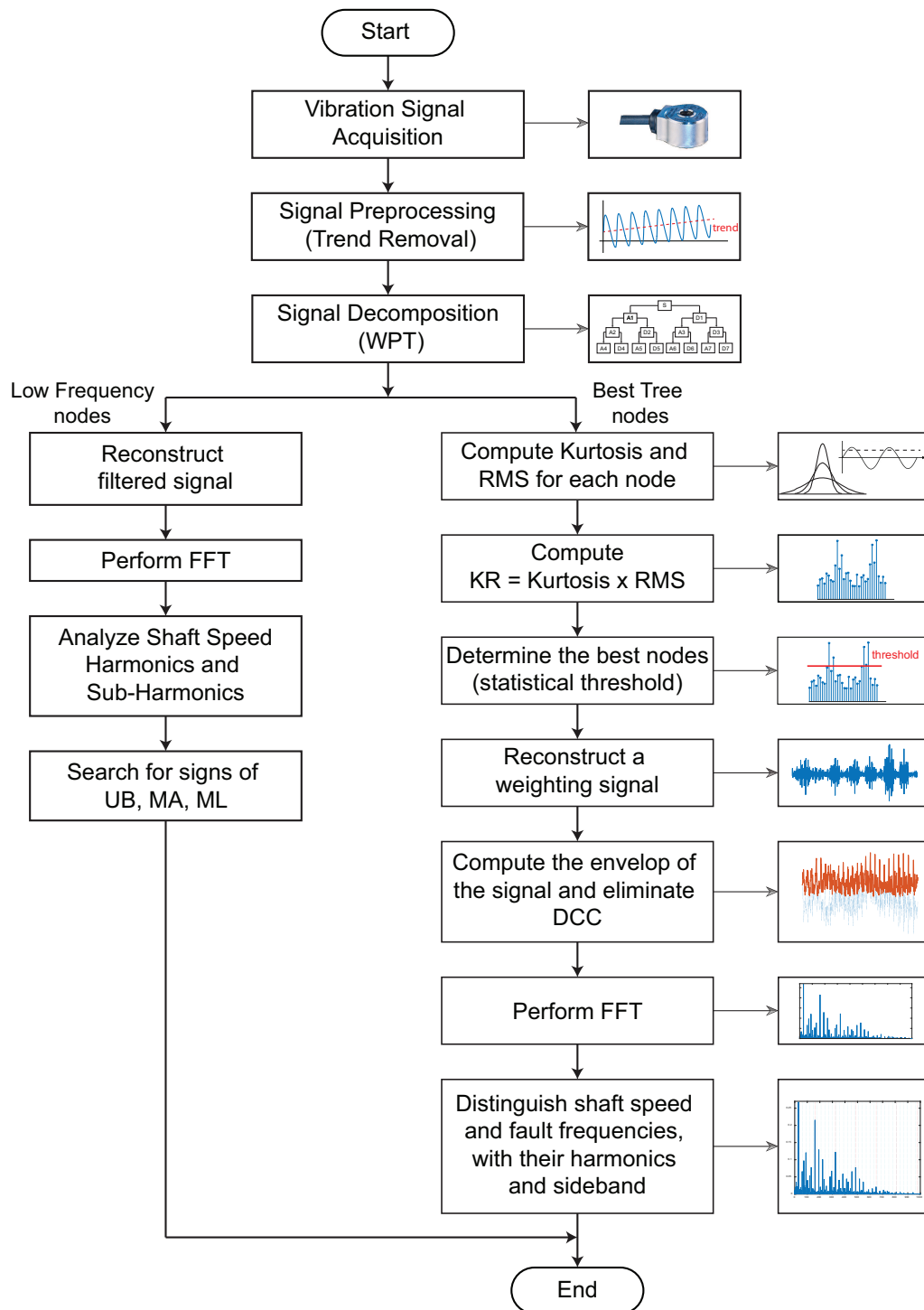


Figure 4.1: Proposed methodology for spindle faults diagnosis

Before any data manipulation, the acquired vibration signal is preprocessed by a trend removal

calculated with the linear model presented in eqn. (4.1), where p_1 and p_2 are computed by *Linear Least Squares*, eqns. (4.2) and (4.3). This eliminates the *Direct Current Component (DCC)*, which not only produces an interference; but, it also does not carry any useful information. This leads to uplift integrally the signal amplitude in frequency domain [Lei, 2016].

$$y_{trend} = p_1 \times x_{trend} + p_2 \quad (4.1)$$

$$p_1 = \frac{\bar{y} (\sum_{i=1}^n x_i^2) - \bar{x} \sum_{i=1}^n x_i y_i}{\sum_{i=1}^n x_i^2 - n\bar{x}^2} \quad (4.2)$$

$$p_2 = \frac{n \sum_{i=1}^n x_i y_i - \sum_{i=1}^n x_i \sum_{i=1}^n y_i}{n \sum_{i=1}^n x_i^2 - (\sum_{i=1}^n x_i)^2} \quad (4.3)$$

After performing the *WPT* the best tree is selected. The entropy of every packet of each level is evaluated and the nodes with the best entropy (minimum entropy $E(s)$) are selected, considering also that the whole frequency range must be covered without overlapping. By covering the analysis of the entire spectrum, this methodology avoids losing the information contained in the various frequency ranges; in contrast to other proposals where the analysis is focused only where most, but not all of the vibration energy is concentrated. The discarded information might actually be useful in prognosis [Ocak *et al.*, 2007]. *Matlab Wavelet Toolbox* allows calculating directly this tree based on eqn. (4.4), where s_i are the wavelet coefficients. The criterion to select which node must be divided and which one must not is: *A node N is split into two nodes if and only if the sum of entropy of its subnodes N_1 and N_2 is lower than the entropy of N*. An example of this criterion is shown in Fig. 4.2, where the entropy for each node is shown and the ones that satisfy the mentioned criterion are highlighted.

Kurtosis and *RMS* values of terminal nodes (last node of each branch) are calculated, *Kurtosis* indicates the impulsiveness of a signal, eqn. (4.5); while, *RMS* provides a measurement of intensity, eqn. (4.6). By multiplying these values, it can be revealed the frequency zone of the impacts that have been overwhelmed by other vibration signals, [Tse and Leung, 2010]. Nodes that provide more information about the fault are selected, considering all the values of $KR = Kurtosis \times RMS$ over the threshold. This threshold is calculated as the average value KR , eqn. (4.7). The coefficients of the best tree nodes are reconstructed (inverse *WPT*) and multiplied for a weighting value before being added to obtain the complete desired signal. These weighting values are considered 1 for all packets with KR that are over the threshold and the value of the percentage with respect to the maximum for the ones that are below, eqn. (4.8).

$$Entropy(s) = - \sum_{i=1}^n s_i^2 \times \log(s_i^2) \quad (4.4)$$

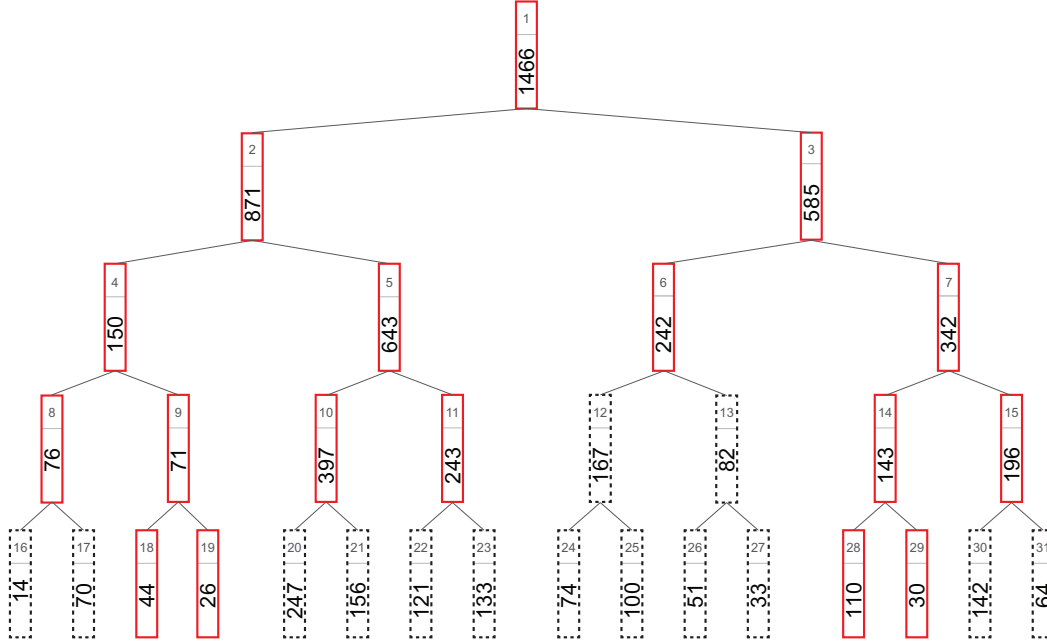


Figure 4.2: Entropy of each node for best tree selection

$$Kurtosis = \frac{\frac{1}{n} \sum_{i=1}^n (x_i - \bar{x})^4}{\left(\frac{1}{n} \sum_{i=1}^n (x_i - \bar{x})^2\right)^2} \quad (4.5)$$

$$RMS = \sqrt{\frac{1}{n} \sum_{i=1}^n |x_i|^2} \quad (4.6)$$

$$Threshold = \frac{1}{n} \sum_{i=1}^n (KR)_i \quad (4.7)$$

$$Weighting\ Values = \begin{cases} 1 & \text{if } KR \geq Threshold \\ \frac{KR}{\max(KR)} & \text{if } KR < Threshold \end{cases} \quad (4.8)$$

Once the signal is processed, bearing faults detection is performed in frequency domain. The envelope of the signal is computed and the *DCC* is eliminated by removing the trend. The envelope generates an smooth wave outlining the extremes of the original signal. This shaping is obtained by computing the absolute value of the analytic signal, eqn. (4.9). This analytic signal is acquired by adding the 90° phase shifted value to it, eqn. (4.10).

$$Envelope = |AnalyticSignal| \quad (4.9)$$

$$AnalyticSignal = signal + i \times signal_{90} \quad (4.10)$$

Envelope analysis is a well known method for detecting rotational defect signals, as it is suitable for repetitive dynamic signal impulses. The key of envelope analysis is to detect the fault by filtering off the low amplitude defect signal with low energy excluding the high amplitude rotational vibration signals. The main advantages of this method are: intensifying useful signal for fault detection, reducing non-periodical signal and its noise and eliminating the low-frequencies and multiples caused frequency of revolutions.

Impactive faults excite the high frequency bearing and structural resonances of the bearing. But, the diagnostic could not be done in the frequency spectrum resulting from the impacts, as this is usually a sum of the resonance frequencies excited. The useful information is contained in the repetition frequency of the impact series. Thus, the envelope analysis technique reduces the high frequency problem to a low frequency problem by isolating the impact-repetition rates.

Finally, the *FFT* is obtained to observe the frequency spectrum and search for fault frequencies. It must be considered that besides the fundamental fault frequencies and their harmonics, some sideband may appear in the spectrum depending the type and magnitude of the fault. Table 4.1 presents the sidebands that must be taken into account when performing the diagnosis. Since the values of fault frequencies are calculated based on equations that do not consider slips a percentage of 1-2% of the calculated frequency is usually considered for diagnosis, [Smith and Randall, 2015].

Table 4.1: Sidebands considered for bearing fault diagnosis

<i>Bearing Fault</i>	<i>Expected Sidebands</i>
<i>IR</i>	Spaced shaft speed and its harmonics
<i>OR</i>	No sidebands
<i>RE</i>	Spaced <i>FTF</i> and its harmonics

4.3 Unbalance, Misalignment and Mechanical Looseness

As *UB*, *MA*, and *ML* require analyzing shaft speed, its harmonics and sub-harmonics low frequencies must be considered. After performing signal decomposition with the *WPT* low frequency nodes (less than 1 kHz) are analyzed. This node selection performs as a low-pass filter, which allows to highlight rotation frequency which trends to be masked by high frequency magnitudes.

The *FFT* is obtained to observe the frequency spectrum. The magnitude of the rotation speed is evaluated for *UB*, a comparison between the fundamental frequency and its first harmonic is performed for detecting *MA*. Finally, harmonics and half harmonics are sought to diagnose *ML*.

Chapter 5

Results

5.1 Introduction

To validate the proposed methodology three signals with fault were taken into account from *CWRU* data center. Based on [Smith and Randall, 2015] categorization a clearly diagnosable signal (Y), a partially diagnosable signal (P) and a not diagnosable (N) signal were considered.

As shown in Fig. 5.1, data clearly diagnosable, Fig. 5.1 (a), (d) and (g), present high amplitudes and peaks that stand out from the rest of the signal. For category partially diagnosable, Fig. 5.1 (b), (e) and (h), amplitudes are notably diminished and peaks are overshadowed by noise and other vibration signals. In the last category, not diagnosable, *IR* signal presents high amplitudes but peaks are completely overwhelmed by noise, Fig. 5.1 (c). On the other hand, *OR* and *RE* present low amplitudes and non peak could be distinguished, Fig. 5.1 (f) and (i), respectively.

For early stage fault analysis, *IMS* data, the initial stage of damage was established by calculating the *Kurtosis* of each sample of the experiment and detecting where the value abruptly changes, [Li *et al.*, 2017]. Figure 5.2 (a), (b) and (c) present the number of sample where the failures are starting considering faults in *IR*, *OR* and *RE* respectively. To compare stages of damage, the selected sample (early stage), a final sample (critical stage) and a sample between this range (medium stage) are considered for each fault, as shown in Fig. 5.3 .

5.2 Results

5.2.1 Raw signal and preprocessing

As first step of the proposed methodology a signal preprocessing is developed, eliminating interference by a trend removal. As shown in Fig. 5.4 (a), the signal trend is fitted to a *linear polynomial curve* and this value is subtracted from the original signal giving as result the signal in Fig. 5.4 (b). This guarantee the removal of the interference near zero frequency in the signal spectrum Fig.

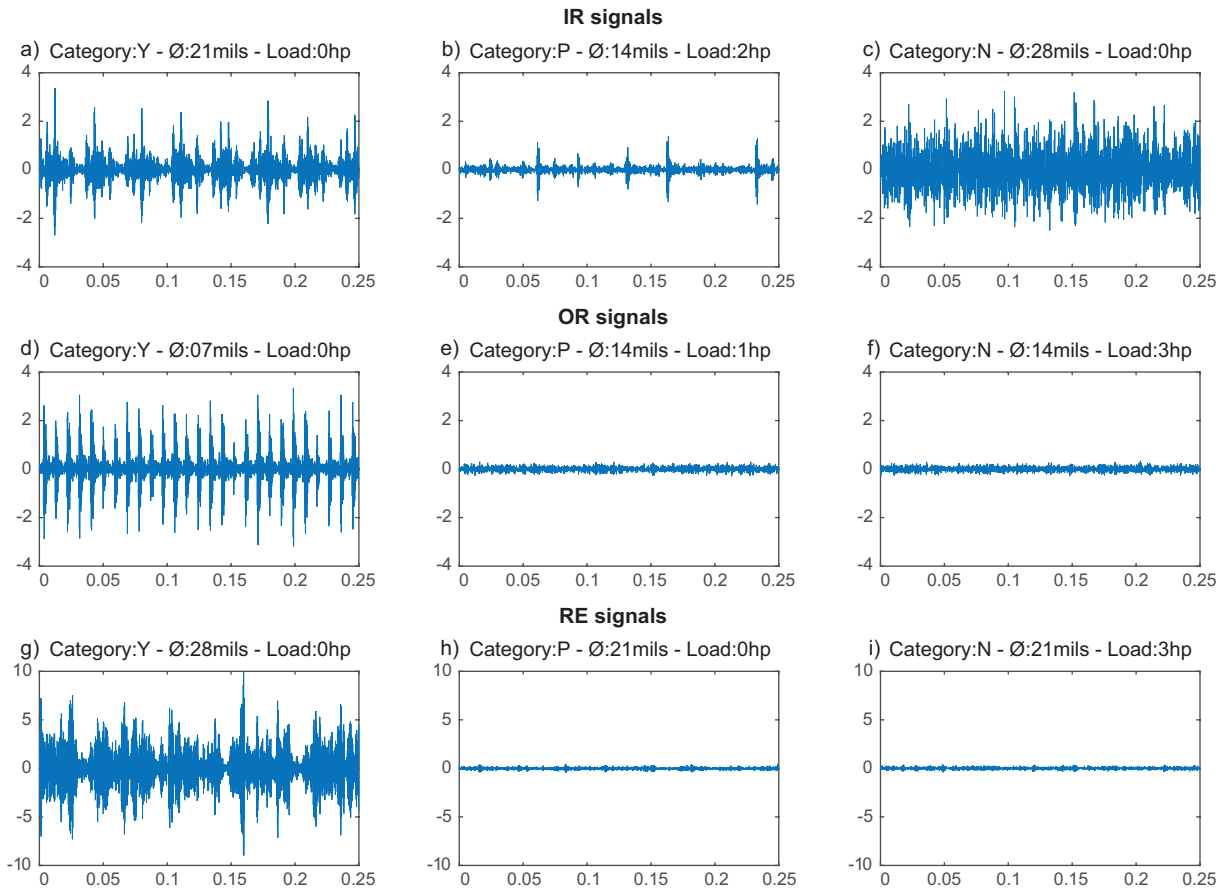


Figure 5.1: Signals considered to validate the proposed methodology (*CWRU* data)

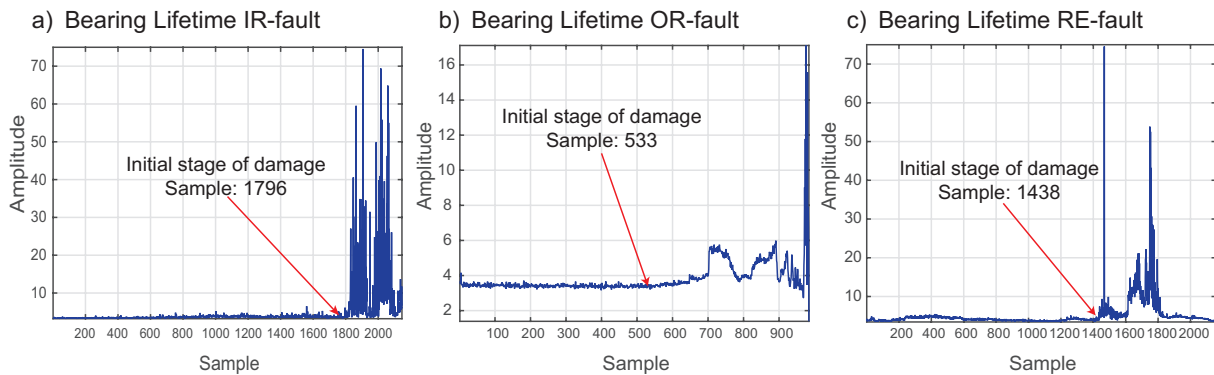


Figure 5.2: Kurtosis calculation for detecting the initial stage of damage (*IMS* data)

5.4 (c), which overshadows the characteristic frequency. The signal without the trend presents a clearer spectrum, Fig. 5.4 (d), as the interference disappears. The characteristic frequency is easily detected as it stands out for being the maximum value of the spectrum; while, in the previous case the maximum value is located near 0 Hz.

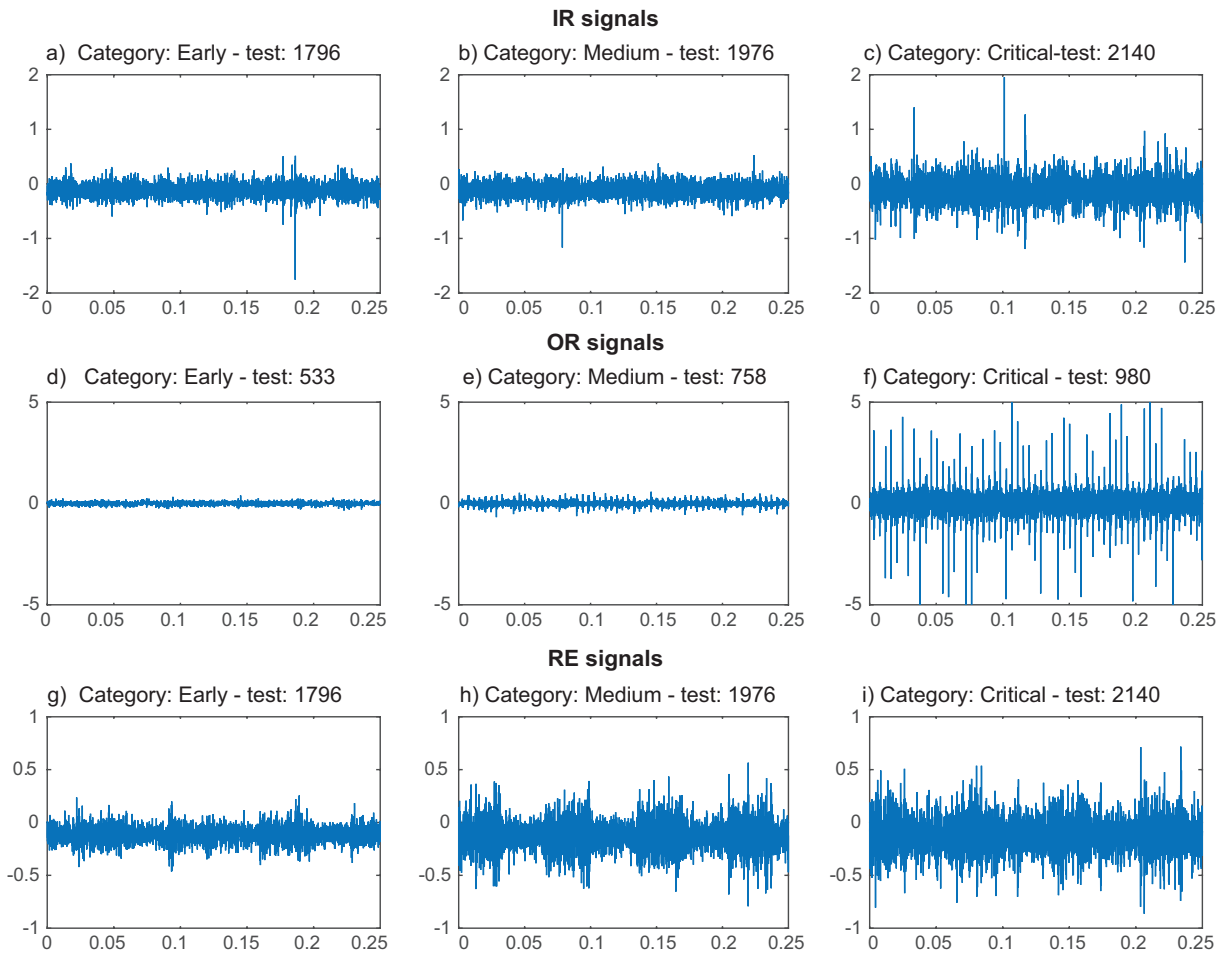


Figure 5.3: Signals considered to validate the proposed methodology (*IMS* data)

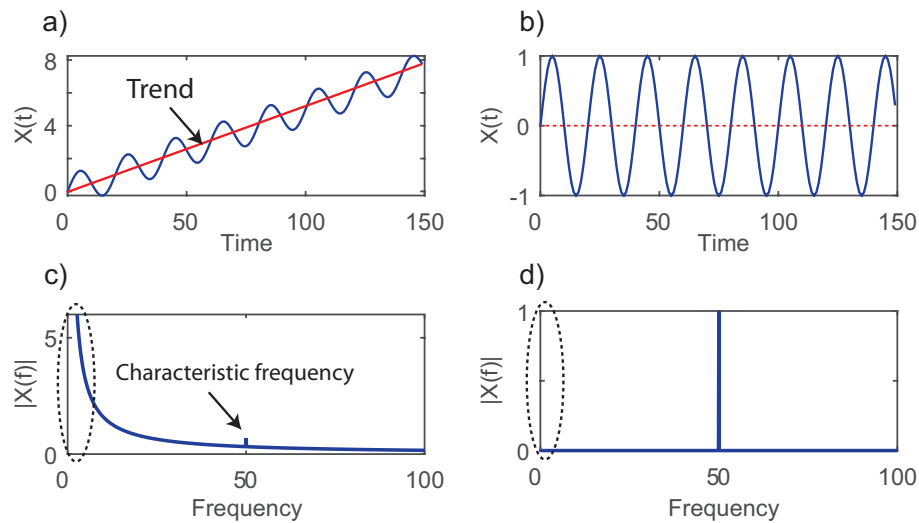


Figure 5.4: Signal Preprocessing: Trend Removal

5.2.2 Signal decomposition

The signal is decomposed by *WPT*. For selecting an adequate level of decomposition, parameters such as sampling frequency (f_s) and fault frequencies must be analyzed. Equation (5.1) presented by [Gao and Yan, 2010] allows to calculate the level of decomposition depending of the frequency component that wants to be considered, in this case the fault frequencies of the bearing elements: f_{fault} ; rearranging variables eqn. (5.2) is presented. Table 5.1 shows the parameters of each selected signal and the computed limits for selecting the appropriate level of decomposition. The fault frequencies were calculated by multiplying the spindle speed (converted to Hz) by the corresponding bearing fault frequency factor. Both parameters are reported in the information of the respective data sets.

$$\frac{f_s}{2^{Level+1}} \leq f_{fault} \leq \frac{f_s}{2^{Level}} \quad (5.1)$$

$$\log_2 \left(\frac{f_s}{2 * f_{fault}} \right) \leq Level \leq \log_2 \left(\frac{f_s}{f_{fault}} \right) \quad (5.2)$$

Table 5.1: Level of decomposition calculated for each signal

<i>Data Case</i>	f_s [kHz]	<i>Fault Type</i>	<i>Speed</i> [RPM]	<i>Freq. Factor</i>	<i>Fault Freq.</i> [Hz]	<i>Level (L) Limits</i>
<i>CWRU</i>	12	<i>IR (Y)</i>	1,797		162.19	$5.21 \leq L \leq 6.21$
		<i>IR (P)</i>	1,752	5.4152	158.12	$5.25 \leq L \leq 6.25$
		<i>IR (N)</i>	1,797		162.19	$5.21 \leq L \leq 6.21$
		<i>OR (Y)</i>	1,796		107.31	$5.81 \leq L \leq 6.81$
		<i>OR (P)</i>	1,772	3.5848	105.87	$5.82 \leq L \leq 6.82$
		<i>OR (N)</i>	1,723		102.94	$5.87 \leq L \leq 6.87$
		<i>RE (Y)</i>	1,797		141.17	$5.41 \leq L \leq 6.41$
		<i>RE (P)</i>	1,796	4.7135	141.09	$5.41 \leq L \leq 6.41$
		<i>RE (N)</i>	1,729		135.83	$5.47 \leq L \leq 6.47$
<i>IMS</i>	20	<i>IR</i>		8.907	296.90	$5.07 \leq L \leq 6.07$
		<i>OR</i>	2,000	7.092	236.40	$5.40 \leq L \leq 6.40$
		<i>RE</i>		4.197	139.90	$6.16 \leq L \leq 7.16$

The computed level limits presented in the last column of Table 5.1 shows that, the only level that is within the established range (considering that L must be a positive integer) is level 6, for all

the analyzed signals except for the last one. As only one level could be selected, and level 6 aim to be the best decomposition level, this value is considered. This depth allows a range of frequencies of 93.75 Hz for each packet, which permits detaching each harmonic from the spectrum. Higher ranges will allow also a good splitting, but computing load increases.

All signals are decomposed with *WPT* until 6th level, and the best tree is selected with *Matlab Toolbox* command: *besttree*. This command computes the optimal subtree, which may be much smaller than the initial one, considering the entropy criterion. The best trees calculated for *CWRU* data are shown in Fig. 5.5 considering one signal with each fault.

5.2.3 Best nodes and weighting values

Kurtosis and *RMS* are computed for terminal nodes (last node of each branch of the best tree). The computed values for the *OR-Y* fault are shown in Fig. 5.6.

Best nodes are established by calculating the threshold, which is computed as the mean value of *KR*, Fig. 5.7 (a). The weighting values are considered 1 for all packets with *KR* that are over the threshold and the ones that are below are calculated by dividing its corresponding value of *KR* by the maximum *KR* of all the packets, Fig. 5.7 (b). In this case, only 5 packets are completely reconstructed, as they contain more information about the fault, greater *KR*.

Both, Fig. 5.7 (a) and (b) present two labels in the *x-axis*; in the bottom, the upper frequency limit of each packet is shown and on the top, the corresponding node of the best tree. This simplifies detecting the best nodes and reveals that high frequencies are the ones that gather more details about the fault, as they present higher *KR*. Most analysis focus on the fault frequency range, (frequency up to 188 Hz); but, as it is shown this range presents one of the lowest *KR*.

5.2.4 Signal reconstruction

Once the weighting values are computed, the coefficients of the best tree must be reconstructed. The signal reconstruction scheme is represented in Fig. 5.8. Each packet is processed and transformed again into a time-acceleration signal. All packets are multiplied by their corresponding weighting value and added together to obtain the final signal, Fig. 5.9

5.2.5 Envelope and post processing

A comparison of the original and the reconstructed signal in frequency domain is shown in Fig. 5.10, where the filtering processes is evident. Nevertheless, it is necessary to reduce the high frequency spectrum to a low frequency to observe the bearing faults. Impact-repetition rates are isolated by calculating the envelope of the signal. For an *OR* fault, Fig. 5.11 presents the reconstructed signal and its envelope. The *DCC* is also calculated and subtracted from the enveloped

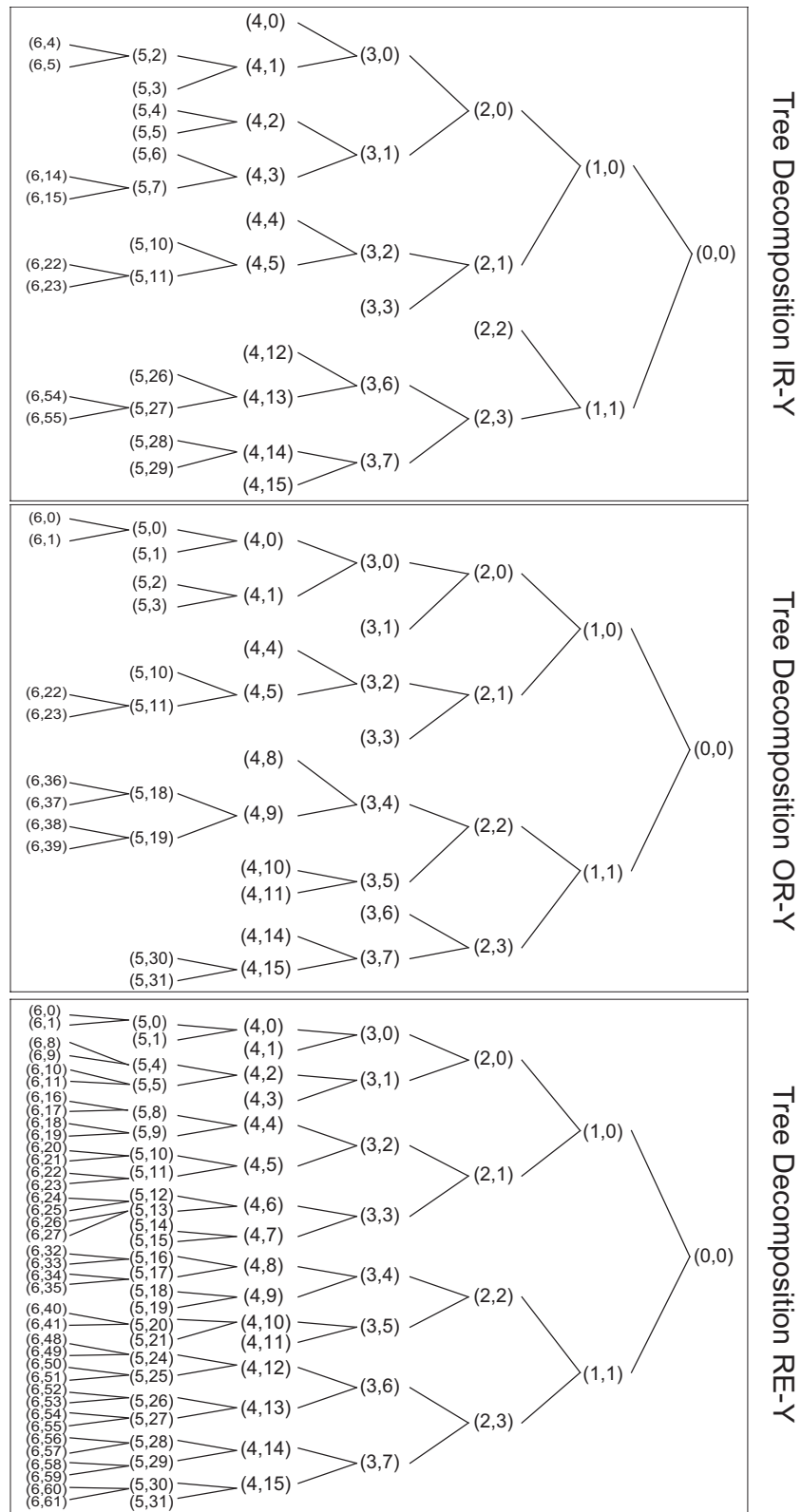


Figure 5.5: Best trees selected for each fault

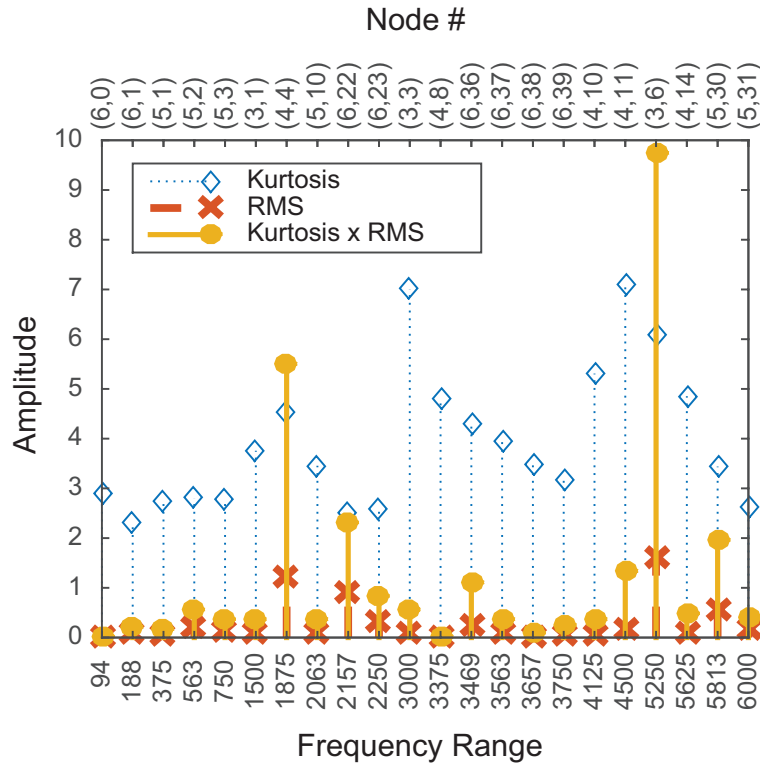


Figure 5.6: Kurtosis, RMS and KR for the signal with OR-Y fault

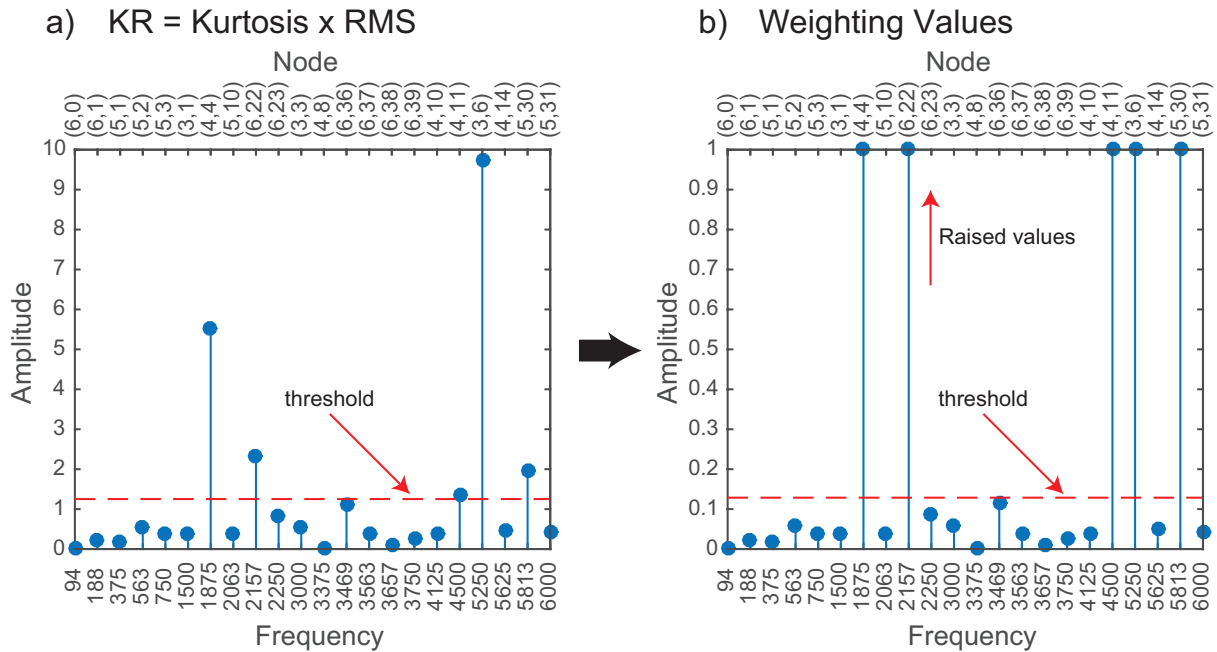


Figure 5.7: Weighting values for the signal with OR-Y fault

signal to obtain the final *Envelope-DCC* signal.

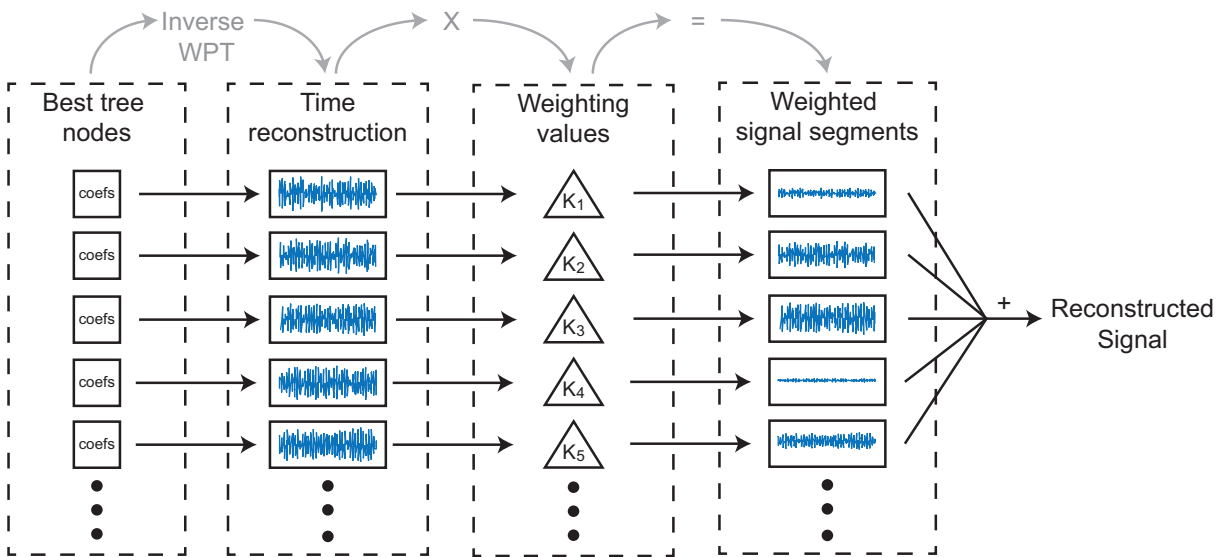
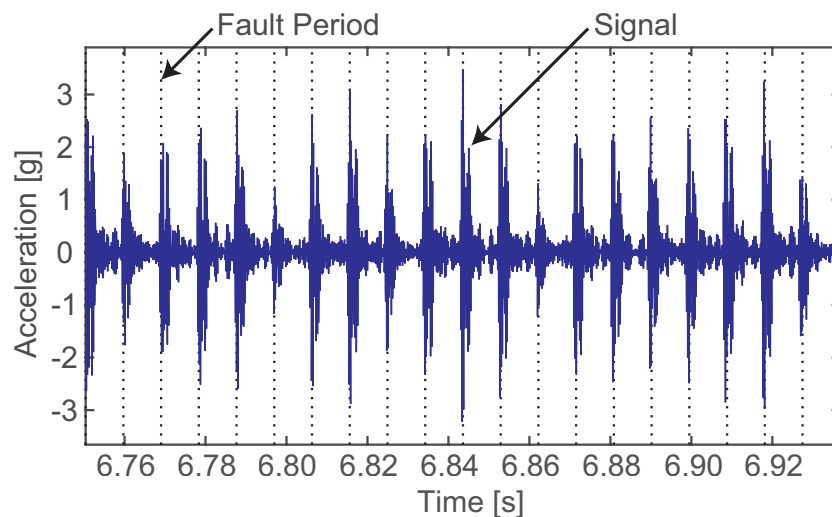


Figure 5.8: Signal reconstruction scheme

Figure 5.9: Reconstructed signal from the *OR-Y* fault

5.2.6 FFT and bearing fault detection

Frequency analysis of the envelope signal enables easier diagnosis of multiple defects as the periodicity of the impacts can be difficult to recognize in the envelope itself (time domain).

In Fig. 5.12, *OR* fault frequency and its harmonics can be clearly identified in spectrum as peaks coincide exactly with the expected frequencies. Other peaks such as spindle speed and its harmonics can also be distinguished. Some unknown peaks also appear in the spectrum, their causes will be discussed later.

On the other hand, Fig. 5.13 presents the spectrum of the signal with an *IR* fault. The fundamental frequency of the fault as well as the harmonics present peaks with considerable magnitudes.

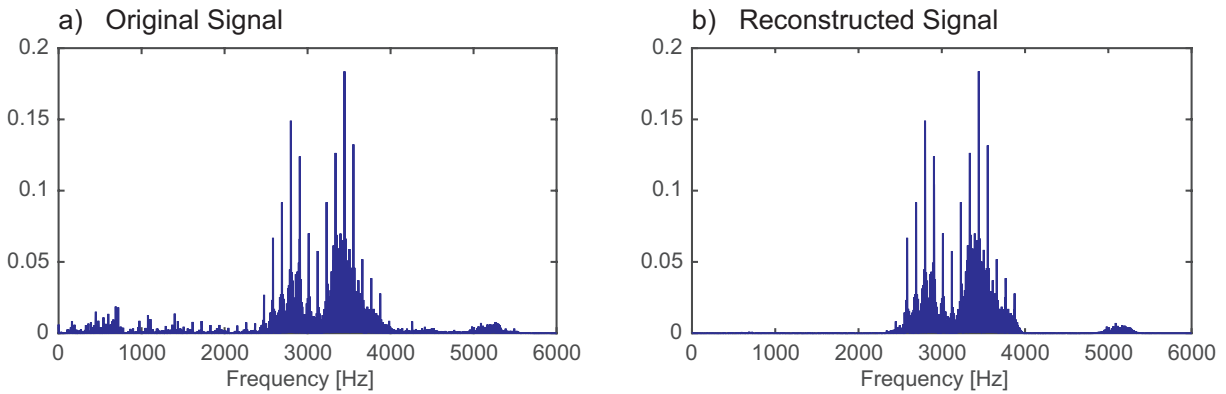


Figure 5.10: FFT spectrum of the (a) original and the (b) reconstructed signal with the *OR-Y* fault

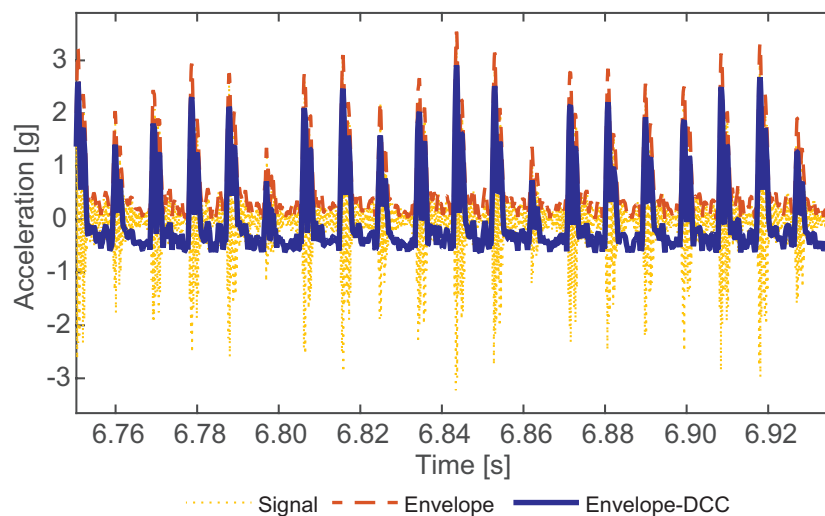


Figure 5.11: Envelope of the reconstructed signal with removed *DCC* from the *OR-Y* fault

One characteristic of *IR* fault is that, according to the magnitude of the fault, each characteristic frequency presents sidebands spaced the distance corresponding to *RPM*. These sidebands, spindle speed and its harmonics are also highlighted.

Finally, the spectrum of the signal with a *RE* fault is presented in Fig. 5.14. Fault frequencies are not as easy to distinguish as in *IR* and *OR* faults; however, considerable peaks are present in the fault frequency and its harmonics, specially the second one. This type of fault present sidebands spaced the frequency corresponding to the *FTF*. Five left sidebands and five right sidebands are presented from each harmonic, between fault harmonics, some sidebands are overlapped. Several peaks coincide with these sidebands, as well as with shaft speed harmonics. The same as for *IR* and *OR*, the remaining peaks are examined in depth later.

Additional results of the application of the methodology to the remaining signals are included in *Appendix C*, for both *CWRU* and *IMS* data.

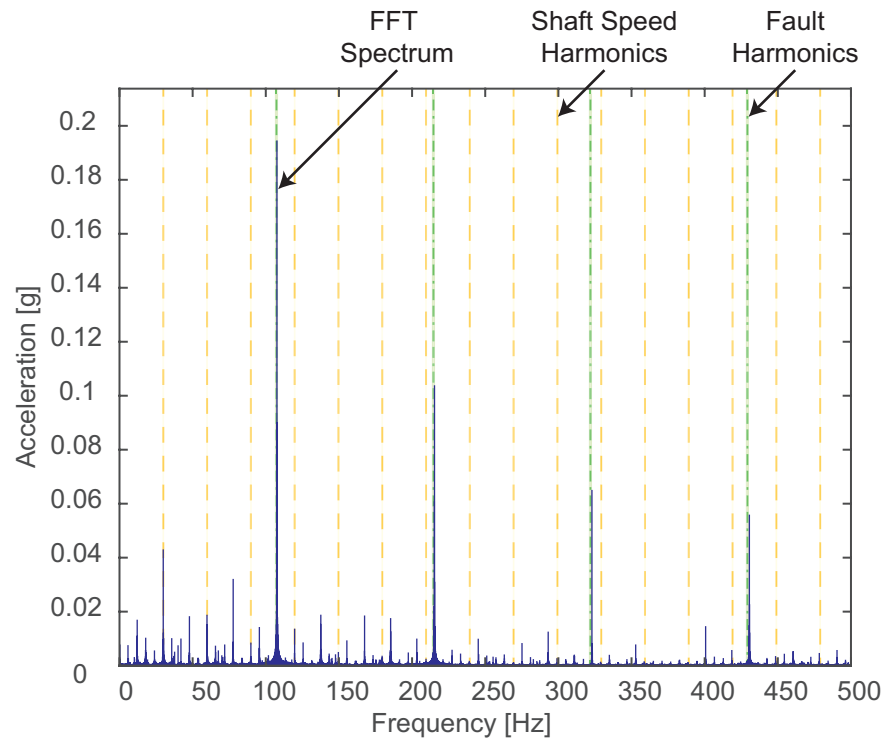


Figure 5.12: *FFT* of the enveloped reconstructed signal with removed *DCC* from the *OR-Y* fault

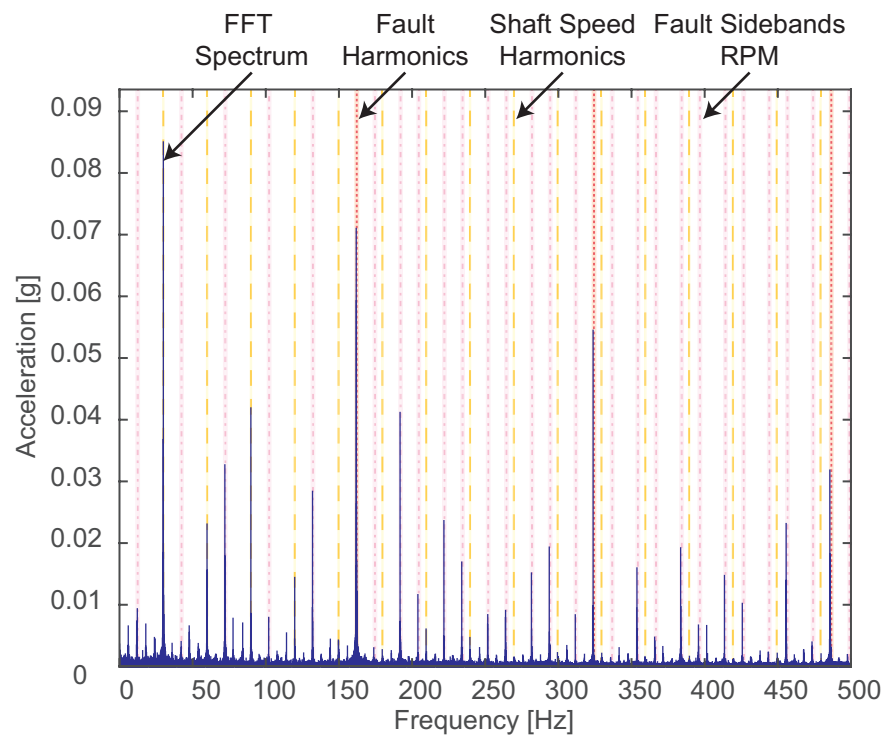


Figure 5.13: *FFT* of the enveloped reconstructed signal with removed *DCC* from the *IR-Y* fault

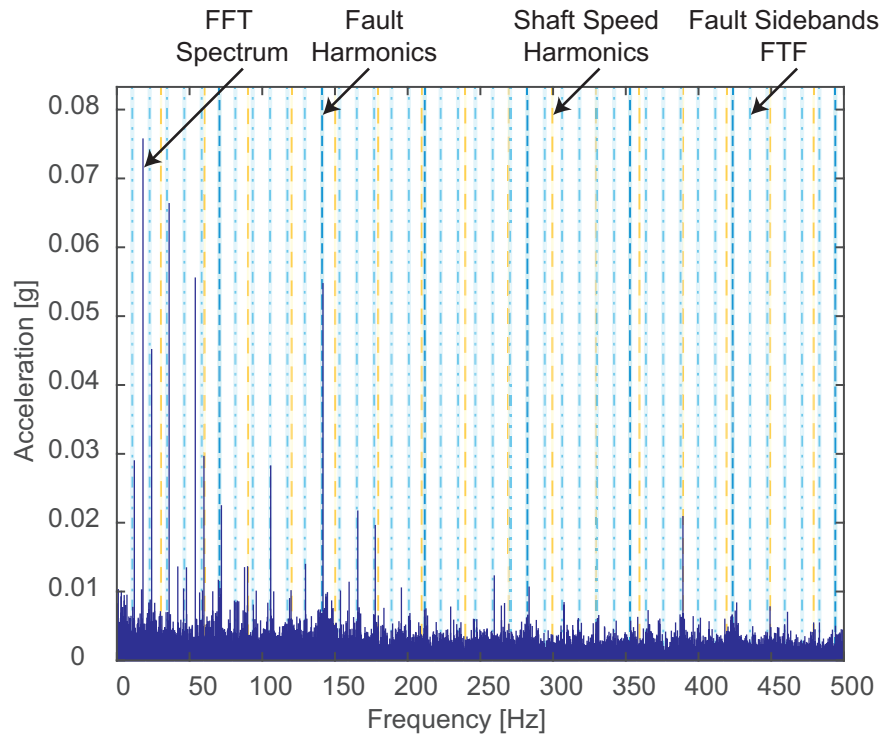


Figure 5.14: *FFT* of the enveloped reconstructed signal with removed *DCC* from the *RE-Y* fault

5.2.7 MA, ML, UB fault detection

The signals analyzed with the proposed methodology for bearing fault detection were also considered for studying *MA* and *ML*, as some present peaks in the spectrum that do not match with the expected frequencies.

To analyze *MA* first and second harmonic of the shaft speed are needed, while for *ML* at least 3 multiples of $1/2$ shaft speed must be considered. In this research, the limit for low frequency nodes reconstruction was considered the fifth shaft speed harmonic. For both data bases, the cutoff frequency is approximately 150 Hz, taking into account that each node of the *WPT* gathers 93.75 Hz, 2 nodes reconstruction is enough for this purpose. By performing this type of low pass filter, low frequencies are not overwhelmed by the high amplitudes of high frequencies, Fig. 5.15.

In Fig. 5.16, *IR* fault signal was analyzed, vertical lines highlight the shaft speed harmonics and the half shaft speed harmonics. The high amplitude of the second harmonic of the rotational frequency ($2X$) compared with the amplitude of the fundamental frequency ($1X$) prove that some *MA* is occurring. For this signal, half harmonics can also be distinguished, but with low magnitudes which indicates that there is probably a *ML* in the test rig. The results for the remaining signals for both *CWRU* and *IMS* data are included in *Appendix C*.

A complementary analysis was performed to the baseline signals (test recorded without faults) of each test rig used in this thesis. Figure 5.17 presents the *FFT* of *CWRU* baseline signal with

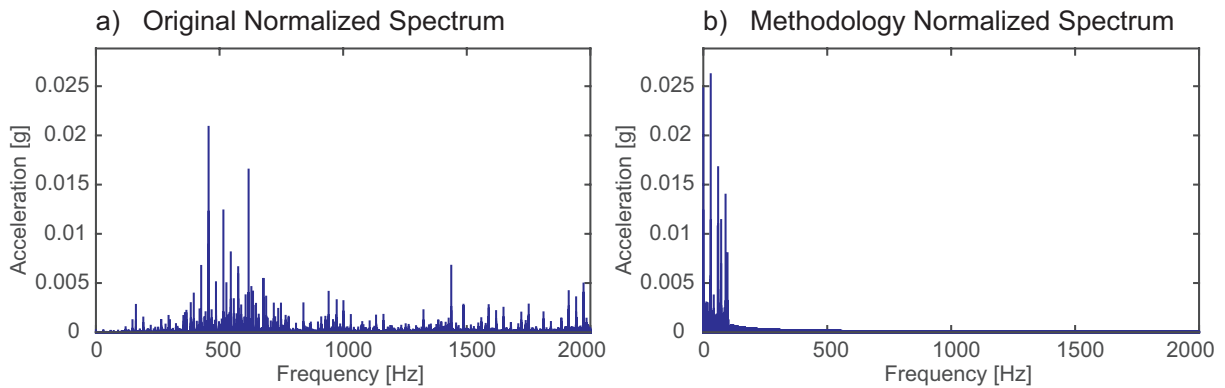


Figure 5.15: *FFT* spectrum of the (a) original signal and the (b) low nodes reconstructed signal - baseline of *CWRU*

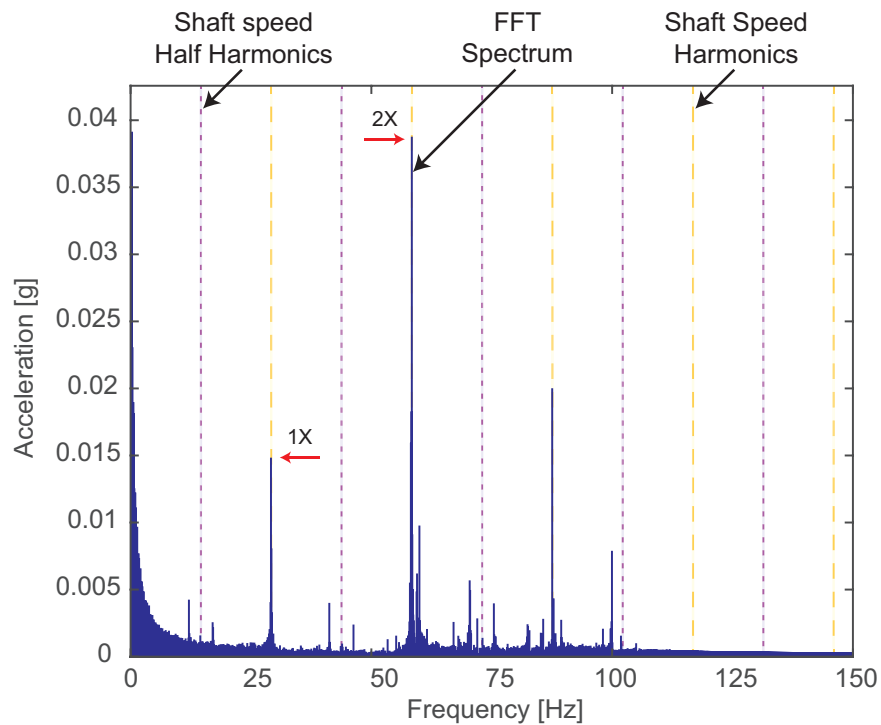


Figure 5.16: *FFT* of the two low nodes reconstructed signal with *IR-P* fault (*CWRU* data)

no load. From this figure, it can be observed that the equipment shows some *MA* as amplitude of the second harmonic is higher than the first. Also, $1/2$, $3/2$, $5/2$ and $7/2$ of the shaft speed frequency present considerable amplitudes, which according to the different faults analyzed, a *ML* is identified as the cause of these peaks. Likewise, $1/4$ speed harmonics were highlighted and relevant peaks were found at this frequencies, which also contributes to the diagnostic of *ML*.

Figures 5.18 and 5.19 show the results of the *MA* and *ML* methodology applied to the baseline signals of *CWRU* and *IMS* data respectively. *CWRU* datasets provide four baseline signals, one for

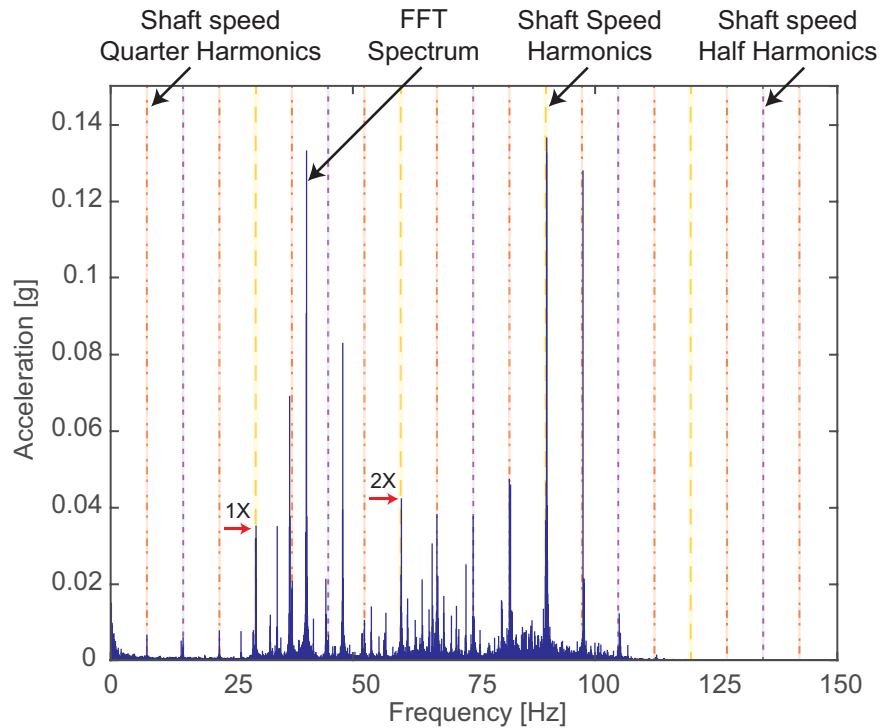


Figure 5.17: *FFT* of the two nodes reconstructed signal 0 load baseline (*CWRU* data)

each case of load applied: 0Hp, 1Hp, 2Hp and 3Hp; their spectrum is shown in Fig. 5.18 (a), (b), (c) and (d) respectively. For *IMS* the baseline signals are considered at the beginning of the test to failure, first sample. One signal was analyzed for the state without fault for each bearing fault case, IR, OR and RE; their spectrum is shown respectively in Fig. 5.19 (a), (b) and (c).

All signals of *CWRU* present an evident *MA* as the amplitude of the second harmonic of the rotational frequency ($2X$) is higher than the amplitude of the fundamental frequency ($1X$). In Fig. 5.18 (a), shaft speed half harmonics present considerable amplitudes, a probable *ML* is also detected. These analysis show that even for bearings in good condition the equipment present faults. In addition, unknown peaks are shown in the spectrum, which represent the equipment's own noises. These reveal that the noises of the recordings of signals with bearing faults are a product of the initial state of the equipment.

For all the baseline signals of *IMS*, the amplitude of the second harmonic of the rotational frequency ($2X$) is higher than the amplitude of the fundamental frequency ($1X$); thus, the test rig presents *MA*. Shaft speed half harmonics also present high magnitude peaks, which lead to a diagnosis of *ML* fault.

Finally for *UB* fault analysis, the signals were obtained from a *GROB 550* machining center, where tool holders were prepared with different conditions of *UB*. Considering the same parameter of five shaft speed harmonics to perform the low pass filter with the proposed methodology a cutoff frequency of 1,000 Hz was established as the spindle speed considered for the analysis was 12,000

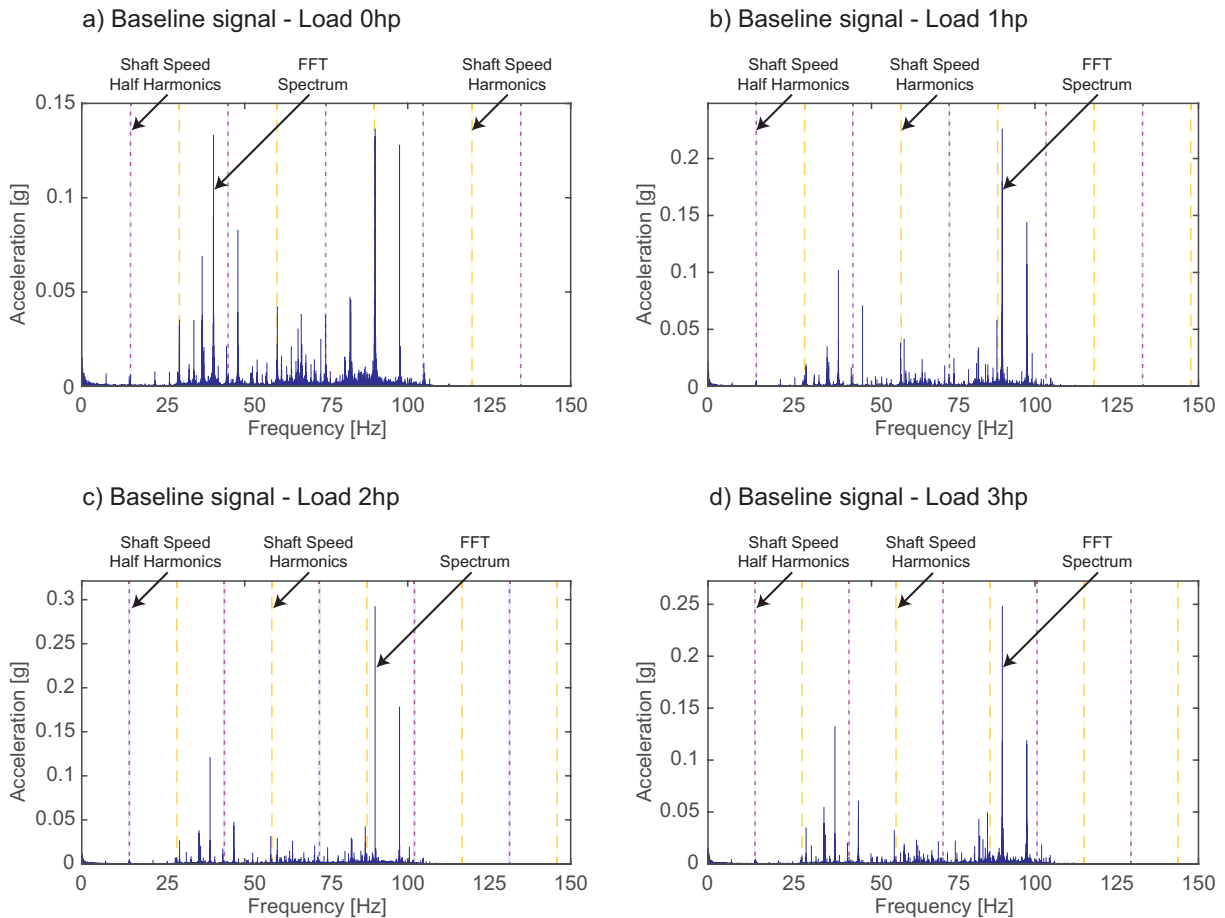


Figure 5.18: *FFT* of the two nodes reconstructed signals baseline (*CWRU* data)

RPM.

Each node of the *WPT* gathers 93.75 Hz. Then, 11 reconstruction nodes are needed to cover the desired spectrum. The original signals of each case of study, Fig. 5.20 (a), (b) and (c), as well as reconstructed signals, Fig. 5.20 (d), (e) and (f), and their spectrum, Fig. 5.20 (g), (h) and (i), were plotted. An increment of the spindle speed harmonic amplitude is observed as expected for *UB*. Figure 5.20 (g) shows the peak of the rotational frequency with an amplitude around 0.03, while Fig. 5.20 (h) and (i) present amplitudes of 0.05 and 0.08 respectively, evidencing that the amplitude increases as the *UB* increases. *MA* and *ML* were discarded as no harmonics or half harmonics of the rotation speed are presented.

5.3 Discussion

In an attempt to present all the results of bearing fault analysis in a quantitative way, Table 5.2 summarizes the magnitudes of the first 3 harmonics of the fault as well as the maximum peak

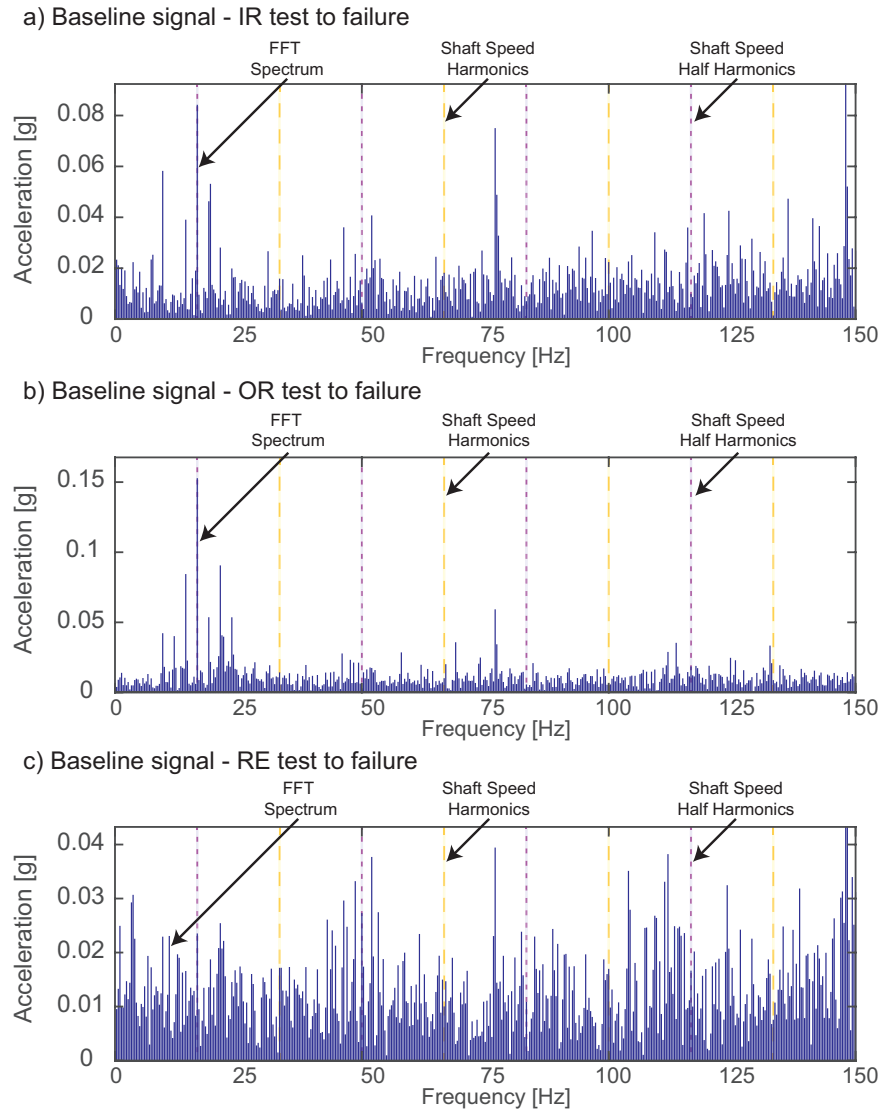


Figure 5.19: *FFT* of the two nodes reconstructed signals baseline (*IMS* data)

of the spectrum. Other significant magnitudes besides the known fault are also listed for each case. Based on the analysis of these parameters and the visual inspection of the cleared spectrum obtained, a categorization of detection difficulty was established:

- **Clear:** The highest peaks coincide exactly with the expected fault frequency, without considering frequencies lower than 50 Hz as they could be part of rotational frequency-dependent faults.
- **Noisy:** High peaks coincide with the expected fault frequency, but there is too many noise and other peaks present higher magnitudes besides the ones lower than 50 Hz.
- **None:** None high peaks were found at the expected fault frequency.

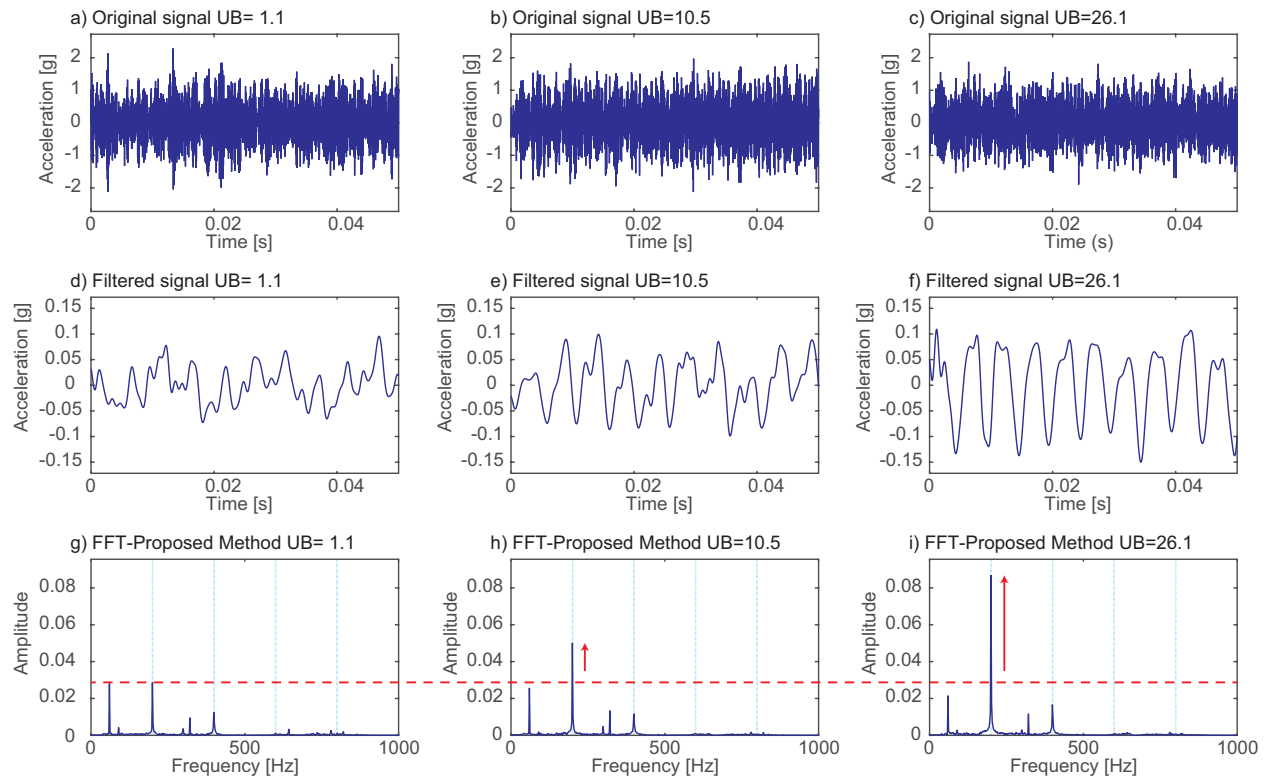


Figure 5.20: *FFT* of the two nodes reconstructed signals baseline (*IMS* data)

From all the studied cases, only one was considered non diagnosable; but, after analyzing the high magnitude peaks, and considering that the database indicates that for the 28 mils diameter faults other bearings were used, periodicity was sought in the remaining peaks. The 110 Hz frequency presented harmonics and sidebands corresponding to an *IR* fault, this could indicate that the fault factor of this bearing is not equivalent to the previous ones. Another peak was found at the frequency of 128 Hz and presented harmonics; however, it could not be attributed to a fault in the *OR* since the frequency can not exceed the *BPFI*, because it contradicts what was found for 110Hz. These results are shown in Fig. 5.21.

For data categorized *noisy* additional significant peaks were evaluated and combined defects were found in each case. In signals from *CWRU* data, *OR* faults present also *IR* harmonics and sidebands, while *RE* faults also have characteristics of *IR* and *OR* faults. Figures 5.22-5.25 highlight these detection of combined faults.

For *OR-N* and *OR-Y* signals, *IR* fault was also diagnosed, as high magnitude peaks coincide with *IR* fault harmonics as well as with their respective sidebands. *IR* fault harmonics present even higher peaks than *OR*. Spectrum of the *OR-N* signal is shown in Fig. 5.22, while for the *OR-Y* signal it is presented in Fig. 5.23.

The combined defects presented in the *RE-P* faulty signal are shown in Fig. 5.24. The highest peaks of the spectrum are found in *IR* fault harmonics and their sidebands. Significant peaks

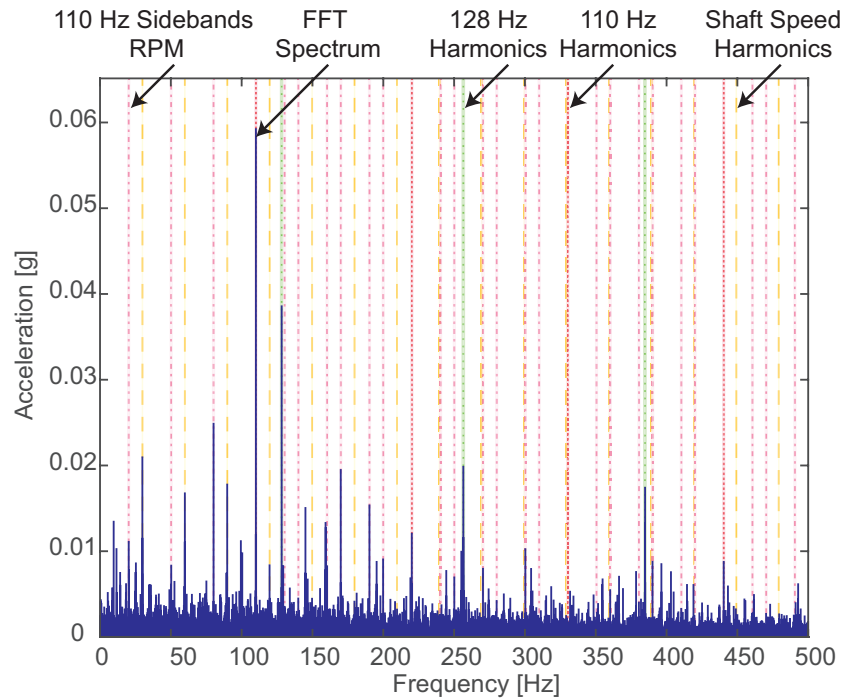


Figure 5.21: Periodicity description of the additional peaks found in *IR-N* signal

were also found at *OR* fault harmonics. For the *RE-N* faulty signal the spectrum shown in Fig. 5.25 reveals that the bearing presents *IR* faults besides the expected ones. *IR* fault harmonics and sidebands present higher peaks than *RE* fault harmonics.

Moreover, additional peaks found in *IMS* data categorized *noisy*, were mostly attributed to *ML*. Analysis of this fault as well as *MA* are demonstrated in Table 5.3. *OR* results present a clear diagnosis at early stages, even earlier than the proposed in the state of the art by [Li *et al.*, 2017], approximately 110 samples before, which leads to more or less 18 hours of pre-detection.

Some noise such as 6 Hz harmonics and some other peaks could not be explained or eliminated, which indicates that an improvement in denoising study would be required.

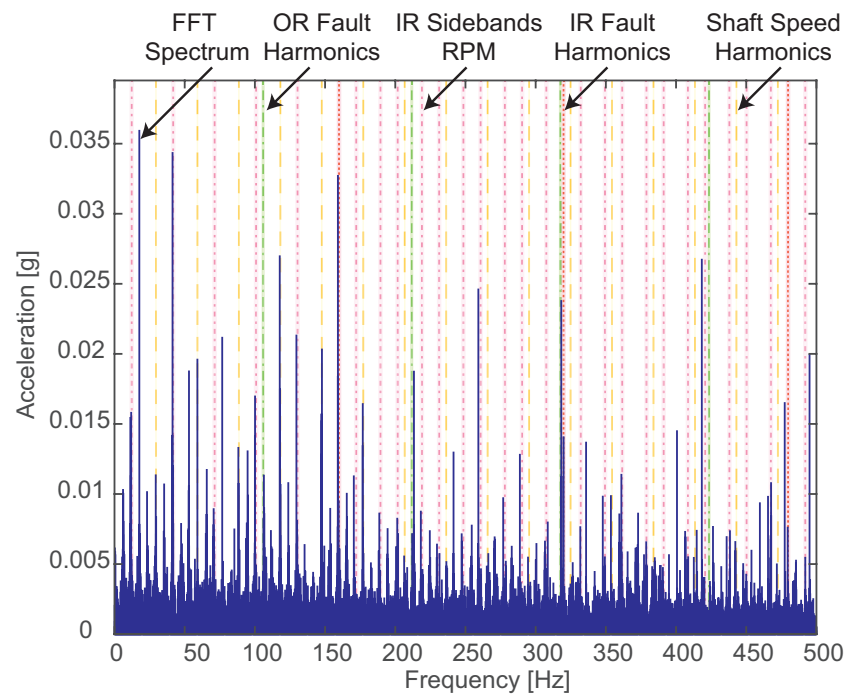


Figure 5.22: Combined defects found in *OR-P* signal, explaining additional peaks

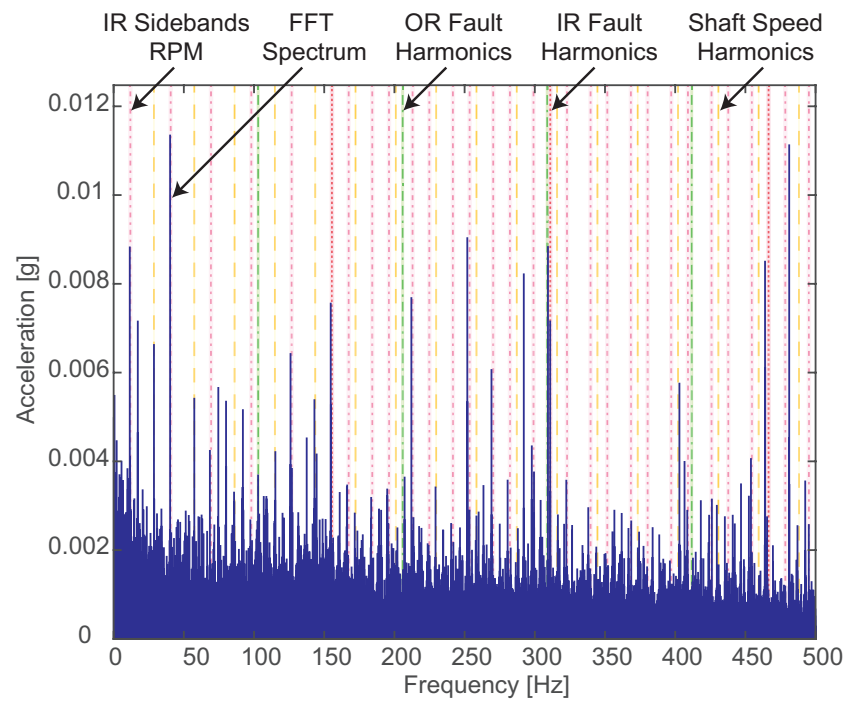


Figure 5.23: Combined defects found in *OR-N* signal, explaining additional peaks

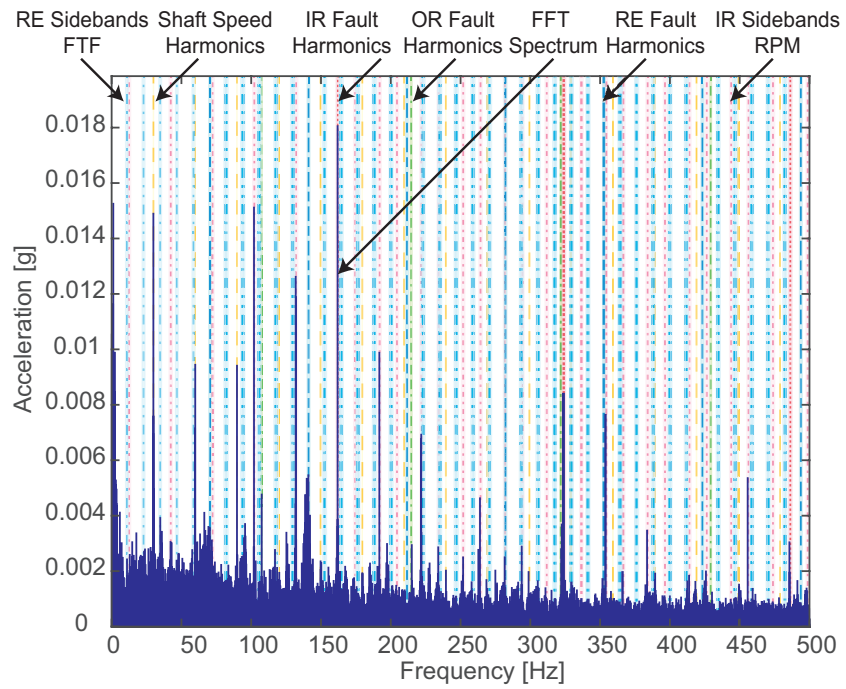


Figure 5.24: Combined defects found in *RE-P* signal, explaining additional peaks

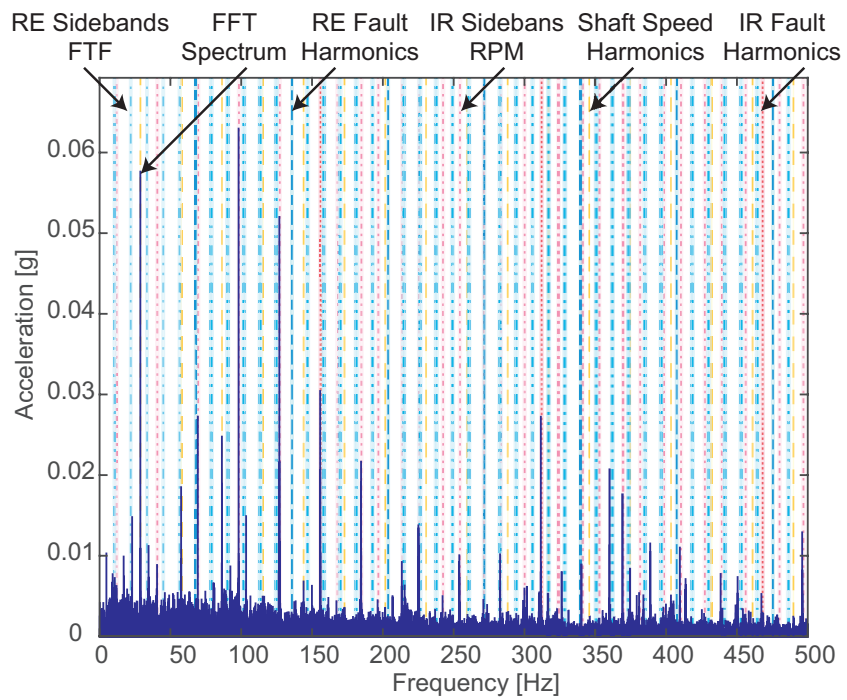


Figure 5.25: Combined defects found in *RE-N* signal, explaining additional peaks

Table 5.2: Results for bearing faults

Data case		Detection difficulty	Fault harmonics amplitude			Maximum amplitude	Additional significant peaks ^a
			1 st	2 nd	3 th		
<i>CWRU</i>	<i>IR(Y)</i>	Clear	0.07100	0.05449	0.03183	0.08503 (1xRPM)	Negligible
	<i>IR(P)</i>	Clear	0.02903	0.01598	0.00317	0.03199 (3xRPM)	Negligible
	<i>IR(N)</i>	None	0.00322	0.00388	0.00209	0.05922 (110.1 Hz)	110 Hz / 128 Hz Harm & SB
	<i>OR(Y)</i>	Clear	0.19434	0.10360	0.06486	0.19434 (fault)	Negligible
	<i>OR(P)</i>	Noisy	0.01131	0.00713	0.02377	0.03592 (17.7 Hz)	IR Harm & SB / 6 Hz Harm
	<i>OR(N)</i>	Noisy	0.00368	0.00155	0.00883	0.01134 (40.2 Hz)	IR Harm & SB / 6 Hz Harm
	<i>RE(Y)</i>	Clear	0.02245	0.05471	0.00656	0.07572 (18 Hz)	6 Hz Harm
	<i>RE(P)</i>	Noisy	0.00355	0.00546	0.00082	0.01805 (BPFI)	IR Harm & SB / OR Harm
	<i>RE(N)</i>	Noisy	0.00459	0.00295	0.00246	0.06297 (BPFO)	IR Harm & SB
<i>IMS</i>	<i>IR(E)</i>	Noisy	0.00443	0.00206	0.00182	0.00789 (58 Hz)	22 Hz / 58 Hz / Noise
	<i>IR(M)</i>	Clear	0.00467	0.00329	0.00250	0.00698 (58 Hz)	15 Hz / 58 Hz / Noise
	<i>IR(C)</i>	Clear	0.00653	0.00744	0.00501	0.00824 (130 Hz)	130 Hz
	<i>OR(E)</i>	Clear	0.02101	0.01369	0.01068	0.02101 (BPFO)	137 Hz
	<i>OR(M)</i>	Clear	0.10200	0.09780	0.04526	0.10200 (BPFO)	72 Hz
	<i>OR(C)</i>	Clear	0.11960	0.06911	0.04805	0.11960 (BPFO)	72 Hz
	<i>RE(E)</i>	Noisy	0.00676	0.00391	0.00439	0.02506 (29 Hz)	15-29-44 Hz / Noise
	<i>RE(M)</i>	Noisy	0.01082	0.00401	0.00560	0.03809 (15 Hz)	15-29-44 Hz / Noise
	<i>RE(C)</i>	Noisy	0.01022	0.01585	0.01058	0.05752 (15 Hz)	15-29-44 Hz / Noise

^aHarm: harmonics, SB: Sidebands

Table 5.3: Results for *MA* and *ML*

Data case		Speed harmonics amplitude			<i>MA</i> fault $\frac{2^{st}}{1^{nd}} > 30\%$	Half Speed harmonics				<i>ML</i> fault $\frac{1}{2}X > 20\% \times 1X$
		1 st	2 nd	$\frac{2^{st}}{1^{nd}}$ (%)		$\frac{1}{2}$	$\frac{3}{2}$	$\frac{5}{2}$	$\frac{7}{2}$	
<i>CWRU</i>	<i>IR</i> (Y)	0.02621	0.01676	63.95	Yes	0.00044	0.00063	0.00041	0.00041	No
	<i>IR</i> (P)	0.01476	0.03870	262.19	Yes	0.00151	0.00090	0.00133	0.00149	No
	<i>IR</i> (N)	0.00266	0.00391	147.01	Yes	0.00038	0.00044	0.00048	0.00051	No
	<i>OR</i> (Y)	0.01774	0.00755	42.53	Yes	0.00040	0.00043	0.00052	0.00039	No
	<i>OR</i> (P)	0.00837	0.03474	414.95	Yes	0.00026	0.00036	0.00586	0.00032	No
	<i>OR</i> (N)	0.02172	0.02206	101.57	Yes	0.00145	0.00141	0.00263	0.00084	No
	<i>RE</i> (Y)	0.02006	0.02406	119.94	Yes	0.01264	0.00636	0.00342	0.00173	No
	<i>RE</i> (P)	0.02817	0.04484	159.17	Yes	0.00348	0.00103	0.00078	0.00070	No
	<i>RE</i> (N)	0.11190	0.18440	164.79	Yes	0.00290	0.00376	0.00943	0.02890	No
<i>IMS</i>	<i>IR</i> (E)	0.01940	0.02229	114.90	Yes	0.02320	0.02129	0.01282	0.02934	Yes
	<i>IR</i> (M)	0.01364	0.02295	168.26	Yes	0.02854	0.03150	0.02131	0.02464	Yes
	<i>IR</i> (C)	0.00924	0.01305	141.18	Yes	0.01407	0.01693	0.01541	0.02353	Yes
	<i>OR</i> (E)	0.01540	0.01811	117.60	Yes	0.14320	0.01549	0.01277	0.01356	Yes
	<i>OR</i> (M)	0.01779	0.01269	71.33	Yes	0.13240	0.03446	0.01971	0.01067	Yes
	<i>OR</i> (C)	0.01532	0.02314	151.04	Yes	0.04366	0.01961	0.01941	0.00930	Yes
	<i>RE</i> (E)	0.01747	0.00955	54.67	Yes	0.01732	0.01683	0.01425	0.01396	Yes
	<i>RE</i> (M)	0.01833	0.01741	94.98	Yes	0.02066	0.01739	0.02838	0.01575	Yes
	<i>RE</i> (C)	0.01279	0.02320	181.39	Yes	0.02357	0.01686	0.01589	0.01715	Yes

5.4 Comparison

For comparison purposes, the results of the proposed methodology were contrasted with the classical envelope *FFT* analysis. Figure 5.26, presents the results considering a baseline signal. To have a same point of comparison, the signals were normalized to contrast their magnitudes. It can be observed that some peaks are magnified while others are diminished, this helps giving more weight to the fault frequencies that are searched and reducing or removing components that are not contributing to the analysis such as noise.

With this methodology high magnitude peaks are more reliable to be part of the fault signal than to be noise, giving more reliability to the signal processing.

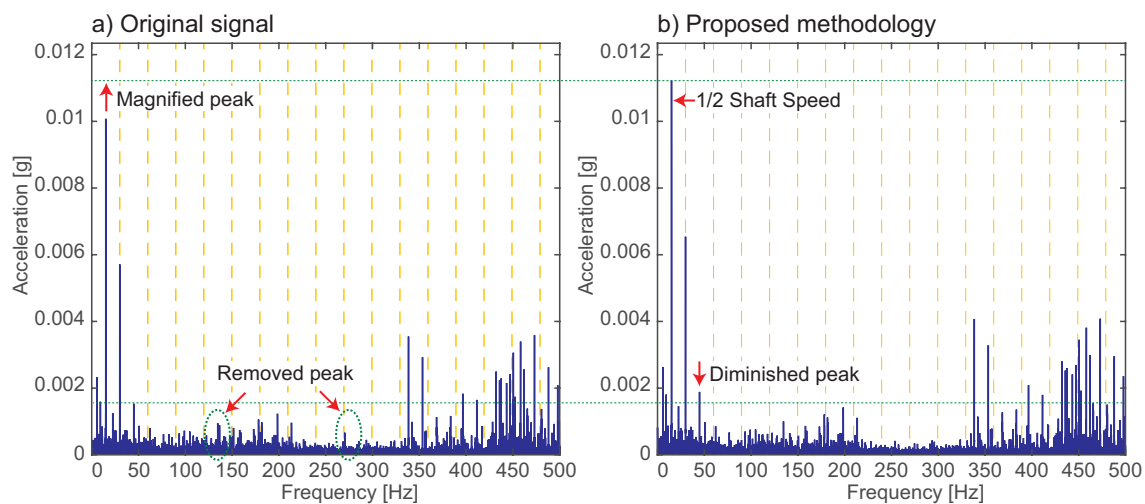


Figure 5.26: Comparison of the traditional envelope *FFT* and the proposed methodology for the base line signal (without fault)

A comparison of a fault signal was also developed and is presented in Fig. 5.27, considering the same parameters of normalization. Even though the fault is clear for both, original signal, Fig. 5.27 (a), and the signal after the application of the proposed methodology, Fig. 5.27 (b), fault peaks are magnified.

Finally, with the purpose of verifying if the methodology could be efficient at industrial level, its response to noise was compared. White *Gaussian* noise, which is distributed throughout the frequency spectrum, was added to the original signal for testing purposes.

The comparison is evidenced in Fig. 5.28 - 5.30, where time domain, *FFT* and envelope *FFT* are shown respectively. By looking to the time domain signals it can be observed that the one after applying the proposed methodology, Fig. 5.28 (b) looks less noisy than the original signal, Fig. 5.28 (a). The shape of the fault is more evident, presenting a periodic peak and its corresponding attenuation. From Fig. 5.29 the spectrum of the original, Fig. 5.29 (a), and the reconstructed, Fig. 5.29 (b), signals can be compared. Low frequency peaks as well as those around 1,000 and 2,000

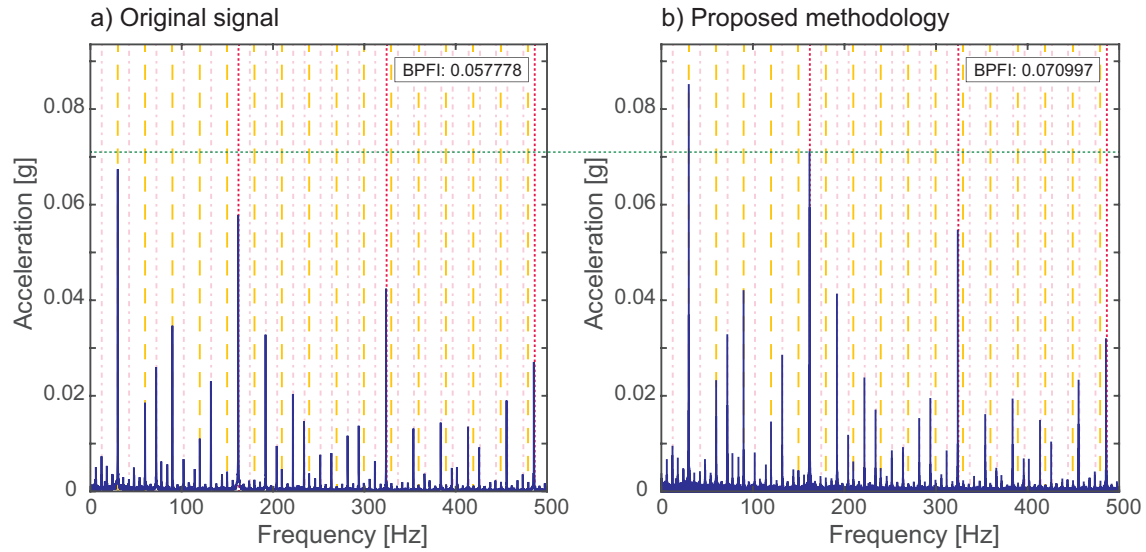


Figure 5.27: Comparison of the traditional envelope *FFT* and the proposed methodology for *IR-Y* signal (*CWRU* data)

Hz are attenuated; reducing noise and extracting the important information about the fault. Finally the comparison of the enveloped spectrum presented in Fig. 5.30 reveals the important increase of the magnitude of the fault frequency peaks. Demonstrating that the attenuation caused by noise is minimum for the proposed methodology.

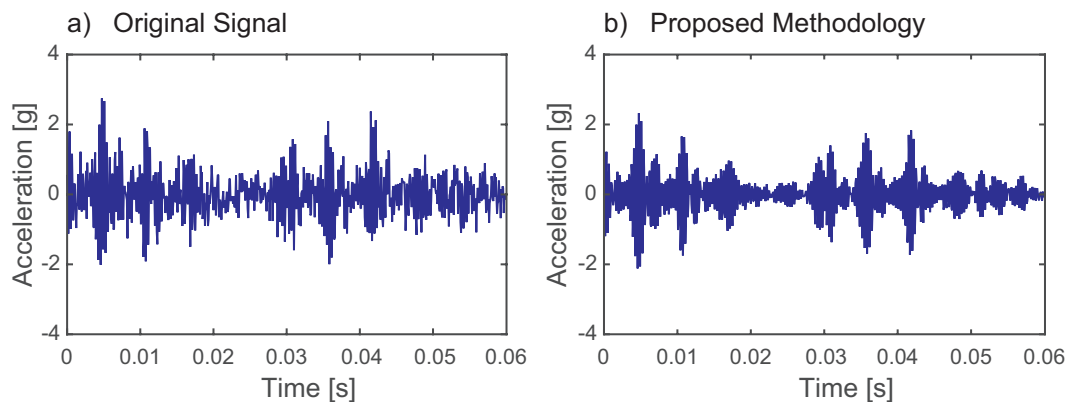


Figure 5.28: Comparison of the initial signal and the obtained with the proposed methodology in time domain for *IR-Y* signal added white *Gaussian* noise $SNR = 10$ (*CWRU* data)

Table 5.4 summarizes the amplitude ratio improvement to noise response. The magnitude considered for comparison was the fundamental fault frequency. The ratio values reflect an intensification in the peaks of 22.88% and 71.03% for noiseless and noisy signals respectively.

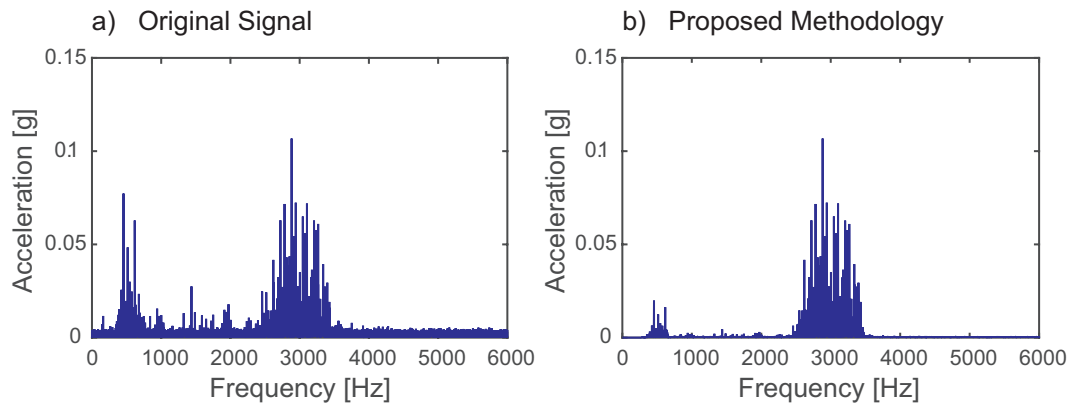


Figure 5.29: Comparison of the *FFT* spectrum of the initial signal and the proposed methodology for *IR-Y* signal added white *Gaussian* noise $SNR = 10$ (*CWRU* data)

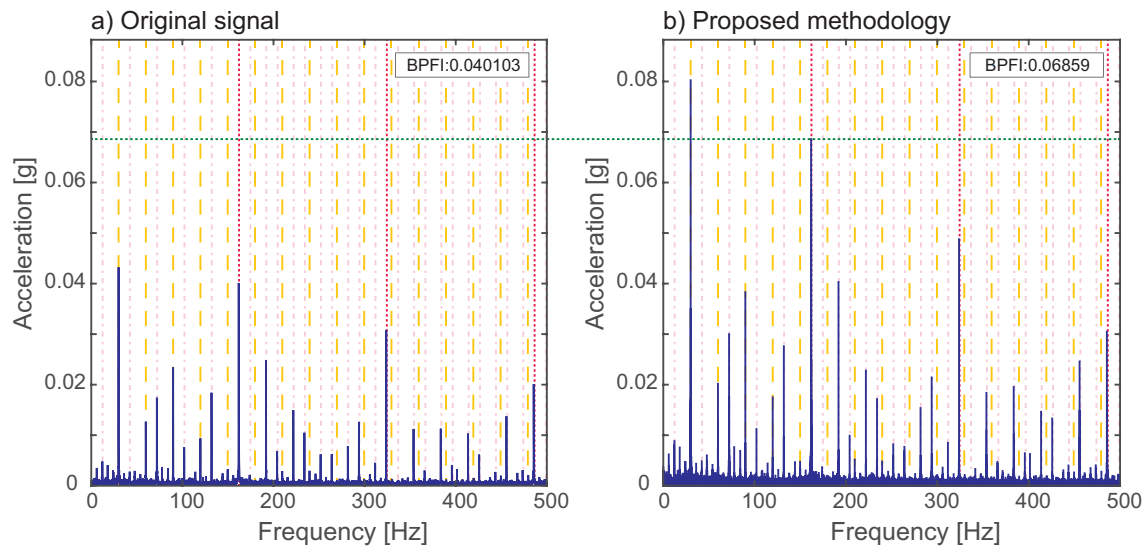


Figure 5.30: Comparison of the traditional envelope *FFT* and the proposed methodology for *IR-Y* signal added white *Gaussian* noise $SNR = 10$ (*CWRU* data)

Table 5.4: Comparison between traditional envelope *FFT* and proposed methodology for noiseless and noisy signals (*IR-Y CWRU* data)

Envelope <i>FFT</i>	Methodology	Ratio	Envelope <i>FFT</i>	Methodology	Ratio
noiseless	noiseless	$\frac{Methodology}{EnvelopeFFT}$	noisy	noisy	$\frac{Methodology}{EnvelopeFFT}$
0.057778	0.070997	1.228790	0.040103	0.068590	1.710346

Chapter 6

Conclusions

6.1 Conclusions

The *WPT* combines computational efficiency and good resolution in time and frequency domain which makes it an optimal tool for analyzing bearing faults. Considering that in high frequencies incipient faults could be detected, this transform allows obtaining better results as it presents good resolution in this range of frequencies unlikely *DWT* and *CWT*

The analysis of high frequencies for bearing fault diagnosis presents two main advantages, first the detection of incipient faults and second the avoidance of external noises that are generally associated with low frequencies.

The proposed methodology presents better results than classical envelope *FFT* as it gives more weight to high energy frequencies. Important magnitudes of the peaks in the spectrum increase while noise is diminished. A comparison showed an increment of the fault frequency 20% for the noiseless signal. And even greater than 70% for signals with added noise.

The proposed methodology allows detecting faults earlier than what has been reported in the state of the art, mainly for *OR* faults, where an earlier detection was proven with around of 18 hours of anticipation. For *IR* and *RE* peaks are identified, but some additional denoising would be recommended for a clearer diagnosis.

6.2 Contributions

A complementary study of the best mother wavelet was developed to deal with the controversy found at the state of the art, where different wavelets were proposed as the best. For this thesis one mother wavelet was selected for each fault according to a comparison of quantitative parameters instead of some visual qualitative parameters that have also been considered in other studies.

The proposed methodology deals with noise, weak signals and achieves detecting faults in

high frequencies; therefore, in early stage of damage. As noise is one of the main problems at industrial environments, this methodology presents a great potential to be applied in *HSM* centers in manufacturing industries.

6.3 Publications

Two published papers were presented during the research.

- "Diagnóstico de Fallas en Husillos de Mecanizado de Alta Velocidad usando Onduletas - Estado del Arte", *Appendix D*. XXIII Annual International Congress of SOMIM (20-22 September 2017, Cuernavaca, Morelos, México)
- "Monitoreo de Husillos usando la Transformada de Onduletas". *Appendix D*. National Congress of Automatic Control 2017 (04-06 October 2017, Monterrey, NL, México)

6.4 Future work

Some research lines have not been covered in this thesis; the following statements are proposed:

- Exploit the potential of Wavelet-Denoising to try to eliminate the remaining noise before reconstructing the signal.
- The proposed method can be used with classifiers that instantly detect what type of fault is present.
- Design of an specific mother wavelet that fits better to the each fault could be done to extract more information from the vibration signal.
- An hybrid method could be developed with approaches as Deep Learning.

Bibliography

- [Chancey *et al.*, 2002] V.C. Chancey, G.T. Flowers, and C.L. Howard. A Harmonic Wavelets Approach for Extracting Transient Patterns From Measured Rotor Vibration Data. *J of Eng for Gas Turbines and Power*, 125(1):81–89, 2002.
- [Chandel and Patel, 2013] A.K. Chandel and R.K. Patel. Bearing Fault Classification based on Wavelet Transform and Artificial Neural Network. *IETE J of Research*, 59(3):219–225, 2013.
- [Chen *et al.*, 2013] D. Chen, J. Fan, and F. Zhang. Extraction the Unbalance Features of Spindle System using Wavelet Transform and Power Spectral Density. *Measurement*, 46(3):1279–1290, 2013.
- [Cui *et al.*, 2016] H. Cui, Y. Qiao, Y. Yin, and M. Hong. An Investigation of Rolling Bearing Early Diagnosis based on High-Frequency Characteristics and Self-Adaptive Wavelet Denoising. *Neurocomputing*, 216:649–656, 2016.
- [CWRU, 1999] CWRU. Case Western Reserve University Bearing Data Center Seeded Fault Test Data. <http://csegroups.case.edu/bearingdatacenter/pages/apparatus-procedures>, Accessed 01-12-2016, 1999.
- [Fan *et al.*, 2013] H.W. Fan, M.Q. Jing, and H. Liu. Experimental Method to Evaluate Unbalance Vibration for Machine Tool Spindle Integrated with Automatic Balancer. In *Applied Mechanics and Materials*, volume 391, pages 398–401. Trans Tech Publ, 2013.
- [Gao and Yan, 2010] R.X. Gao and R. Yan. *Wavelets: Theory and Applications for Manufacturing*. Springer Science & Business Media, 2010.
- [He *et al.*, 2009] W. He, Z.N. Jiang, and K. Feng. Bearing Fault Detection based on Optimal Wavelet Filter and Sparse Code Shrinkage. *Measurement*, 42(7):1092–1102, 2009.
- [IMS, 2004] IMS. NSF I/UCR Center for Intelligent Maintenance Systems. www.imscenter.net, Accessed 05-12-2016, 2004.
- [Kankar *et al.*, 2011] P.K. Kankar, S.C. Sharma, and S.P. Harsha. Rolling Element Bearing Fault Diagnosis using Wavelet Transform. *Neurocomputing*, 74(10):1638 – 1645, 2011.

- [Kedadouche *et al.*, 2016a] M. Kedadouche, Z. Liu, and V.H. Vu. A New Approach based on OMA-Empirical Wavelet Transforms for Bearing Fault Diagnosis. *Measurement*, 90:292–308, 2016.
- [Kedadouche *et al.*, 2016b] M. Kedadouche, M. Thomas, and A. Tahan. A Comparative Study Between Empirical Wavelet Transforms and Empirical Mode Decomposition Methods: Application to Bearing Defect Diagnosis. *Mechanical Systems and Signal Processing*, 81:88 – 107, 2016.
- [Khanam *et al.*, 2014] S. Khanam, N. Tandon, and J.K. Dutt. Fault Size Estimation in the Outer Race of Ball Bearing using Discrete Wavelet Transform of the Vibration Signal. *Procedia Technology*, 14:12–19, 2014.
- [Law *et al.*, 2012] L.S. Law, J.H. Kim, W.Y.H. Liew, and S.K. Lee. An Approach based on Wavelet Packet Decomposition and Hilbert-Huang Transform (WPD-HHT) for Spindle Bearings Condition Monitoring. *Mechanical Systems and Signal Processing*, 33:197–211, 2012.
- [Lei, 2016] L.Y. Lei. *Intelligent Fault Diagnosis and Remaining Useful Life Prediction of Rotating Machinery*. Elsevier. Joe Hayton, 2016.
- [Li *et al.*, 2017] Y. Li, X. Liang, M. Xu, and W. Huang. Early Fault Feature Extraction of Rolling Bearing based on ICD and Tunable Q-factor Wavelet Transform. *Mechanical Systems and Signal Processing*, 86, Part A:204 – 223, 2017.
- [Liu, 2012] J. Liu. Shannon Wavelet Spectrum Analysis on Truncated Vibration Signals for Machine Incipient Fault Detection. *Measurement Science and Technology*, 23(5):055604, 2012.
- [Mais, 2002] J. Mais. *Spectrum Analysis: the Key Features of Analyzing Spectra*, 2002.
- [Mori *et al.*, 1996] K. Mori, N. Kasashima, T. Yoshioka, and Y. Ueno. Prediction of Spalling on a Ball Bearing by Applying the Discrete Wavelet Transform to Vibration Signals. *Wear*, 195(1-2):162–168, 1996.
- [Nguï *et al.*, 2013] W.K. Nguï, M.S. Leong, L.M. Hee, and A.M. Abdelrhman. Wavelet Analysis: Mother Wavelet Selection Methods. In *Applied mechanics and materials*, volume 393, pages 953–958. Trans Tech Publ, 2013.
- [Nikolaou and Antoniadis, 2002] N.G. Nikolaou and I.A. Antoniadis. Rolling Element Bearing Fault Diagnosis using Wavelet Packets. *NDT & E Int*, 35(3):197 – 205, 2002.
- [Ocak *et al.*, 2007] H. Ocak, K.A. Loparo, and F.M. Discenzo. Online Tracking of Bearing Wear Using Wavelet Packet Decomposition and Probabilistic Modeling: A Method for Bearing Prognostics. *J. of Sound and Vibration*, 302(4):951–961, 2007.

- [Pandya *et al.*, 2012] D.H. Pandya, S. Upadhyay, and S.P. Harsha. ANN Based Fault Diagnosis of Rolling Element Bearing using Time-Frequency Domain Feature. *Int J of Eng Science and Technology*, 4(6):2878–2886, 2012.
- [Paya *et al.*, 1997] B.A. Paya, I.I. Esat, and M.N.M. Badi. Artificial Neural Network based Fault Diagnostics for Rotating Machinery using Wavelet Transforms as a Preprocessor. *Mechanical Systems and Signal Processing*, 11(5):751 – 765, 1997.
- [Peng *et al.*, 2007] Z.K. Peng, F.L. Chu, and P.W. Tse. Singularity Analysis of the Vibration Signals by Means of Wavelet Modulus Maximal Method. *Mechanical Systems and Signal Processing*, 21(2):780–794, 2007.
- [Prabhakar *et al.*, 2002] S. Prabhakar, A.R. Mohanty, and A.S. Sekhar. Application of Discrete Wavelet Transform for Detection of Ball Bearing Race Faults. *Tribology Int*, 35(12):793 – 800, 2002.
- [Purushotham *et al.*, 2005] V. Purushotham, S. Narayanan, and S.A.N. Prasad. Multi-Fault Diagnosis of Rolling Bearing Elements using Wavelet Analysis and Hidden Markov Model based Fault Recognition. *NDT & E Int*, 38(8):654 – 664, 2005.
- [Rafiee and Tse, 2009] J. Rafiee and P.W. Tse. Use of Autocorrelation of Wavelet Coefficients for Fault Diagnosis. *Mechanical Systems and Signal Processing*, 23(5):1554–1572, 2009.
- [Rafiee *et al.*, 2010] J. Rafiee, M.A. Rafiee, and P.W. Tse. Application of Mother Wavelet Functions for Automatic Gear and Bearing Fault Diagnosis. *Expert Systems with Applications*, 37(6):4568 – 4579, 2010.
- [Randall, 2011] R.B. Randall. *Vibration-based Condition Monitoring: Industrial, Aerospace and Automotive Applications*. EBL-Schweitzer. John Wiley & Sons, 2011.
- [Rathbone, 1939] T.C. Rathbone. Vibration Tolerance. *Power Plant Engineering*, 43(1939):721–724, 1939.
- [Scheffer and Girdhar, 2004] C. Scheffer and P. Girdhar. *Practical Machinery Vibration Analysis and Predictive Maintenance*. Elsevier Wordmark, 1st edition, 2004.
- [Shi *et al.*, 2004] D.F. Shi, W.J. Wang, and L.S. Qu. Defect Detection for Bearings using Envelope Spectra of Wavelet Transform. *J of Vibration and Acoustics*, 126(4):567–573, 2004.
- [Smith and Randall, 2015] W.A. Smith and R.B. Randall. Rolling Element Bearing Diagnostics Using the Case Western Reserve University Data: A Benchmark Study. *Mechanical Systems and Signal Processing*, 64:100–131, 2015.

- [Tse and Leung, 2010] P.W. Tse and C.T. Leung. *Advanced System For Automatically Detecting Faults Occurring in Bearings*. Nova Science Publishers, 2010.
- [Tse *et al.*, 2001] P.W. Tse, Y.H. Peng, and R. Yam. Wavelet Analysis and Envelope Detection for Rolling Element Bearing Fault Diagnosis Their Effectiveness and Flexibilities. *J of Vibration and Acoustics, Trans of the ASME*, 123:303–10, 2001.
- [Tse *et al.*, 2004] P.W. Tse, W.X. Yang, and H.Y. Tam. Machine Fault Diagnosis through an Effective Exact Wavelet Analysis. *J of Sound and Vibration*, 277(4):1005–1024, 2004.
- [Wang *et al.*, 2011] S. Wang, W. Huang, and Z.K. Zhu. Transient Modeling and Parameter Identification Based on Wavelet and Correlation Filtering for Rotating Machine Fault Diagnosis. *Mechanical Systems and Signal Processing*, 25(4):1299 – 1320, 2011.
- [Xul *et al.*, 2017] J. Xul, X. Zheng, J. Zhang, and X. Liu. Vibration Characteristics of Unbalance Response for Motorized Spindle System. *Procedia Eng.*, 174:331–340, 2017.
- [Yan and Gao, 2005] R. Yan and R.X. Gao. An Efficient Approach to Machine Health Diagnosis based on Harmonic Wavelet Packet Transform. *Robotics and Computer-Integrated Manufacturing*, 21(4-5):291–301, 2005.
- [Yan and Gao, 2011] R. Yan and R.X. Gao. Wavelet Domain Principal Feature Analysis for Spindle Health Diagnosis. *Structural Health Monitoring*, 10(6):631–642, 2011.
- [Yan *et al.*, 2014] R. Yan, R.X. Gao, and X. Chen. Wavelets for Fault Diagnosis of Rotary Machines: A Review with Applications. *Signal Processing*, 96:1–15, 2014.
- [Yan, 2007] R. Yan. *Base Wavelet Selection Criteria for Non-stationary Vibration Analysis in Bearing Health Diagnosis*. University of Massachusetts Amherst, 2007.
- [Yanping *et al.*, 2006] Z. Yanping, H. Shuhong, H. Jinghong, S. Tao, and L. Wei. Continuous Wavelet Grey Moment Approach for Vibration Analysis of Rotating Machinery. *Mechanical Systems and Signal Processing*, 20(5):1202–1220, 2006.
- [Zhang and Gao, 2004] L. Zhang and R.X. Gao. Customized Wavelet for Bearing Defect Detection. *J of Dynamic Systems, Measurement, and Control*, 126:740–745, 2004.
- [Zhang *et al.*, 2005] L. Zhang, R.X. Gao, and K.B Lee. Wavelet-based Enveloping for Spindle Health Diagnosis. In *Instrumentation and Measurement Technology Conf, 2005. Proc of the IEEE*, volume 2, pages 1203–1208, 2005.

- [Zhang *et al.*, 2006] L. Zhang, R.X. Gao, and K.B. Lee. Spindle Health Diagnosis based on Analytic Wavelet Enveloping. *IEEE Trans on Instrumentation and Measurement*, 55(5):1850–1858, Oct 2006.
- [Zhu *et al.*, 2009] Z.K. Zhu, R. Yan, L. Luo, Z.H. Feng, and F.R Kong. Detection of Signal Transients based on Wavelet and Statistics for Machine Fault Diagnosis. *Mechanical Systems and Signal Processing*, 23(4):1076–1097, 2009.

Appendix A

Acronyms Definition

Table A.1: Acronyms Definitions

<i>Acronyms</i>	<i>Definition</i>	<i>Acronyms</i>	<i>Definition</i>
ANN	Artificial Neural Network	AWT	Analytic Wavelet Transform
BPFI	Ball-Passing Frequency Inner-Race	BPFO	Ball-Passing Frequency Outer-Race
BS	Bent Shaft	BSF	Ball Spin Frequency
C	Cage	CWRU	Case Western Reserve University
CWT	Continuous Wavelet Transform	DCC	Direct Current Component
DWT	Discrete Wavelet Transform	EEMD	Ensemble Empirical Mode Decomposition
EMA	Exponential Moving Average	ESER	Energy to Shannon Entropy Ratio
EWA	Exact Wavelet Analysis	EWT	Empirical Wavelet Transform
FEM	Finite Element Model	FFT	Fast Fourier Transform
FTF	Fundamental Train Frequency	HHT	Hilbert Huang Transform
HMM	Hidden Markov Models	HSM	High Speed Machining
HW	Harmonic Wavelet	ICD	Intrinsic Characteristic-scale Decomposition
IFFT	Inverse Fast Fourier Transform	IMF	Intrinsic Mode Function
IMS	Intelligent Maintenance Systems	IR	Inner Race
ITD	Intrinsic Time Decomposition	K-S	Kolmogorov-Smirnev
MA	MisAlignment	MEC	Maximum Energy Criterion
MFCC	Mel Frequency Complex Ceptrum	ML	Mechanical Looseness
MLP	Multiplayer Perception	MSEC	Minimum Shannon Entropy Criterion
OMA	Operational Modal Analysis	OR	Outer Race
PFA	Principal Feature Analysis	PSD	Power Spectral Density

Table A.1: Acronyms Definitions (Continued)

<i>Acronyms</i>	<i>Definition</i>	<i>Acronyms</i>	<i>Definition</i>
QFWT	Q Factor Wavelet Transform	RBF	Radial Basis Functions
RE	Rolling Element	SCS	Sparse Code Shrinkage
SGWT	Second Generation Wavelet Transform	SSA	Statistical Signal Analysis
STFT	Short Time Fourier Transform	SVM	Support Vector Machine
UB	UnBalance	WGM	Wavelet Grey Moment
WGMV	Wavelet Grey Moment Vector	WPT	Wavelet Packet Transform
WT	Wavelet Transform	WTMM	Wavelet Transform Modulus Maxima
WVD	Wigner-Ville Distribution		

Appendix B

Wavelet Parameters Selection

B.1 Wavelet Transform Selection

To select an appropriate *WT* a comparison between *CWT*, *DWT* and *WPT* was performed considering some quantitative parameters. Figure B.1, shows the 3D scalograms of an *OR* faulty signal from *CWRU* data performed with each *WT*, considering: same duration, same *MW* (*db4*) and same level of decomposition: 5th level. The 3D scalogram allows to visualize frequency, time and coefficients of the wavelet decomposition, enabling determining time-frequency resolution as well as the magnitude of the coefficients which allows to localize the defect.

The purpose of this methodology is to detect incipient faults to avoid machine damage; faults must be identified in the first stages. To achieve this objective, faults must be detected at high frequencies, and for this reason a good resolution in this range is required.

The *FFT* graph, Fig. B.1 (a), shows high amplitude peaks in frequencies where the energy of the signal is concentrated, this is evidenced in the high frequency zone between 2.5 and 4 kHz, with the maximum peak at approximately 3.5 kHz. This range is the one that requires great resolution in the wavelet decomposition.

It must be considered that wavelets are very good at detecting discontinuities, or singularities. Abrupt transitions in signals, as in faults, results in high magnitude of the coefficients. That is why, when comparing the different *WT* the amplitude of the coefficients should also be considered. By analyzing the three scalograms from Fig. B.1 (b), (c) and (d) it can be distinguished that *WPT* generates highest magnitudes of the coefficients (greater than 5), this parameter indicates that this transform makes the wavelet fits better to the signal.

As *WT* works as a series of filters, better decomposition allows obtaining better results. *DWT* presents a bad frequency resolution, only 6 frequency ranges are obtained ($N^\circ \text{ DWT ranges} = \text{level} + 1$). As bearing faults impulses are of high frequency in nature, signal decomposition in high frequencies must present a good resolution. In this range *DWT* presents many frequencies contained in each segment, so it can not be established which ranges must be evaluated. In Fig. B.2 (a)

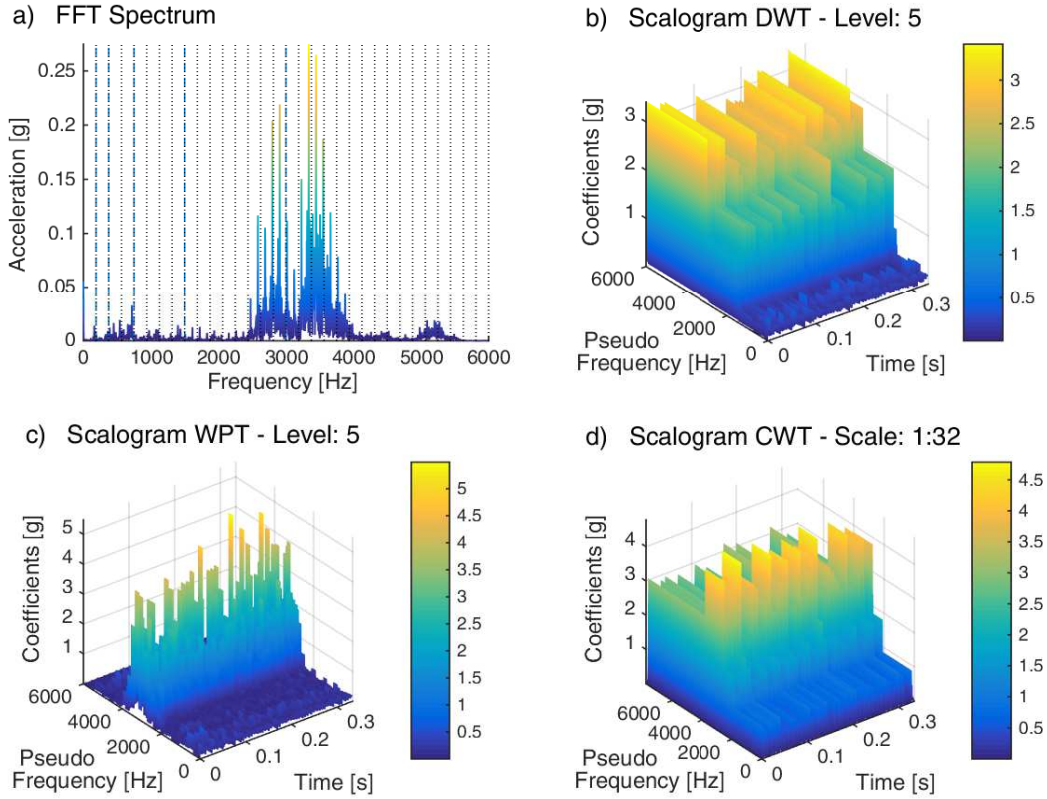


Figure B.1: WT 3D scalogram comparison applied to a signal with OR fault

it can be observed that the coefficients with magnitudes above the average are in the range between 1,500 and 6,000 Hz. So, from the 6 frequency ranges it would be necessary to analyze the range the last two, from 1,500 to 3,000 Hz and from 3,000 to 6,000 Hz as both present high coefficient values. The upper limit of each range in *DWT* can be calculated as $DWT \text{ range limit} = \frac{fs/2}{2^{level+1-range}}$. This range covers an spectrum of 4,500 Hz which implies a bad resolution.

Instead, *WPT*, Fig. B.2 (b), shows a grate resolution as it decomposes the signal into 32 frequency ranges of equal proportions ($N^\circ WPT \text{ ranges} = 2^{level}$). With this transform four ranges present coefficients magnitudes above the average (15, 16, 18 and 19). The upper limit of each range in *WPT* can be calculated as $WPT \text{ range limit} = range \times \frac{fs/2}{2^{level}}$. It would be necessary to analyze only the ranges from 2,625 to 3,000 Hz and 3,187.5 to 3,562.5 Hz. The sum of these ranges cover an spectrum of 750 Hz which is much smaller than *DWT*

Meanwhile, *CWT*, Fig. B.2 (c), decomposes the signal into 32 frequency ranges as *WPT*; but, not of equal proportions, as each range depends on the center frequency of the mother wavelet. For high frequencies this transform has bad resolution, but for low frequencies it has an excellent decomposition. In this case the range that must be evaluated can not be easily calculated, but from

Fig. B.2 (c) it can be distinguished that coefficients with magnitude above the average are between 3,000 and 8,000 Hz. This implies an spectrum range of more o less 5,000 Hz which leads to a bad resolution.

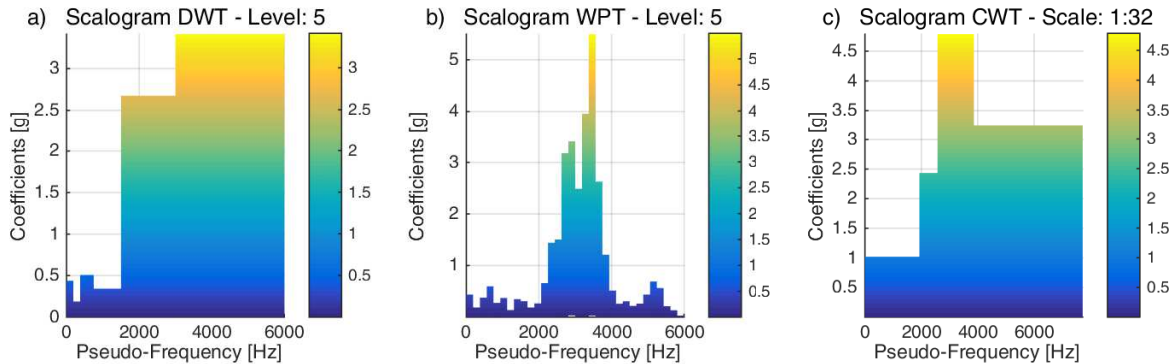


Figure B.2: WT frequency-coefficients comparison applied to a signal with *OR* fault

For selecting the best *WT* also computing time is considered. Contemplating exactly the same parameters for each analysis, processing time for *CWT* was 0.0916 s, for *DWT*: 0.0285 s and finally for *WPT*: 0.0479 s. This shows that *DWT* works 66.88 % faster than *CWT* and *WPT* speed is 47.7 % higher than *CWT*.

WPT combines computational efficiency, an acceptable resolution in the whole frequency ranges; hence, this transform is selected for the developed methodology.

B.2 Mother Wavelet Selection

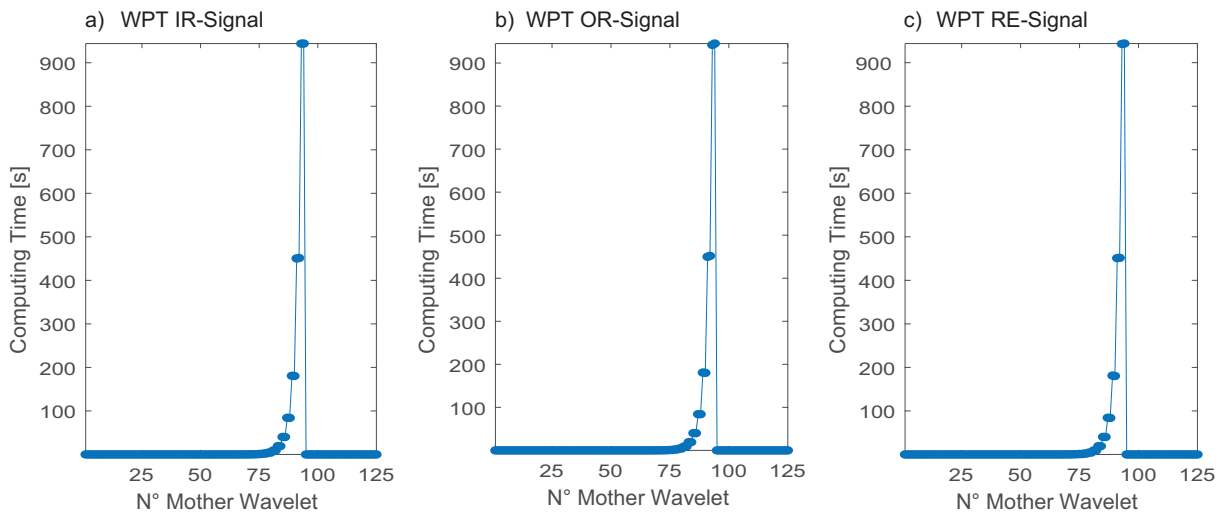
Matlab Wavelet Toolbox has 125 different mother wavelets grouped by families, for *WPT*, these are described in Table B.1.

For preselecting some mother wavelets a computing time analysis is first preformed. One signal for each fault (*IR*, *OR* and *RE*) was considered in this stage. The signals were splitted into 20 segments, and the *WPT* was applied for each segment with each of the mentioned mother wavelets. The computing time required for the analysis of every segment was measured, then the average time was computed. Figure B.3 shows the average time of the 20 segments for each wavelet, the number of the mother wavelets was considered in the same order that is presented in Table B.1.

As it can be seen, some wavelets required excessive amount of time, the slowest wavelet requires 944 seconds for computing the *WPT* of each segment compared to the fastest that needs only 0.009 seconds. Wavelets from *sym31* to *sym45* were discarded as they need more than 900 times the computing time of the other wavelets.

Table B.1: Mother wavelets for *WPT*

Wavelet Families	Wavelets	N ^o wavelets
Daubechies	'db1',..., 'db45'	45
Coiflets	'coif1',..., 'coif5'	5
Symlets	'sym2',..., 'sym45'	44
Discrete Meyer	'dmey'	1
Biorthogonal	'bior1.1', 'bior1.3', 'bior1.5' 'bior2.2', 'bior2.4', 'bior2.6', 'bior2.8' 'bior3.1', 'bior3.3', 'bior3.5', 'bior3.7' 'bior3.9', 'bior4.4', 'bior5.5', 'bior6.8'	15
Reverse Biorthogonal	'rbio1.1', 'rbio1.3', 'rbio1.5' 'rbio2.2', 'rbio2.4', 'rbio2.6', 'rbio2.8' 'rbio3.1', 'rbio3.3', 'rbio3.5', 'rbio3.7' 'rbio3.9', 'rbio4.4', 'rbio5.5', 'rbio6.8'	15
	Total	125

Figure B.3: Mother wavelet computing time for signals with *IR*, *OR*, and *RE* faults

Another characteristic that was considered for preselecting wavelets is that mother wavelets are divided in two main groups, orthogonal and biorthogonal. The principal difference between both is that low-pass and high-pass filters of orthogonal wavelets are of the same length and are not symmetric, while biorthogonal wavelets filters do not have the same length and the low pass filters

are always symmetric while the high pass filters could be either symmetric or anti-symmetric, Fig. B.4. Other difference is that coefficients obtained from orthogonal filters are real numbers, while biorthogonal are either real or integers. As orthogonal filters have more regular structure they lead to easy implementation and scalable architecture. Under these considerations, biorthogonal wavelets are not considered in this analysis. The studied wavelets and their corresponding order for the following figures are shown in Table B.2.

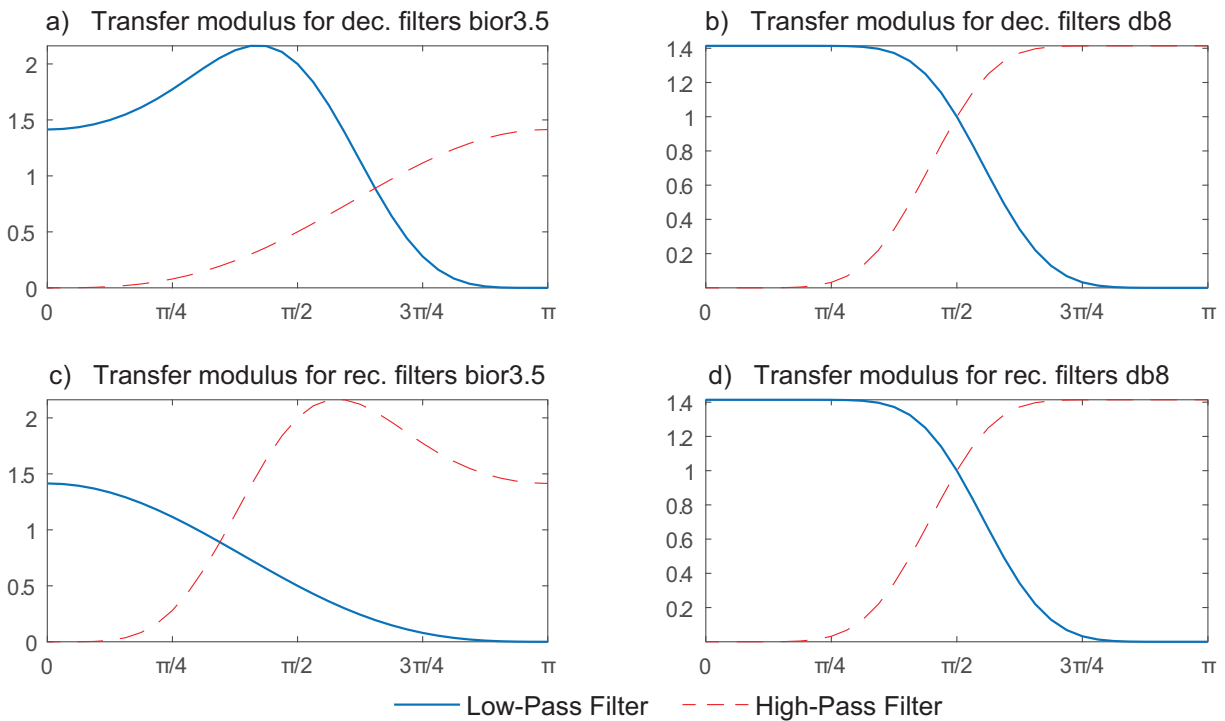


Figure B.4: Orthogonal vs Biorthogonal transfer modulus for decomposition and reconstruction filters

Table B.2: Selected mother wavelets for *WPT*

Wavelet Families	Wavelets	N ^o wavelets
Daubechies	'db1', ..., 'db45'	1, ..., 45
Coiflets	'coif1', ..., 'coif5'	46, ..., 50
Symlets	'sym2', ..., 'sym30'	51, ..., 79
Discrete Meyer	'dmey'	80

[Ngui *et al.*, 2013] presented a review of different quantitative methods of selecting the best *MW* for various applications. In the area of bearing failures three methods have been proposed.

[Rafiee *et al.*, 2010] presented a method named "SUMVAR" (SUMmation of VARiances) for analyzing the best *MW* among 324 with *CWT*, it was first tested in gears and then applied in bearings, [Rafiee and Tse, 2009]. This method is based in the variance of the coefficients, considering that the more variance the signal has, the greater the ability to properly classify faults. [Yan, 2007] proposed the measurement of the *Maximum Energy Criterion (MEC)* and the *Minimum Shannon Entropy Criterion (MSEC)* to select the wavelet that extracts the largest amount of energy from the signal as well as the one that yields large magnitude at a few coefficients and negligible magnitude at the others. *MEC* and *MSEC* are combined by calculating the *Energy-to-Shannon Entropy Ratio (ESER)*. Finally, [Kankar *et al.*, 2011] developed the selection of the *MW* analyzing only the *MSEC*. Many other research have also use these methods; but, there is not a consensus of which wavelet is better.

Variance, eqn (B.1); *MEC*, eqn (B.2); *MSEC*, eqn (B.3) and *ESER*, eqn (B.5) are considered in conjunction with an efficient computing time to select the best wavelet in this research. Considering that each bearing fault has its own different shape, instead of founding one best *MW* for the three faults, *IR*, *OR* and *RE*, as some other research, one wavelet is considered for each one.

- "SUMVAR" Criterion based on the *Variance (V)* of the coefficients

$$V = \frac{1}{N-1} \sum_{i=1}^N |W_{(s,i)} - \mu|^2 \quad (\text{B.1})$$

where μ is the mean of $W_{(s,i)}$, N is the number of wavelet coefficients, and $W_{(s,i)}$ is the wavelet coefficients.

- *Maximum Energy Criterion*

$$E_{energy}(s) = \sum_{i=1}^N |W_{(s,i)}|^2 \quad (\text{B.2})$$

- *Minimum Shannon Entropy Criterion*

$$E_{entropy}(s) = - \sum_{i=1}^N p_i * \log_2(p_i) \quad (\text{B.3})$$

where p_i is the energy probability distribution of the wavelet coefficients, defined as:

$$p_i = \frac{|W_{(s,i)}|^2}{E_{energy}(s)} \quad (\text{B.4})$$

with $\sum_{i=1}^N p_i = 1$, and $p_i * \log_2(p_i) = 0$ if $p_i = 0$

- *Energy-to-Shannon Entropy Ratio*

$$R(s) = \frac{E_{energy}(s)}{E_{entropy}(s)} \quad (\text{B.5})$$

To analyze the best *MW*, the level of decomposition of the *WPT* must be selected according to the range of frequencies where the components with highest energy are found. To select an appropriate range eight signals of each fault were selected from *CWRU* data, prioritizing the ones cataloged by [Smith and Randall, 2015] as data clearly diagnosable, which present less noise. The characteristics of these signals are listed in Table B.3. The spectrum of the signals according to their fault are shown in Fig. B.5.

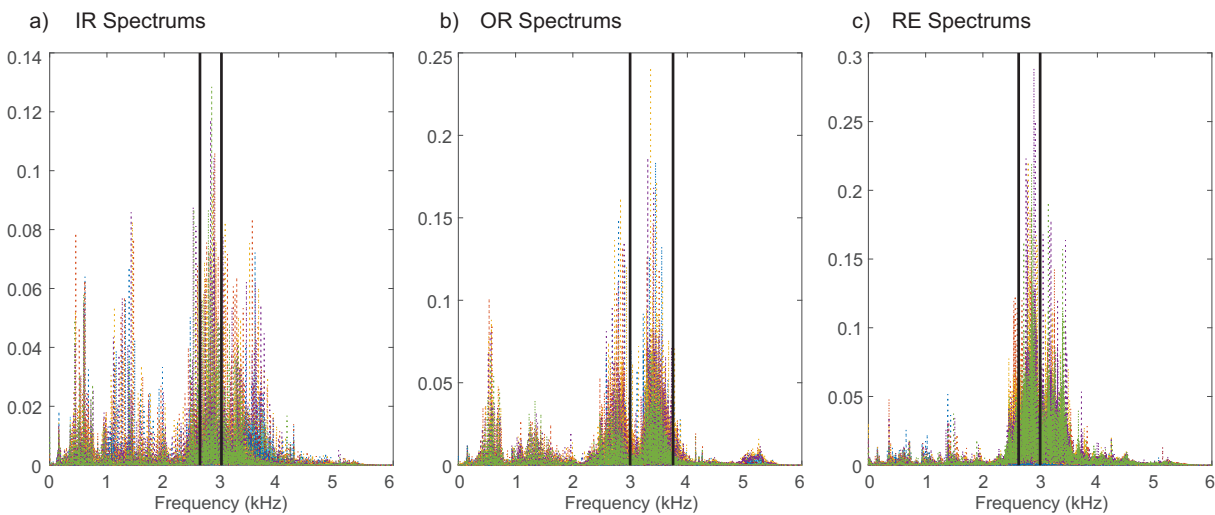


Figure B.5: FFT signals energy

For *IR* the maximum peaks of the signals were found around 2,800 Hz, Fig. B.5 (a); the same as for *RE*, Fig. B.5 (c); while for *OR* the maximum magnitudes were observed around 3,400 Hz, Fig. B.5 (b). With a 4th level of decomposition the 8th range of frequencies (2,625-3,000 Hz) can cover the high energy components of *IR* and *RE* failures. For the *OR* a bigger range is needed to avoid splitting the high energy components, a 3rd level of decomposition is required and the 5th range (3,000-3,750 Hz) must be evaluated.

Besides considering all parameters mentioned above, one extra criterion was analyzed for calculating performance features of *MW*. *WT* is based on convolutions, if these convolutions are performed on finite-length signals, as the ones considered for this thesis, border distortions as shown in Fig. B.6 arise.

When the signal is reconstructed, these distortions disappear, but as quantitative parameters work over the coefficients, border effects must be dismissed. To avoid this problem, the first and the last 100 values of each packet were not considered for performance calculations. This signal cutting implies only a loss of less than 3% of the content of each package.

MEC, *MSEC*, *ESER* and Variance of the coefficients are calculated for four signals of each fault. For *OR* signals considered were the ones with a fault diameter of 0.007 in, for *IR* signals with fault diameter of 0.021 in and for *RE* 0.028 in. Results of each quantitative parameter are shown in Fig. B.7-B.9 for *OR*, *IR* and *RE* respectively.

Table B.3: CWRU signals considered for MW analysis

Fault Type	Fault Diameter	Load	Speed	Fault Frequency	Category ^a
OR	0.007 in	0 hp	1,797 RPM	107.36 Hz	Y
	0.007 in	1 hp	1,772 RPM	105.87 Hz	Y
	0.007 in	2 hp	1,750 RPM	104.56 Hz	Y
	0.007 in	3 hp	1,730 RPM	103.36 Hz	Y
	0.021 in	0 hp	1,797 RPM	107.36 Hz	Y
	0.021 in	1 hp	1,772 RPM	105.87 Hz	Y
	0.021 in	2 hp	1,750 RPM	104.56 Hz	Y
	0.021 in	3 hp	1,730 RPM	103.36 Hz	Y
IR	0.014 in	0 hp	1,797 RPM	162.19 Hz	Y
	0.014 in	1 hp	1,772 RPM	159.93 Hz	Y
	0.014 in	2 hp	1,750 RPM	157.94 Hz	P
	0.014 in	3 hp	1,730 RPM	156.14 Hz	Y
	0.021 in	0 hp	1,797 RPM	162.19 Hz	Y
	0.021 in	1 hp	1,772 RPM	159.93 Hz	Y
	0.021 in	2 hp	1,750 RPM	157.94 Hz	Y
	0.021 in	3 hp	1,730 RPM	156.14 Hz	Y
RE	0.021 in	0 hp	1,797 RPM	141.17 Hz	P
	0.021 in	1 hp	1,772 RPM	139.21 Hz	Y
	0.021 in	2 hp	1,750 RPM	137.48 Hz	N
	0.021 in	3 hp	1,730 RPM	135.91 Hz	N
	0.028 in	0 hp	1,797 RPM	141.17 Hz	Y
	0.028 in	1 hp	1,772 RPM	139.21 Hz	Y
	0.028 in	2 hp	1,750 RPM	137.48 Hz	Y
	0.028 in	3 hp	1,730 RPM	135.91 Hz	Y

^aBased on [Smith and Randall, 2015], where category Y is for data clearly diagnosable, P is for data partially diagnosable and N for data not diagnosable

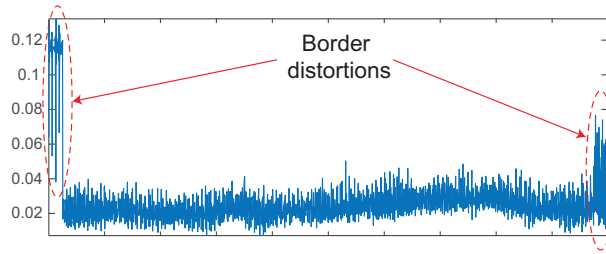


Figure B.6: Border Effects

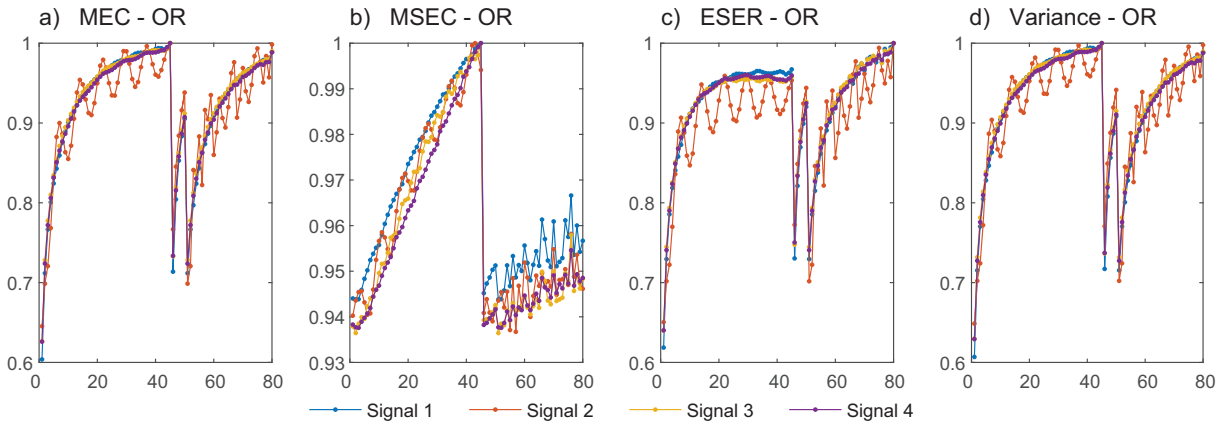


Figure B.7: *MW* quantitative parameters for 4 signals with *OR* fault

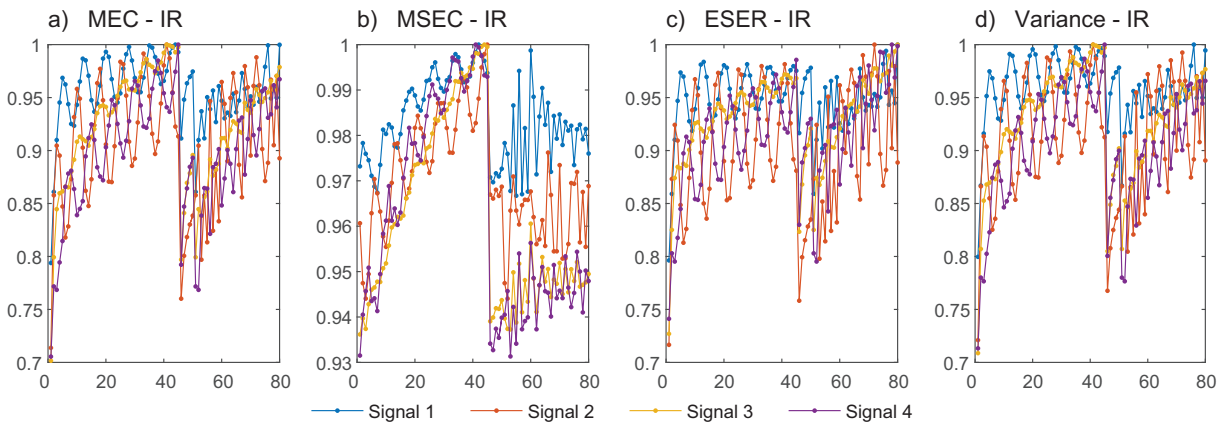
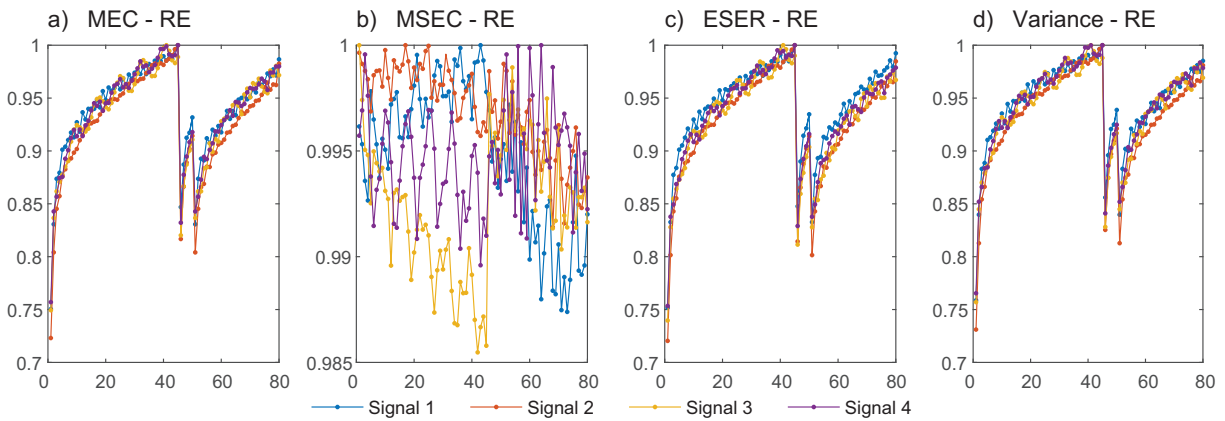
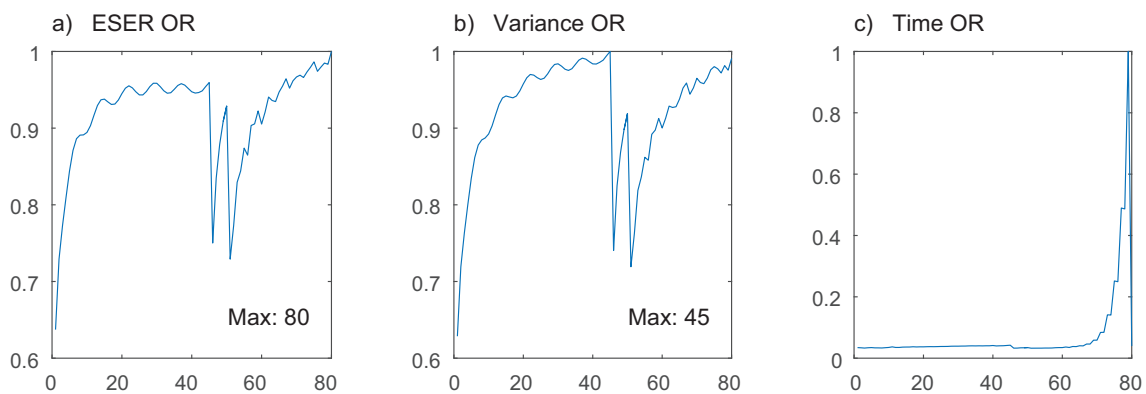
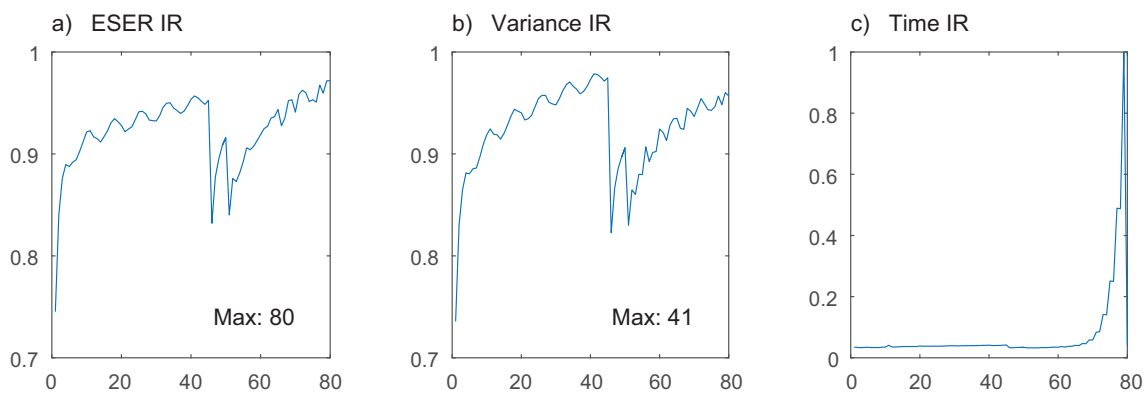


Figure B.8: *MW* quantitative parameters for 4 signals with *IR* fault

The average *ESER*, Variance and Time were considered for selecting the best *MW*, to be able to average these parameters between the signals, first, values were normalized by dividing each value by the maximum of each signal. These parameters are shown in Fig. B.10-B.12 for each fault, where the maximum values of *ESER* and Variance are presented.

Finally, to make a decision based on the three presented parameters, these were counterpoised. Figures B.13- B.15 present the results. Considering the maximum *ESER*, maximum Variance, and minimum computing time, the most suitable *MW* for *OR* failures is *dmey*. The relationship *ESER*-

Figure B.9: *MW* quantitative parameters for 4 signals with *RE* faultFigure B.10: Averaged *MW* quantitative parameters for signals with *OR* faultFigure B.11: Averaged *MW* quantitative parameters for signals with *IR* fault

Time and Variance-*ESER* gives great advantage to this wavelet, while the relationship Variance-Time favors not for much *db45*. For *IR* faults when analyzing Variance-*ESER* there was a tie between *dmey* and *db41*. But, when inspecting *ESER*-Time, in which *dmey* performs better, the difference between both wavelets is not as high as in Variance-Time where *db41* presents better

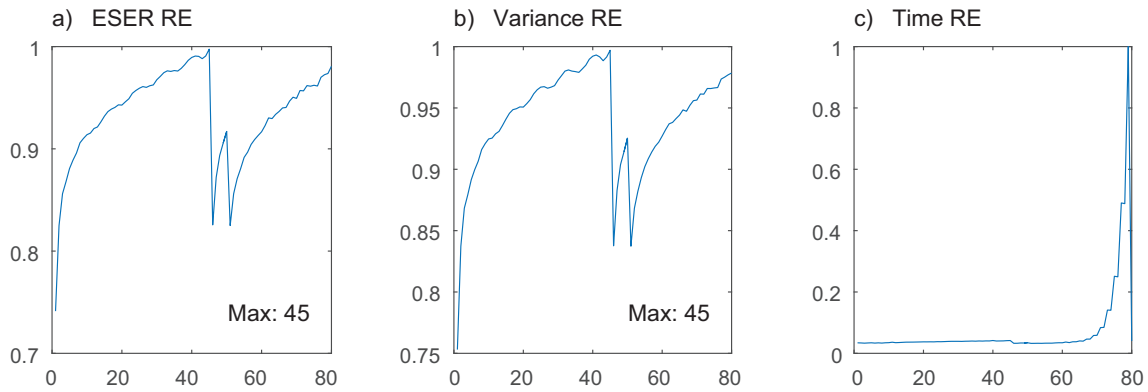


Figure B.12: Averaged *MW* quantitative parameters for signals with *RE* fault

results. This makes *db41* the wavelet that maximizes both parameters. For the last fault, it was evident that *db45* had the best performance for all relationships.

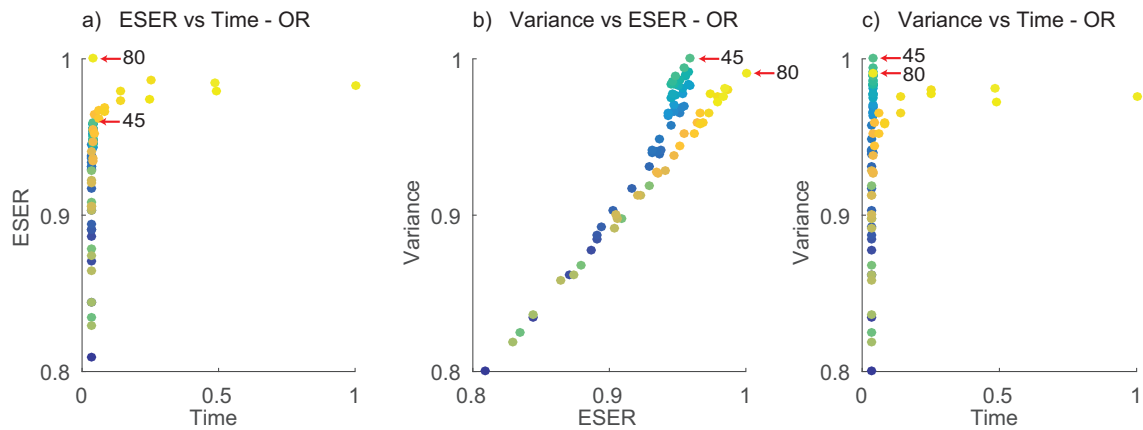


Figure B.13: Quantitative parameters comparison for signals with *OR* faults

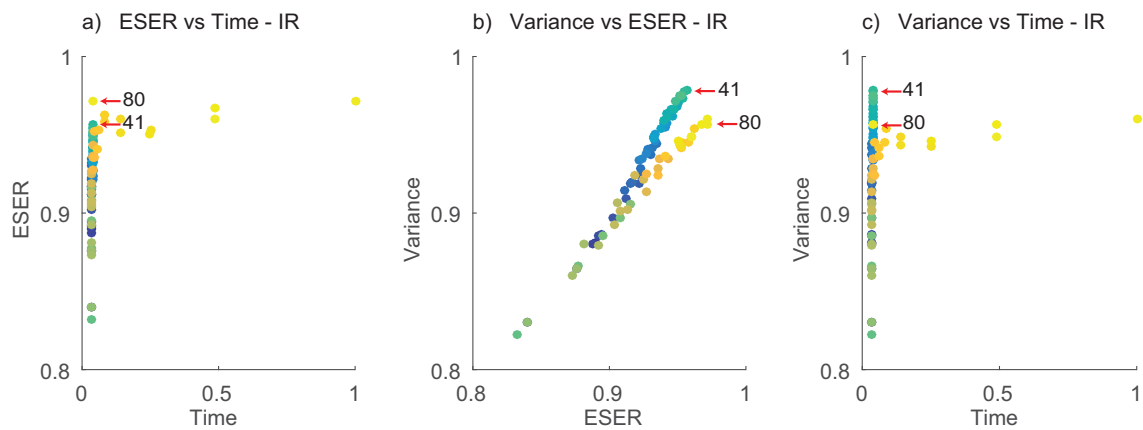


Figure B.14: Quantitative parameters comparison for signals with *IR* faults

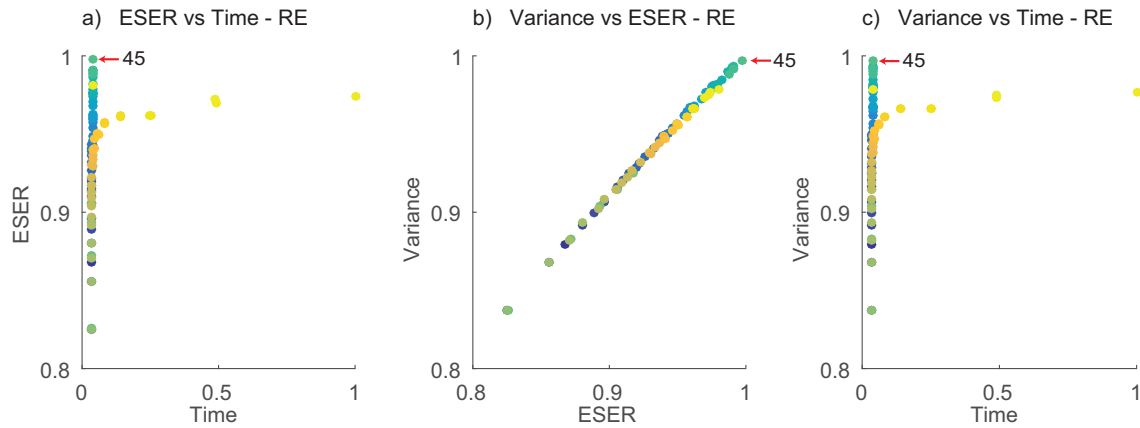


Figure B.15: Quantitative parameters comparison for signals with *RE* faults

An additional analysis was performed for selecting one *MW* for the three types of faults. The average of the quantitative parameters was computed, Fig. B.16. The comparison of the parameters was done as for individual faults, Fig. B.17. The best performance was obtained by *dmey*.

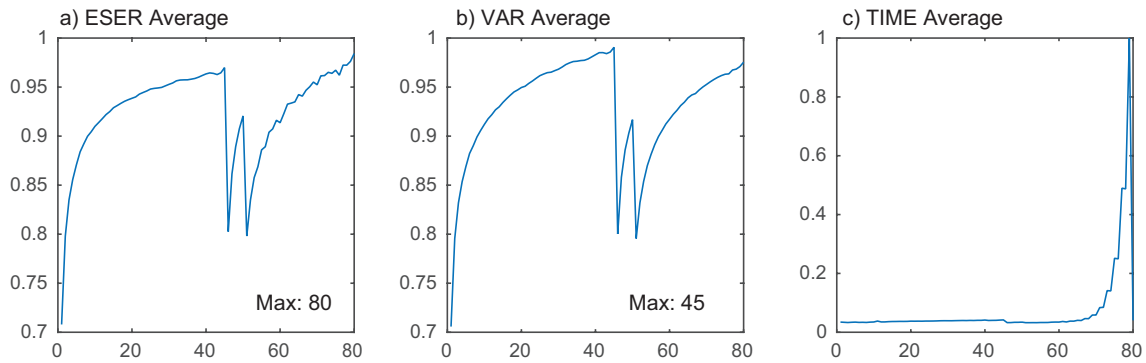


Figure B.16: Averaged *MW* quantitative parameters for the three type of faults

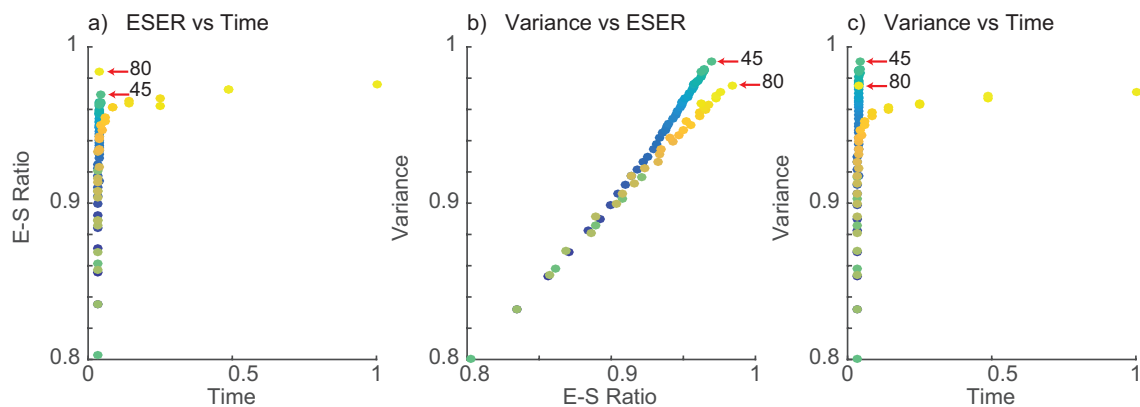


Figure B.17: Quantitative parameters comparison for the three type of faults

Appendix C

Additional results of the proposed methodology

C.1 Bearing Faults

The complete analysis for *CWRU* data is presented in Fig. C.1 - C.3, where (a), (b) and (c) show the clearly diagnosable (Y), partially diagnosable (P) and a not diagnosable (N) cases respectively. As in some cases many peaks are shown, to make more evident the coincidence between the peaks and the fault frequencies a cleared spectrum is presented in Fig. C.4 - C.6. Peaks that correspond to known frequencies (shaft speed and sidebands) were hidden.

For *IMS* data complete results are shown in Fig. C.7 - C.9, in these cases, (a), (b) and (c) represent early, medium and critical stage of damage respectively. The cleared spectrums of these signals are presented in Fig. C.10 - C.12.

Guidelines were plotted in all cases to show the fault frequency, their sidebands and the rotational frequencies with their respective harmonics.

C.2 Unbalance, Misalignment and Mechanical Looseness

A complementary analysis for *CWRU* data is presented in Fig. C.13 - C.15 considering the second part of the methodology to analyze possible *MA* and *ML*. For each fault, (a), (b) and (c) show the clearly diagnosable (Y), partially diagnosable (P) and a not diagnosable (N) cases respectively.

For *IMS* data the complementary results are shown in Fig. C.16 - C.18; (a), (b) and (c) represent early, medium and critical stage of damage respectively.

For both data bases guidelines were plotted showing the shaft speed harmonics, and half speed harmonics.

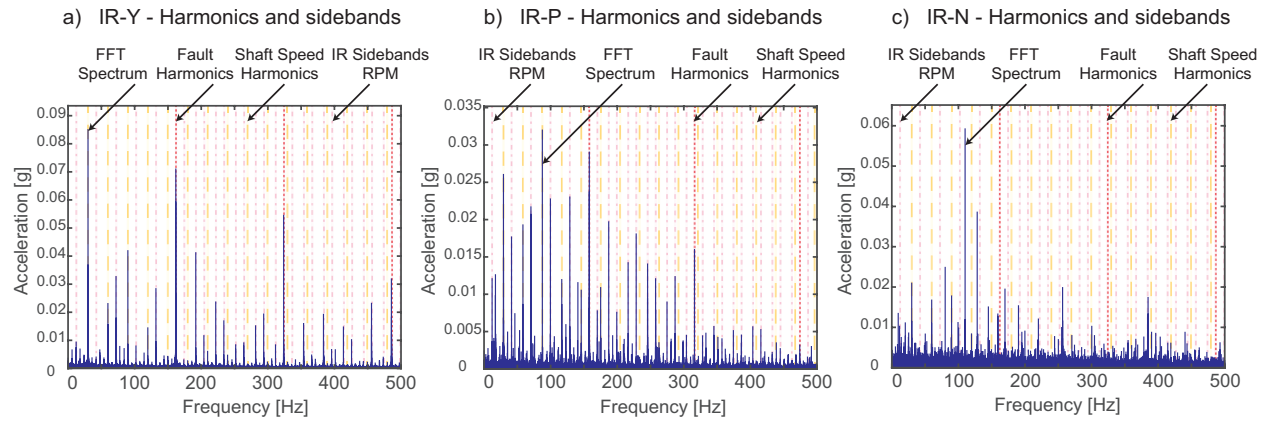


Figure C.1: Spectrum of *IR* faulty signals considering harmonics and sidebands (*CWRU* data base)

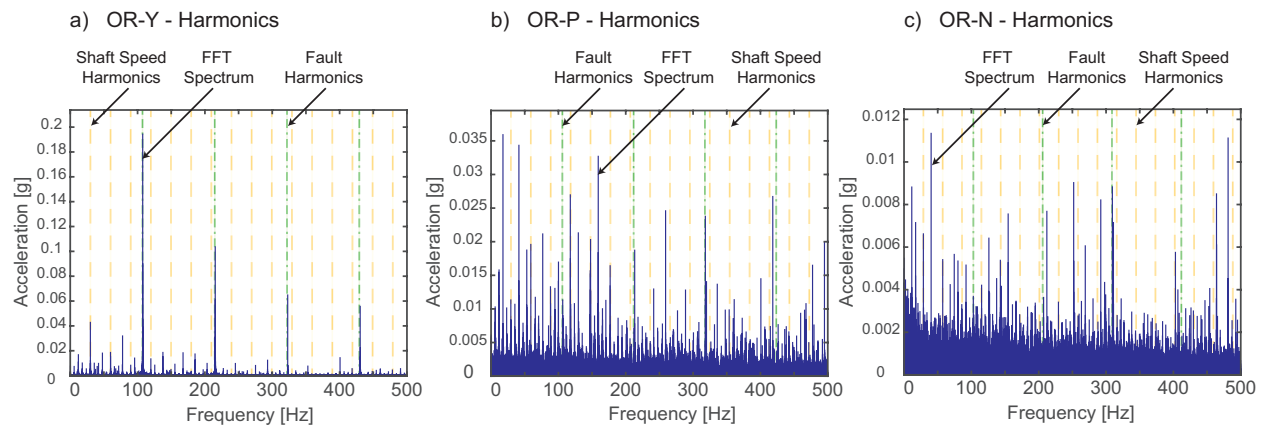


Figure C.2: Spectrum of *OR* faulty signals considering harmonics (*CWRU* data base)

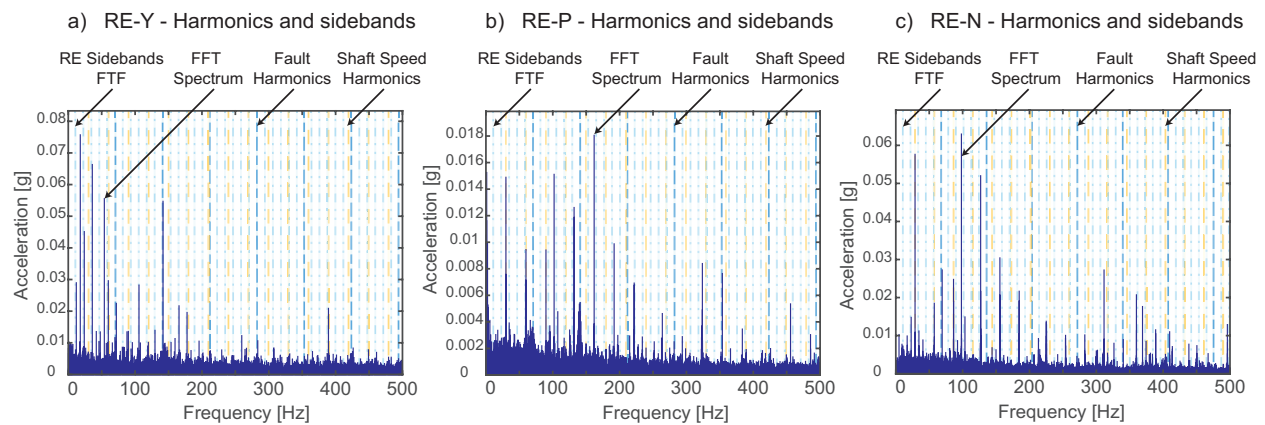


Figure C.3: Spectrum of *RE* faulty signals considering harmonics and sidebands (*CWRU* data base)

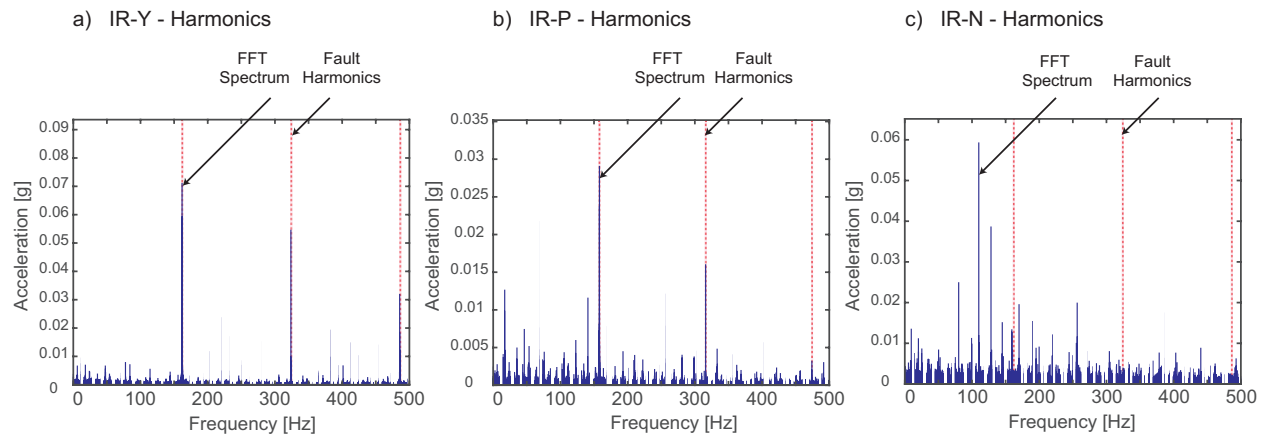


Figure C.4: Cleared spectrum of *IR* faulty signals (*CWRU* data base)

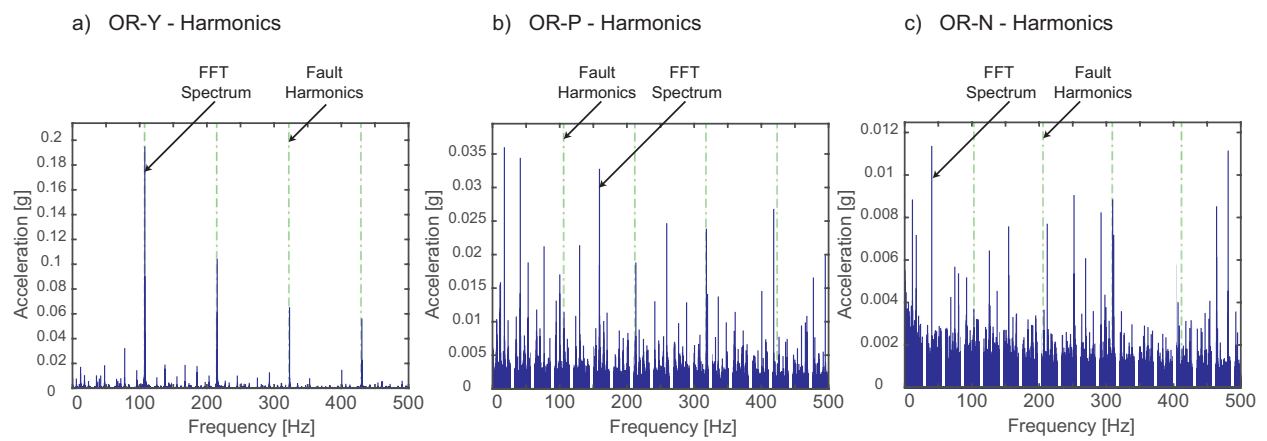


Figure C.5: Cleared spectrum of *OR* faulty signals (*CWRU* data base)

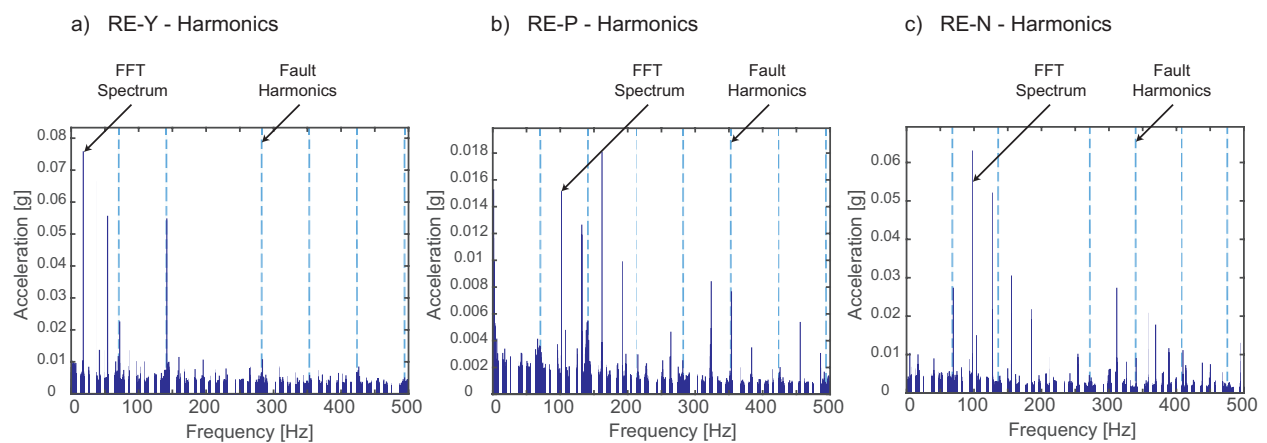
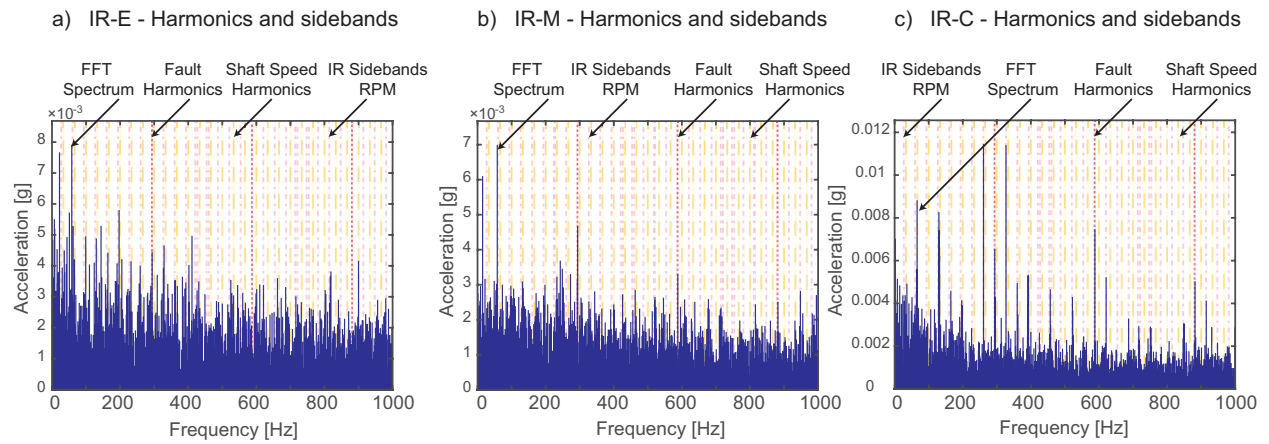
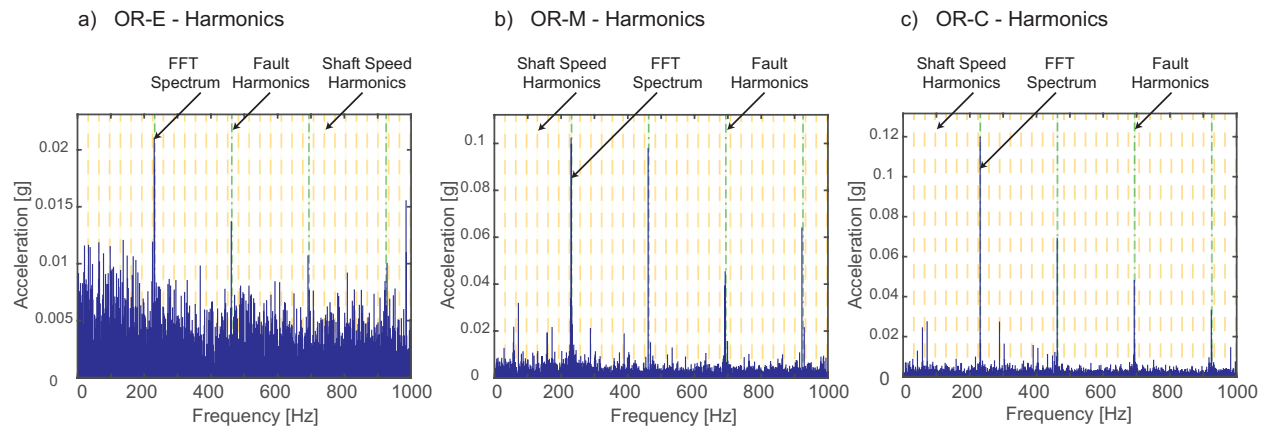
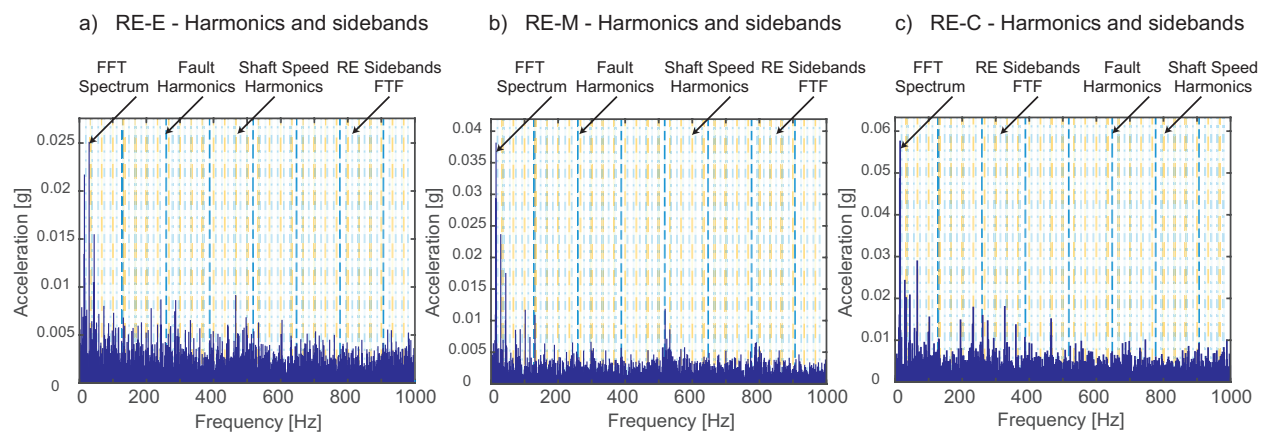


Figure C.6: Cleared spectrum of *RE* faulty signals (*CWRU* data base)

Figure C.7: Spectrum of *IR* faulty signals considering harmonics and sidebands (*IMS* data base)Figure C.8: Spectrum of *OR* faulty signals considering harmonics (*IMS* data base)Figure C.9: Spectrum of *RE* faulty signals considering harmonics and sidebands (*IMS* data base)

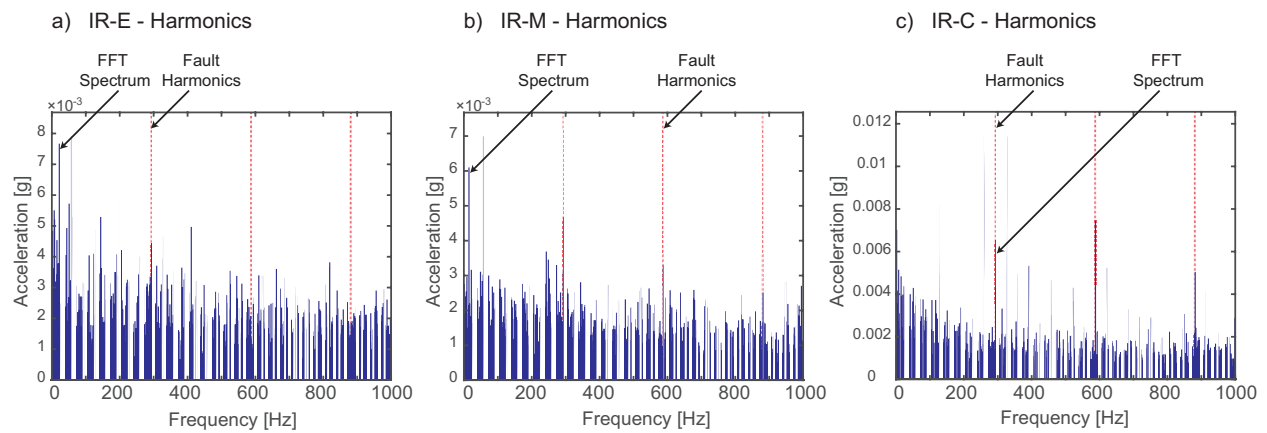


Figure C.10: Cleared spectrum of *IR* faulty signals (*IMS* data base)

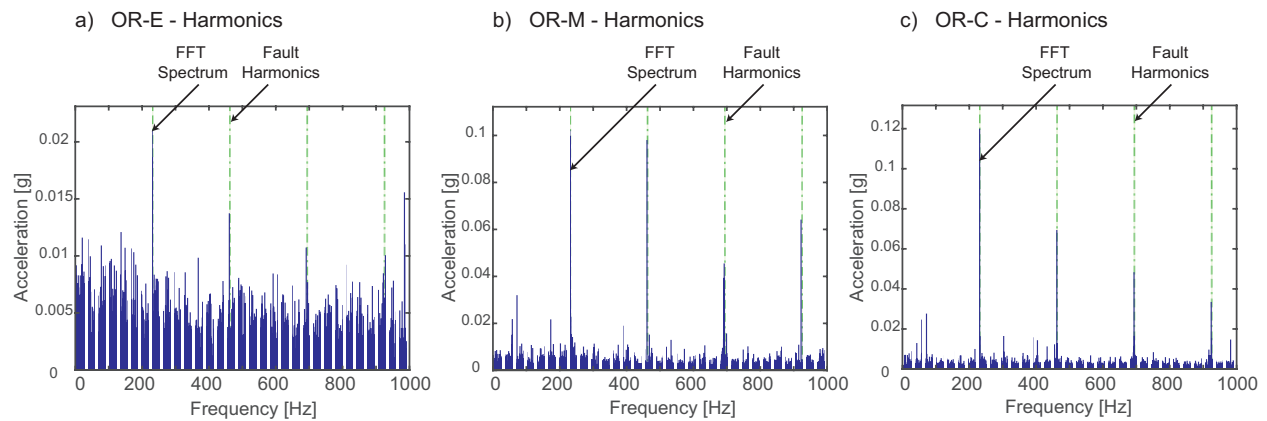


Figure C.11: Cleared spectrum of *OR* faulty signals (*IMS* data base)

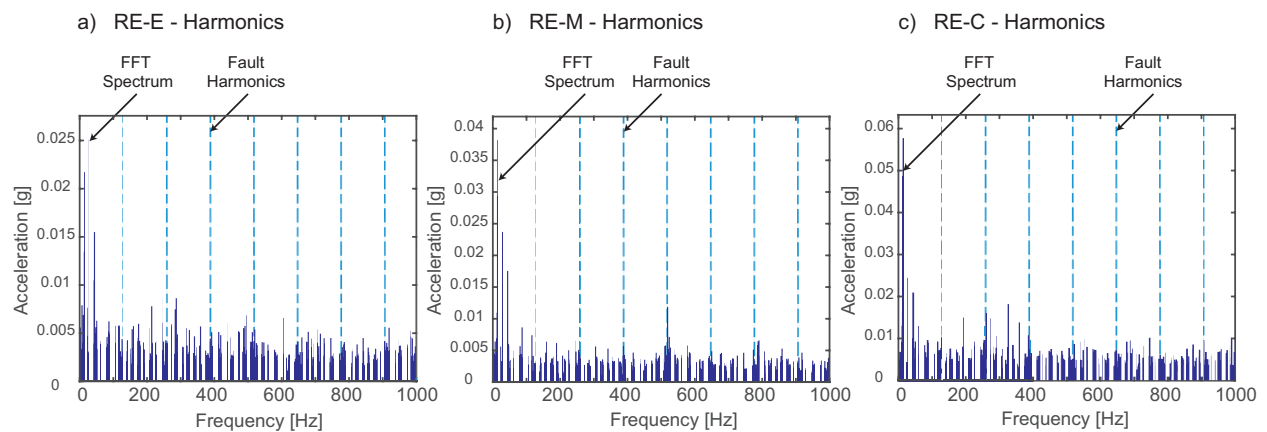


Figure C.12: Cleared spectrum of *RE* faulty signals (*IMS* data base)

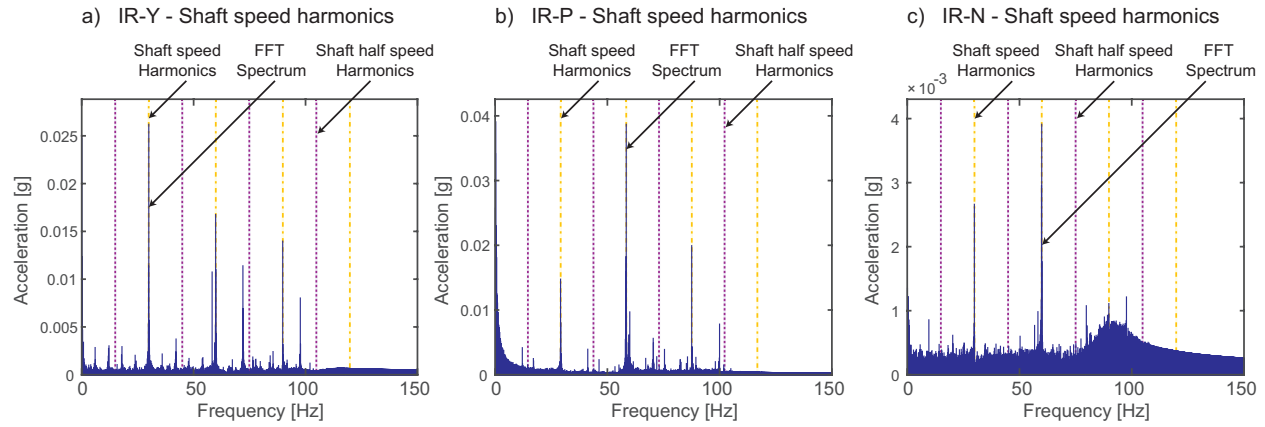


Figure C.13: Spectrum of *IR* faulty signals considering speed harmonics and half speed harmonics (*CWRU* data base)

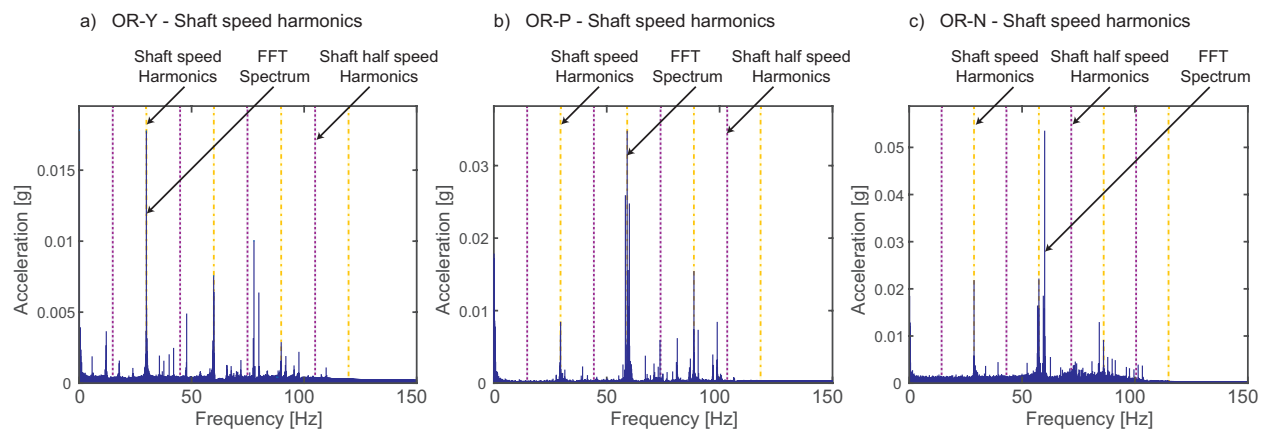


Figure C.14: Spectrum of *OR* faulty signals considering speed harmonics and half speed harmonics (*CWRU* data base)

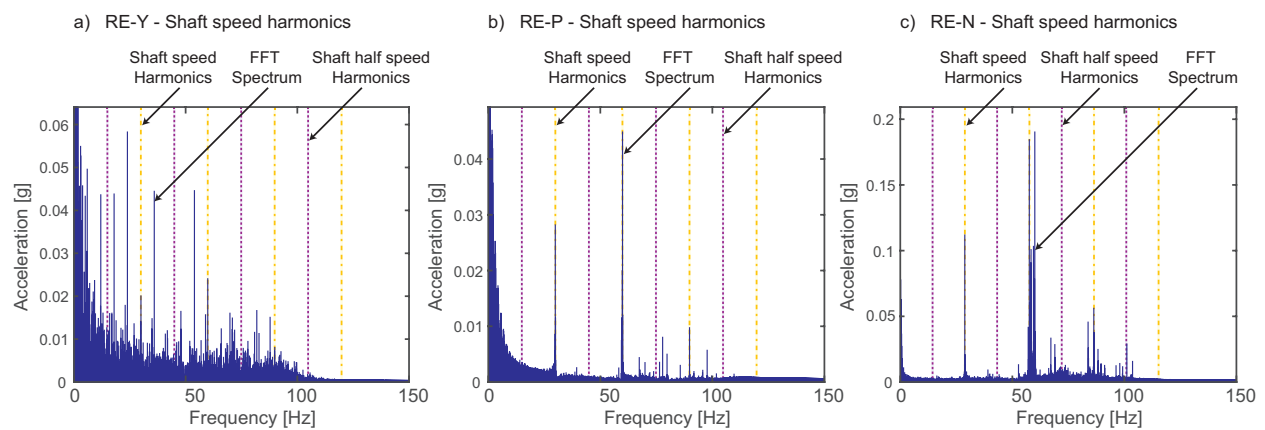


Figure C.15: Spectrum of *RE* faulty signals considering speed harmonics and half speed harmonics (*CWRU* data base)

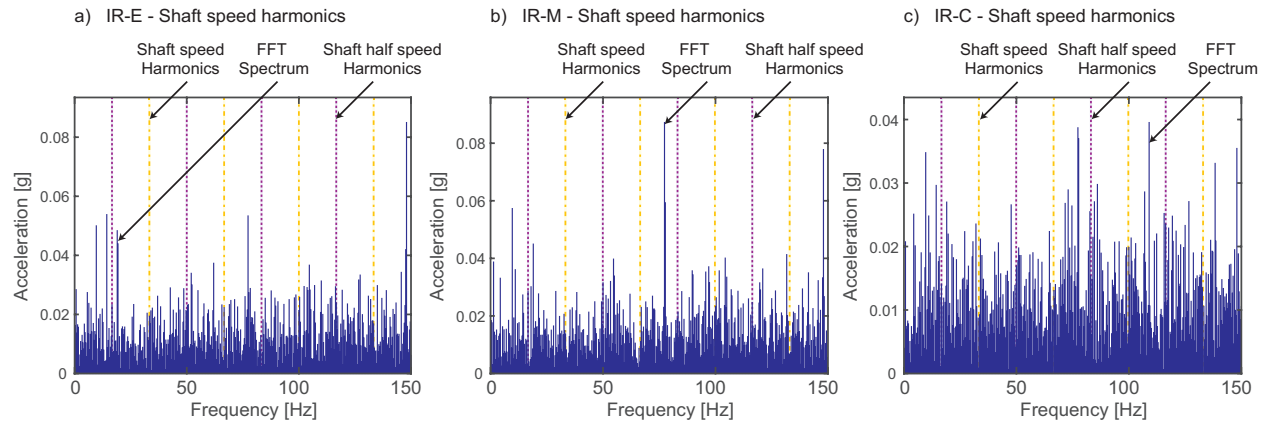


Figure C.16: Spectrum of *IR* faulty signals considering speed harmonics and half speed harmonics (*IMS* data base)

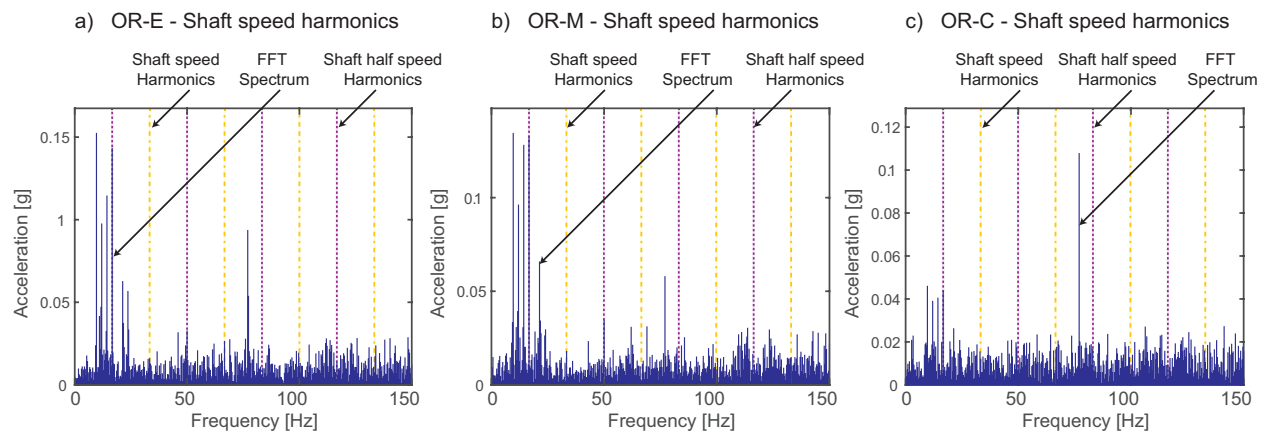


Figure C.17: Spectrum of *OR* faulty signals considering speed harmonics and half speed harmonics (*IMS* data base)

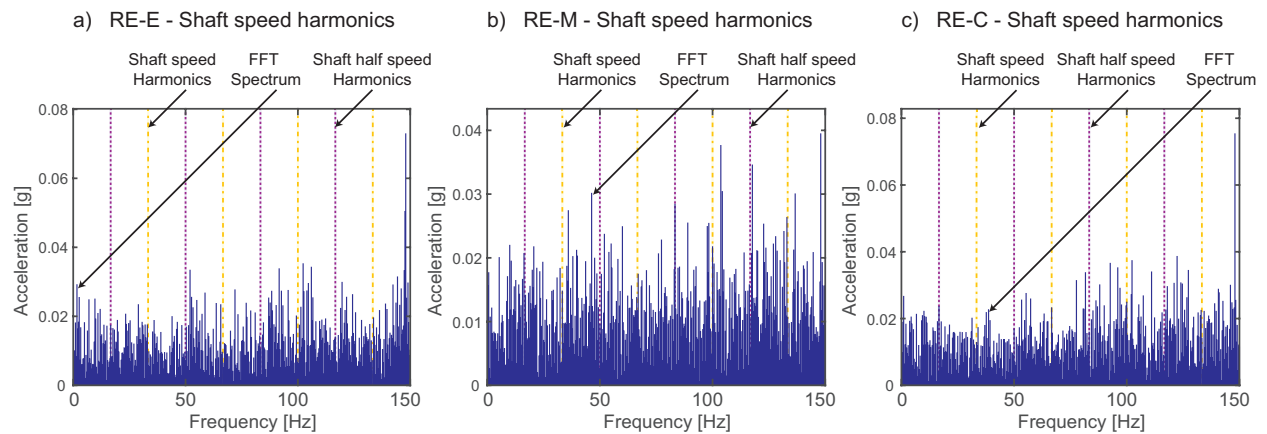


Figure C.18: Spectrum of *RE* faulty signals considering speed harmonics and half speed harmonics (*IMS* data base)

Appendix D

Published articles

Tema A1b. Automatización y Control Mecánico y A2b. Manufactura

“Diagnóstico de Fallas en Husillos de Mecanizado de Alta Velocidad usando Onduletas – Estado del Arte”

Cristina Villagómez Garzón, George Batallas Moncayo, Diana Hernández-Alcántara, Antonio Jr Vallejo Guevara, David Ibarra-Zarate and Ruben Morales-Menendez
Tecnológico de Monterrey, Escuela de Ingeniería y Ciencias
Monterrey Nuevo León, México
Email: {A00819778, A01361945, dianahalc, avallejo, david.ibarra, rmm} @itesm.mx

RESUMEN

La detección y diagnóstico de fallas es una estrategia muy eficiente para dar mantenimiento y servicio en muchas industrias. Particularmente, en sistemas de mecanizado de alta de velocidad, la calidad de las piezas depende en buena parte del desempeño del husillo, donde los rodamientos representan los componentes mecánicos más vulnerables, estadísticamente el 30% de los paros de operación se debe a una falla en los rodamientos. Un sistema de detección y diagnóstico de fallas en rodamientos es una herramienta de competitividad industrial, no solo por evitar productos fuera de especificación, sino por evitar daños extremos. Se presenta una revisión bibliográfica de la investigación del uso de la Transformada de Onduletas para el análisis de vibraciones mecánicas que permitan la detección y diagnóstico confiables de fallas en rodamientos de husillos.

Palabras Clave: Detección, Diagnóstico, Fallas, Rodamientos, Husillos, Mecanizado.

ABSTRACT

Detection and fault diagnosis is a very efficient strategy for maintenance and service in many industries. Particularly in high speed machining systems, the quality of the parts is highly dependent on the performance of the spindle where the bearings represent the most vulnerable mechanical components; statistically, the 30% of breakdowns are due to bearing failures. A detection and fault diagnosis system in bearings is a tool of industrial competitiveness not only to avoid products out of specification; but to avoid extreme damages. A full review of the research about the use of Wavelet Transform for the analysis of mechanical vibrations that allow a reliable fault detection and diagnosis in spindle bearings is presented.

Keywords: Detection, Diagnosis, Failures, Bearings, Spindles, Machining.

1. Introducción

El monitoreo de la condición de una máquina, sistema o proceso es la manera más eficiente de administrar el mantenimiento en muchas industrias, ya que los ahorros económicos pueden ser excepcionales en muchos casos, sin considerar los daños materiales (y humanos) que se pueden evitar. El mantenimiento basado en la condición de una máquina o proceso que requiere operar continuamente, demanda de aplicaciones (algoritmos computacionales) que determinen o estimen la condición interna de la maquina mientras ésta se encuentre en operación.

En el caso de los sistemas de mecanizado de alta velocidad existen dos grandes alternativas para realizar esta tarea, el análisis de vibraciones y el análisis de lubricantes; siendo el estudio de las vibraciones el de mayor interés práctico.

Un centro de maquinado aun en condiciones normales tiene un cierto nivel de vibraciones, cuando se presenta una falla,

estas vibraciones cambian de tal manera, que pueden asociarse a dicha falla.

En este trabajo se presentarán algoritmos de detección y diagnóstico de fallas para husillos en centros de mecanizado de alta velocidad; aunque existen muchos enfoques y herramientas matemáticas, el estudio se limita al uso de la *Transformada de Onduletas (WT, Wavelets Transform)*. Se conservan los términos en inglés para evitar confusiones. La Tabla 1 resume los acrónimos utilizados.

Este artículo está organizado como se indica. La *Sección 2* describe el problema, mientras que la *Sección 3* presenta una revisión bibliográfica de los trabajos más importantes que se han publicado utilizando *WT*. La *Sección 4* ejemplifica este tipo de enfoque utilizando datos experimentales. Finalmente, la *Sección 5* concluye la investigación.

Monitoreo de Husillos usando la Transformada de Onduletas ^{*}

George Batallas Moncayo, Cristina Villagómez Garzón ^{*}
Diana Hernández Alcantara, Antonio Jr Vallejo Guevara ^{*}
David Ibarra Zarate and Ruben Morales-Menendez ^{*}

^{*} *Tecnológico de Monterrey, Escuela de Ingeniería y Ciencias
Monterrey NL, México, {A01361945, A00819778, dianahalc, avallejo,
david.ibarra, rmm}@itesm.mx*

Abstract: El diagnóstico y prevención de fallas ha permitido evolucionar las estrategias de mantenimiento en las industrias, mejorando la eficiencia y optimizando los paros en la producción. En el caso de los sistemas de mecanizado, el diagnóstico oportuno de fallas evita productos fuera de especificación y/o daños extremos. Un maquinado óptimo es altamente dependiente del desempeño y condición del husillo, dentro del cual los rodamientos representan los componentes mecánicos con más probabilidad de falla. A partir de una revisión bibliográfica exhaustiva, se presentan los avances en el uso de la Transformada de Onduletas para el análisis de vibraciones mecánicas de rodamientos en husillos. Adicionalmente, se propone una metodología para detectar y diagnosticar fallas en este tipo de aplicaciones.

Keywords: Diagnóstico fallas, Vibraciones, Husillos, Rodamientos, Onduletas

1. INTRODUCCIÓN

El monitoreo de la condición de una máquina, sistema o proceso es la manera más eficiente de administrar el mantenimiento. La economía del proceso puede ser excepcional. Para llevar a cabo un mantenimiento basado en la condición de una máquina en operación continua, se requieren algoritmos eficientes que determinen el estado interno en línea, mientras está operando.

Un centro de maquinado aún en condiciones normales presenta un cierto nivel de vibraciones. Cuando ocurre una falla, estas vibraciones se modifican y en ellas se puede encontrar el motivo del desperfecto. Este análisis puede realizarse utilizando diferentes herramientas matemáticas, una de las más usadas por su capacidad de manejar señales complejas gracias a su multiresolución es la *Transformada de Onduletas* (*WT*, *Wavelet Transform*). En la Tabla 1 se muestra un resumen de todos los acrónimos utilizados en este artículo, se conservarán los términos en inglés por ser muy familiares y para evitar confusiones en su traducción.

La *WT* se asemeja a la *Transformada de Fourier* (*FT*, *Fourier Transform*) al descomponer una función con base a otras preestablecidas, mientras la *FT* utiliza senos y cosenos; la *WT* maneja como funciones base distintas onduletas. La *WT* está definida como:

$$F(a, b) = \int_{-\infty}^{\infty} f(x)\psi_{(a,b)}^*(x)dx \quad (1)$$

^{*} Los autores le agradecen al *Tecnológico de Monterrey* y al *CONACyT* por sus apoyos parciales.

donde el ^{*} representa el conjugado complejo y la función $\psi(\dots)$ se selecciona de acuerdo a ciertas reglas de diseño.

La *WT* tiene beneficios en tiempo y frecuencia debido a su ventana modificable, seleccionando el tiempo mediante traslaciones y los rangos de frecuencia por medio de dilataciones. En el procesamiento de señales no estacionarias presenta un mejor rendimiento que los análisis tradicionales, Kankar et al. (2011) y Lauro et al. (2014). Además, a diferencia de la *FT*, tiene un conjunto infinito de funciones base, lo que hace que la *WT* sea muy versátil. Entre los beneficios intrínsecos de esta transformada están la reducción de ruido, la compresión de datos, filtrado, entre otros.

Este artículo está organizado en 5 secciones. En la *Sección 2* se describe el problema y en la *Sección 3* se presenta una revisión bibliográfica de los trabajos más importantes usando *WT*. La *Sección 4* ejemplifica la metodología desarrollada para la detección de fallas, y finalmente, la *Sección 5* concluye el trabajo.

2. DESCRIPCIÓN DEL PROBLEMA

La relación entre las señales de vibración y el estado de una máquina fueron inicialmente identificadas por Rathbone (1939), concluyendo que el efecto negativo era proporcional a la amplitud de la señal de vibración. Más tarde, en 1960 se vio que el monitoreo y análisis de la vibración podía prevenir dichos daños. Posteriormente, se empezaron a analizar las señales de vibración con técnicas como la *Transformada Rápida de Fourier* (*FFT*, *Fast Fourier Transform*) para buscar relaciones más claras o explícitas en problemas más complejos. Con el desarrollo de la era digital se mejoró la velocidad y capacidad de procesamiento en el área de detección, Randall (2011).

Appendix E

Developed Programs

For the developed methodology four *Matlab* functions were developed, two for plotting the scalograms, the first one in two dimensions and the second one in three dimensions; and two for processing the signals, one for bearing faults diagnosis and the other for shaft faults diagnosis. Parameters are shown in the following code.

```
1 % Loading signal
2 load DE12k_0_007_OR_C; Signal=X130_DE_time;
3
4 % Parameters
5 Level=6; % Level for WPT
6 MW='dmey'; % Mother Wavelet
7 fs=12000; % Sampling Frequency
8 RPM=2000; % Spindle Speed
9
10 % Decomposition: WPT (Matlab Toolbox)
11 Tree=wpdec(Signal,Level,MW);
12
13 % Scalogram Plots 2D y 3D
14 figure(1)
15 ScalogramWPT2D(Tree,fs)
16 figure(2)
17 ScalogramWPT3D(Tree,fs)
18
19 % Final signal after processing for bearing fault diagnosis
20 Fsignal=MetodologiaGBCV(Signal1,fs,'OR');
21
22 % Final signal after processing for shaft fault diagnosis
23 Fsignal_2=MetodologiaGBCV_2(Signal1,fs,RPM);
```

An scalogram can be plotted for any signal, the parameters needed are: the tree of the *WPT* and the sampling frequency. The tree is easily obtained with the *Matlab Toolbox* function: *wpdec* selecting the level of decomposition and the *MW*. An example is shown in Fig. E.1, for the 2D scalogram and in Fig. E.2 for the 3D scalogram.

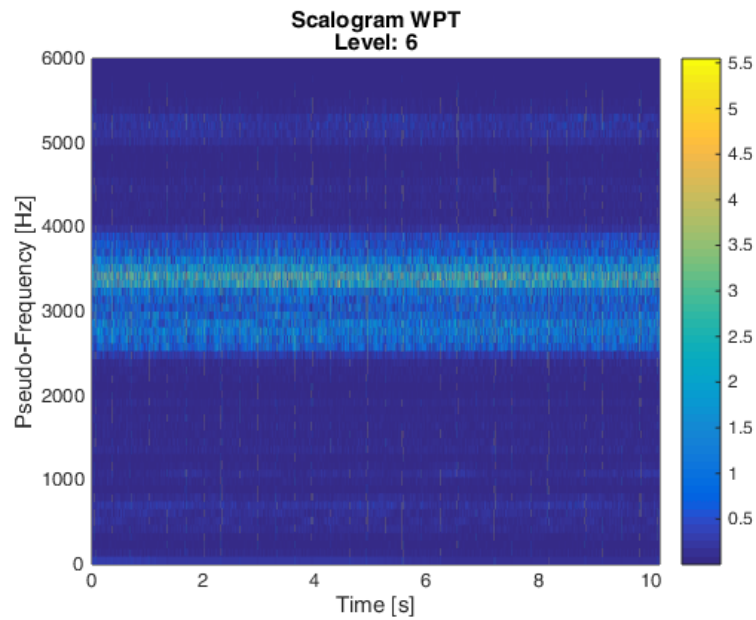


Figure E.1: *WPT* 2D scalogram function

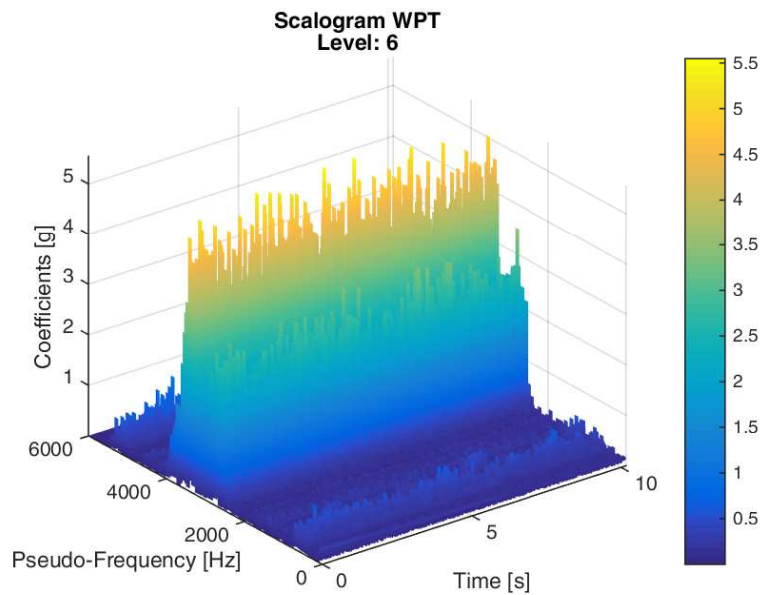


Figure E.2: *WPT* 3D scalogram function

The developed functions to plot the scalogram are shown below.

```

1 function ScalogramWPT2D(Tree , fs )
2 % -Tree:TreeWPT -fs:Sampling frequency
3 level=get(Tree , 'Depth');
4 [SPEC,TIMES,FREQ,TNFO] = wpspectrum(Tree , fs);
5 SPEC=flipud(SPEC);
6 FREQ1=0; SPEC1=[];
7
8 for i=1:length(FREQ)
9     FREQ1=vertcat(FREQ1,FREQ(i));
10    FREQ1=vertcat(FREQ1,FREQ(i));
11    SPEC1=vertcat(SPEC1,SPEC(i,:));
12    SPEC1=vertcat(SPEC1,SPEC(i,:));
13 end
14 FREQ1=FREQ1(1:length(FREQ)*2)';
15
16 pcolor(TIMES,FREQ1,SPEC1); shading('interp'); colorbar
17 xlabel('Time [s]');ylabel('Pseudo-Frequency [Hz]');zlabel('Coefficients [g]')
18 title({'Scalogram WPT';['Level: ',num2str(level)]})
19 axis tight

1 function ScalogramWPT3D(Tree , fs )
2 % -Tree:TreeWPT -fs:Sampling frequency
3 level=get(Tree , 'Depth');
4 [SPEC,TIMES,FREQ,TNFO] = wpspectrum(Tree , fs);
5 SPEC=flipud(SPEC);
6 FREQ1=0; SPEC1=[];
7
8 for i=1:length(FREQ)
9     FREQ1=vertcat(FREQ1,FREQ(i));
10    FREQ1=vertcat(FREQ1,FREQ(i));
11    SPEC1=vertcat(SPEC1,SPEC(i,:));
12    SPEC1=vertcat(SPEC1,SPEC(i,:));
13 end
14 FREQ1=FREQ1(1:length(FREQ)*2)';
15
16 surf(TIMES,FREQ1,SPEC1);shading('interp');colorbar
17 xlabel('Time [s]');ylabel('Pseudo-Frequency [Hz]');zlabel('Coefficients [g]')
18 title({'Scalogram WPT';['Level: ',num2str(level)]})
19 axis tight

```

The functions developed for processing the signal based on the proposed methodology are presented below.

```

1 %% METHODOLOGY FOR BEARING FAULT DIAGNOSIS USING WPT
2 % By GEORGE BATALLAS & CRISTINA VILLAGOMEZ
3
4 function FilteredSignal = MetodologiaGBCV(Signal , fs , fault)
5 %\////////////////////////////////////
6 % Wavelet Parameters
7 %\////////////////////////////////////
8 WaveIR='db41';
9 WaveOR='dmey';
10 WaveRE='db45';
11 Nlevel=6;
12 %\////////////////////////////////////
13 % Signal Parameters
14 %\////////////////////////////////////
15 switch fault
16 case 'IR'
17     wavelet=WaveIR;
18 case 'OR'
19     wavelet=WaveOR;
20 case 'RE'
21     wavelet=WaveRE;
22 end
23 %\////////////////////////////////////
24 % Signal Preprocessing Trend Removal
25 %\////////////////////////////////////
26 time=0:1/fs:(length(Signal)-1)/fs;
27 fitness = fit(time',Signal,'poly1');
28 trend = fitness.p1*time+fitness.p2;
29 Signal=Signal-trend';
30 %\////////////////////////////////////
31 % Wavelet Packet Decomposition and Best Tree
32 %\////////////////////////////////////
33 dwtmode('mode');
34 T=wpdec(Signal ,Nlevel , wavelet);
35 [SPEC,TIMES,FREQ] = wpspectrum(T, fs);
36 % BestTree
37 BT=besttree(T);
38 BTnodesN = leaves(BT); BTnodesL = leaves(BT,'dp');
39 for i=1:length(BTnodesN)
40     FREQS(i)=BTnodesL(i,2)*(fs/2)/(2^BTnodesL(i,1));
41 end
42 FREQS=horzcat(FREQS(2:end),6000);

```

```

43 %\////////////////////////////////////
44 % Best Nodes Selection [ Kurtosis x RMS ]
45 %\////////////////////////////////////
46 for m=1:length(BTnodesN)
47     COEFS=wpccoef(BT, BTnodesN(m));
48     K(m) = kurtosis(COEFS(100:end-100));
49     RMS(m)=      rms(COEFS(100:end-100));
50 end
51 K=sum(K,1, 'omitnan');
52 KR=K.*RMS;
53 %\////////////////////////////////////
54 % Threshold KR Best Nodes
55 %\////////////////////////////////////
56 limm=mean(KR);
57 %\////////////////////////////////////
58 % Threshold Normalized Weighting
59 %\////////////////////////////////////
60 for i=1:length(KR)
61     if(KR(i)>=limm)
62         KRW(i)=1;
63     else
64         KRW(i)=KR(i)/max(KR);
65     end
66 end
67 %\////////////////////////////////////
68 % Reconstructed Signal With Weighting Values
69 %\////////////////////////////////////
70 BSignal=0;
71 for i=1:length(BTnodesN)
72     BSignal=BSignal+KRW(i).*wprcoef(T, BTnodesN(i));
73 end
74
75 FilteredSignal=BSignal;

1 %% METHODOLOGY FOR SHAFT FAULT DIAGNOSIS USING WPT
2 % By GEORGE BATALLAS & CRISTINA VILLAGOMEZ
3
4 function FilteredSignal = MetodologiaGBCV_2(Signal, fs, RPM)
5 %\////////////////////////////////////
6 % Wavelet Parameters
7 %\////////////////////////////////////
8 Wave='db44';
9 Nlevel=6;
10 %\////////////////////////////////////
11 % Shaft Speed and 5 SSHz harmonics

```

```

12 %\////////////////////////////////////
13 SSHz=RPM/60;
14 fcorte=ceil(SSHz*5);
15 %\////////////////////////////////////
16 % Signal Preprocessing Trend Removal
17 %\////////////////////////////////////
18 time=0:1/fs:(length(Signal)-1)/fs;
19 fitness = fit(time',Signal,'poly1');
20 trend = fitness.p1*time+fitness.p2;
21 Signal=Signal-trend';
22 %\////////////////////////////////////
23 % Wavelet Packet Decomposition and Cutoff Frequency
24 %\////////////////////////////////////
25 T=wpdec(Signal,Nlevel,wavelet);
26 [SPEC,TIMES,FREQ,TNFO] = wpspectrum(T,fs);
27 % Selecting first nodes 5 SSHz harmonics
28 if fcorte>FREQ(1)
29     cutF=find(FREQ<=fcorte,1,'last');
30 else
31     cutF=1;
32 end
33 %\////////////////////////////////////
34 % Reconstructed Signal only Low Frequencies
35 %\////////////////////////////////////
36 BSignal=0;
37 for i=1:cutF
38     BSignal=BSignal+wprcoef(T,TNFO(i));
39 end
40 %\////////////////////////////////////
41 % DC REMOVAL
42 %\////////////////////////////////////
43 fitness = fit(t',BSignal,'poly1');
44 trend = fitness.p1*t+fitness.p2;
45 BSignal=BSignal-trend';
46 BSignal=BSignal-mean(BSignal);
47
48 FilteredSignal=BSignal;

```


Curriculum Vitae



Silvia Cristina Villagómez Garzón was born in Quito Ecuador on March 2nd, 1990. She received the degree of Mechatronics Engineer from the *Universidad de las Fuerzas Armadas - ESPE*, Sangolquí Ecuador in Dec 2014 with the thesis "*Automation of the Equipment for Analysis of Coriolis Acceleration with Hydraulic Analogy for the Laboratory of Mechanisms at ESPE*". She has worked in design, manufacture and commissioning of protection, control and distribution panels, as well as in automation in low and medium voltage at TCONTROL (Ecuador). She was part of the Automotive Consortium Research Group working for an industrial project at Bocar SA de CV. She pursuit a Master Degree in Manufacturing Systems at *Tecnológico de Monterrey*, Escuela de Ingeniería y Ciencias, from January 2016 to December 2017.

This document was typed in using L^AT_EX by Silvia Cristina Villagómez Garzón and partially by George Francisco Batallas Moncayo.